Perirhinal feedback input controls neocortical memory formation via layer 1

DISSERTATION

zur Erlangung des akademischen Grades

Doctor of Philosophy

(PhD)

im Fach Biologie

eingereicht an der

Lebenswissenschaftlichen Fakultät

der Humboldt-Universität zu Berlin

Von

M.Sc.

Jiyun Shin

Präsidentin der Humboldt-Universität zu Berlin

Prof. Dr. Sabine Kunst

Dekan der Lebenswissenschaftlichen Fakultät

Prof. Dr. Bernhard Grimm

Gutachter/innen:

1. Prof. Dr. Matthew Larkum
2. Prof. Dr. Michael Brecht
3. Prof. Dr. James Poulet

Tag der mündlichen Prüfung: 18.12.2020

Perirhinal feedback input controls neocortical memory formation via layer 1

PhD Candidate:

Jiyun Shin

Supervisor:

Prof. Matthew Larkum

September 2020

Neurocure Cluster of Excellence,

Institut für Biologie

Humboldt Universität zu Berlin, Berlin, Germany

Table of Contents

Abstract

Declarative memory formation is believed to rely on interactions between the medial temporal lobe (MTL) and neocortex. However, the distributed nature of neocortical networks has hindered investigation on cellular targets and mechanisms of memory formation in the neocortex. The six-layered mammalian neocortex has an anatomical organization in which top-down inputs converge on its outermost layer, layer 1 (L1). We investigated this organization to examine how layer-specific MTL inputs modulate neocortical activity and memory formation. To this end, we first adapted a cortical- and hippocampal-dependent learning paradigm, in which animals were trained to associate direct cortical microstimulation and reward, and characterized learning behavior of rats and mice during this task. We next showed that neurons in the deep layers of the perirhinal cortex not only provide monosynaptic inputs to L1 of the primary somatosensory cortex (S1), where microstimulation was presented, but also actively reflect the behavioral outcome. Chemogenetic suppression of perirhinal inputs to L1 of S1 disrupted early memory formation but did not affect animals' performance after learning. The learning was followed by an emergence of a distinct subpopulation of layer 5 (L5) pyramidal neurons (~10%) characterized by high-frequency burst firing, which could be reduced by blocking perirhinal inputs to L1. Interestingly, similar proportion of apical dendrites (~10%) of L5 pyramidal neurons also displayed significantly enhanced calcium (Ca^{2+}) activity during memory retrieval in expert animals. Importantly, disrupting dendritic Ca^{2+} activity impaired learning, suggesting that apical dendrites of L5 pyramidal neurons have a critical role in neocortical memory formation. Taken together, these results suggest that MTL inputs control learning via a perirhinal-mediated gating process in L1, manifested by elevated dendritic Ca^{2+} activity and burst firing in L5 pyramidal neurons. The present study provides insights into cellular mechanisms of learning and memory representations in the neocortex.

Zusammenfassung

Es wird angenommen, dass deklarative Gedächtnisbildung auf Wechselwirkungen zwischen dem medialen Temporallappens (MTL) und dem Neokortex beruht. Die Untersuchung der zellulären Ziele und Mechanismen von Gedächtnisbildung im Neokortex wird erschwert durch die über den Kortex verteilte Struktur neokortikaler Netzwerke. Der in sechs Schichten gegliederte Neokortex von Säugetieren besitzt eine anatomische Organisation, in der Top-Down-Inputs inseiner äußersten Schicht, Schicht 1 (L1), konvergieren. Wir haben diese Organisation untersucht, um zu verstehen, wie schichtspezifische MTL-Inputs die neokortikale Aktivität und die Gedächtnisbildung modulieren. Zu diesem Zweck haben wir ein Kortex- und Hippocampus-abhängiges Lernparadigma angepasst, in dem Tiere darauf trainiert wurden, direkte kortikale Mikrostimulation und Belohnung zu assoziieren, und das Verhalten von Ratten und Mäusen während dieser Aufgabe charakterisiert. Als nächstes haben wir gezeigt, dass Neuronen in den tiefen Schichten des perirhinalen Kortex nicht nur monosynaptische Inputs in L1 des primären somato-sensorischen Kortex (S1) liefern, wo die Mikrostimulation eingebracht wurde, sondern auch aktiv den Verhaltensausgang der Mikrostimulation reflektieren. Die chemogenetische Unterdrückung der perirhinalen Inputs in L1 von S1 störte die anfängliche Gedächtnisbildung, hatte jedoch keinen Einfluss auf die Leistung der Tiere nach abgeschlossenem Lernen. Dem Lernen folgte das Auftreten einer klaren Subpopulation von Pyramidenneuronen der Schicht 5 (L5) (~10%), die durch hochfrequentes Burst-Feuern gekennzeichnet war und durch Blockieren der perirhinalen Inputs zu L1 reduziert werden konnte. Interessanterweise zeigte ein ähnlicher Anteil an apikalen Dendriten (~10%) von L5-Pyramidenneuronen ebenfalls eine signifikant erhöhte Calcium (Ca^{2+})-Aktivität während des Gedächtnisabrufs bei Expertentieren. Wichtig ist, dass die Störung der dendritischen Ca^{2+}-Aktivität das Lernen beeinträchtigte, was darauf hindeutet, dass apikale Dendriten von L5-Pyramidenneuronen eine entscheidende Rolle bei der Bildung des neokortikalen Gedächtnisses spielen. Zusammengenommen legen diese Ergebnisse nahe, dass MTL-Eingaben das Lernen über einen perirhinalen vermittelten Gating-Prozess in L1 steuern, der sich in einer erhöhten dendritischen Ca^{2+}-Aktivität und einem Burst-Firing in pyramidalen L5-Neuronen manifestiert. Die vorliegende Studie bietet Einblicke in zelluläre Lernmechanismen und Gedächtnisrepräsentationen im Neokortex.

Chapter 1. Introduction

The brain actively reconstructs the external world and generates internal models enabling the animal to make predictions, thereby adapt its behavior to maximize survival (Keller and Mrsic-Flogel, 2018). While phylogenetic internal models (e.g. innate behaviors) develop during evolution, ontogenetic accumulation of experiences during the organism's development can update existing models as well as generate new models about the current environment (Krubitzer and Kahn, 2003; Marler, 2004; Tierney, 1986). For example, encountering a predator at a certain location will update the animal's internal model of the environment so that the location is now associated with danger. Based on this model, the animal can predict the likelihood of meeting a predator at each location and will avoid the place associated with danger in the future. The ability to update internal models by experience (i.e. learning) and to store that information (i.e. memory) is one of the most remarkable properties of the brain, which can even last for the animal's entire lifetime. One of the fundamental goals of neuroscience is to understand the neuronal mechanisms of memory formation, storage and retention.

Lesion studies from animals and human patients have suggested brain regions associated with memory. In particular, Dr. Brenda Milner's studies with patient H.M. shed light on the current understanding of the role of the medial temporal lobe (MTL) structures (the hippocampus and parahippocampal region) on declarative memory (Milner, 2005; Scoville and Milner, 1957). Due to severe epilepsy, H.M had to undergo a lobotomy, in which most of the hippocampus and parts of its surrounding areas were bilaterally removed. After the surgery, although his epilepsy was alleviated, H.M. could no longer remember new events and information. On the contrary, his remote memory, for instance, his childhood memories, remained relatively intact. Altogether this case led to the idea that there are two complementary memory systems in the brain, in which the hippocampus and associated areas play a crucial role in recent memory whereas long-term memory is stored in the neocortex (Kumaran et al., 2016; McClelland et al., 1995, 2020).

While MTL regions have been subjected to extensive research on memory, less is known about how memory is processed and represented in the neocortex. Multimodal information entering the hippocampus is processed in a serial manner via the trisynaptic circuit (van Strien et al., 2009), where it is stripped from its original modality and

transformed into associational and contextual information (Buzsáki and Tingley, 2018). In contrast, hippocampal output is broadcast back to distributed neocortical networks (Hübener and Bonhoeffer, 2010; Josselyn et al., 2015), each consisting of repeated modules processing specific sensory modalities. This distributed nature of the neocortical system complicates the attempts to identify the exact loci of memory storage and challenged research into the cellular mechanisms of memory processing in the neocortex. Nevertheless, regardless of information modality they process, neocortical areas share a stereotypical organization, namely laminar or columnar organization where different cortical afferents target particular layers (Douglas and Martin, 2004; Mountcastle, 1997). By focusing on this organizational principle of the neocortex, this study aims to understand how top-down MTL inputs can modulate local circuits in the neocortex to mediate neocortical memory formation.

1.1 Complementary memory systems and their interactions

Large body of studies in animals and human patients showed that hippocampal lesions result in severe anterograde amnesia accompanied by temporally-graded retrograde amnesia (Lee et al., 2016; Ramos, 2013; Scoville & Milner, 1957; Winocur et al., 2001). These results emphasize the importance of the hippocampus in learning and memory but at the same time point out its time-limited role in memory storage. On the contrary, when the damage included neocortical areas, remote memory was often disrupted (Graham and Hodges, 1997; Wiltgen et al., 2004). These observations gave rise to one of the prevailing models of memory, the complementary memory systems model. This model posits that memory is initially formed in the MTL system and then gradually transferred to the neocortex for long-term storage (Alvarez and Squire, 1994; McClelland et al., 1995). But note that whether remote memory becomes completely independent of the hippocampus is still controversial (Clark et al., 2005; Metzler et al., 1991; Moscovitch and Nadel, 1997; Nadel et al., 2000; Teyler and DiScenna, 1986; Teyler and Rudy, 2007). According to the complementary memory systems model, the MTL system is actively engaged in the memory transfer by co-activating neocortical areas and strengthening the connectivity within the neocortical system (Squire and Alvarez, 1995).

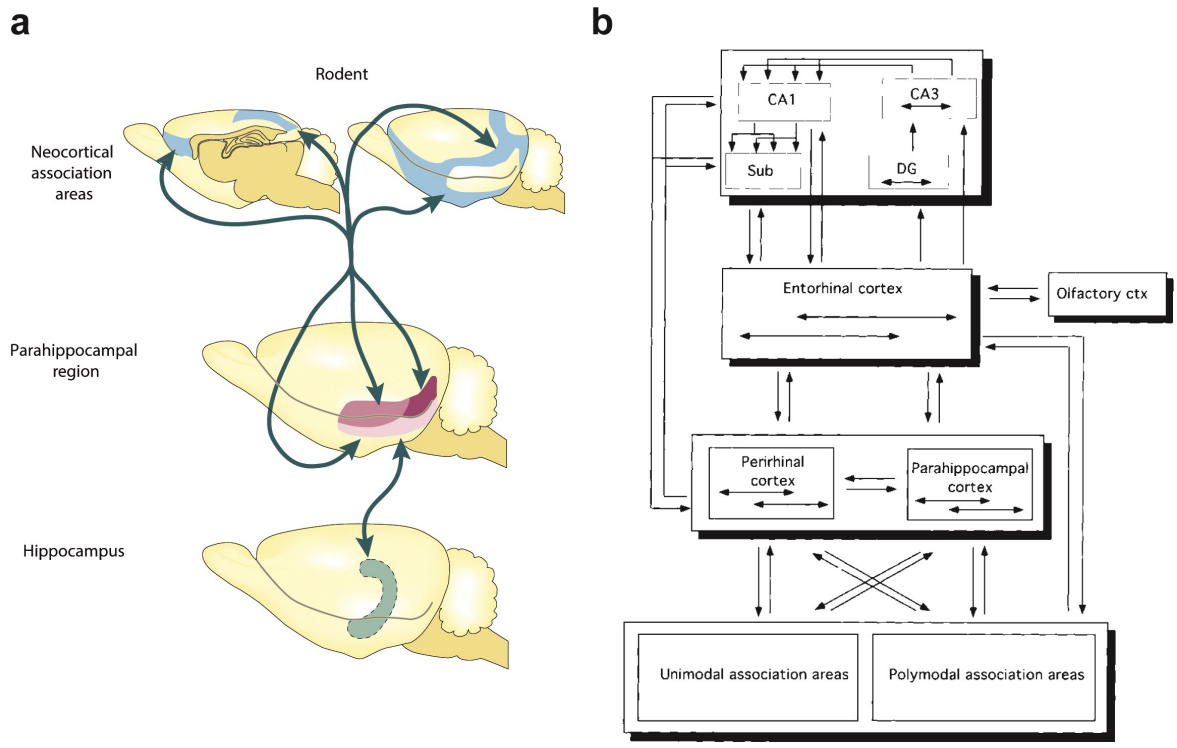

Figure 1.1. Connectivity between complementary memory systems. a) Neocortical areas (blue) receiving external sensory inputs project to the parahippocampal region, including the perirhinal cortex (purple), postrhinal cortex (dark purple) and entorhinal cortex (light purple). These areas provide the majority of inputs to the hippocampus (green). Hippocampal outputs return to the parahippocampal region that in turn projects back to the same neocortical areas that provide inputs to this region. **b)** Detailed connectivity map between brain areas constituting memory systems. The hippocampus and neocortex is connected via parahippocampal areas. Adapted with permission from Eichenbaum, 2000 (a), Lavenex & Amaral, 2000 (b).

The interaction between the MTL system and neocortex is bidirectional and reciprocal (Figure 1.1). Since the hippocampus does not have direct access to sensory information, this information has to be provided by the neocortex (Eichenbaum, 2000; Lavenex and Amaral, 2000). Sensory information is first processed in unimodal sensory areas and association areas, which provide inputs to the parahippocampal region. For example, the perirhinal cortex receives inputs from multiple sensory areas associated with gustatory, olfactory, somatosensory, auditory and visual processing (Agster & Burwell, 2009; Burwell, 2006; Burwell et al., 1995; Witter et al., 1989). The entorhinal cortex conveys this multimodal information to the hippocampus, where higher-order integration and abstraction can be made. The hippocampus, in turn, sends output to the parahippocampal region, which projects back to the same neocortical areas from which it receives inputs (Burwell, 2006; Burwell et al., 1995). Anatomical studies revealed that projections from the neocortex to the MTL system are feedforward type whereas MTL projections re-entering to

the neocortex are feedback type, supporting the notion of hierarchical organization of neocortical-hippocampal loop (Lavenex and Amaral, 2000).

Information flow between the neocortex and the hippocampus is dynamic and brain state-dependent. It has been suggested that memory encoding occurs predominantly during active state when information flow from neocortex to the hippocampus is high, whereas memory consolidation occurs mostly during immobile or sleep state when reactivation of previous experience happens (Buzsáki, 1989). A plethora of experimental evidence supports that coordinated activities in the hippocampus and neocortex could act as a network mechanism for memory consolidation. For instance, enhancing or disrupting a temporal coupling of hippocampal sharp-wave ripples (SWRs) and neocortical slow oscillations or spindles improve or impair memory, respectively (Latchoumane et al., 2017; Maingret et al., 2016). In addition, a recent study demonstrated that bidirectional information flow between the neocortex and the hippocampus occurs during SWRs (Rothschild et al., 2016).

Consistent with the complementary memory systems model, memory traces in the brain reorganize over time. The involvement of the hippocampus declines while the neocortical areas gradually increase their engagement in remote memory (Bontempi et al., 1999; Frankland and Bontempi, 2005; Kitamura et al., 2017; Maviel et al., 2004; Wiltgen et al., 2004). These neocortical areas with persistent memory representations include medial prefrontal cortex, temporal cortex and parietal areas such as retrosplenial cortex and posterior parietal cortex (Maviel et al., 2004). The reorganization of memory traces from the MTL memory system to neocortical memory system is termed systems memory consolidation (Alvarez and Squire, 1994; Dudai et al., 2015; Kumaran et al., 2016; Marr, 1971; McClelland et al., 1995; Moscovitch and Nadel, 1997; Winocur and Moscovitch, 2011). During systems memory consolidation, the hippocampus reactivates distributed memory representations in the neocortex and strengthens connections within the neocortical memory system (Takashima et al., 2009). This process does not only involve the stability of memories but also transforms the nature of the memory, including generalization, semanticization and abstraction (Winocur and Moscovitch, 2011).

1.2 Distributed memory networks in the neocortex

The neocortex is the most recently evolved structure in the brain and is often credited for the immense success of the mammalian kingdom (Rakic, 2009). It gives rise to higher-order cognitive capabilities spanning from perception, memory, prediction, planning and imagination (Lodato and Arlotta, 2015). The neocortex consists of different modules associated with particular sensory modalities and is organized in a hierarchical manner, where primary sensory cortices lies at the bottom and the higher-order association areas are situated at the top of the hierarchy (Felleman and Van Essen, 1991; Harris et al., 2019). Learning and memory function is often attributed to higher-order areas processing multimodal information (Eichenbaum, 2000; Frankland and Bontempi, 2005), such as the prefrontal cortex (Eichenbaum, 2017), retrosplenial cortex (Makino and Komiyama, 2015; Sousa et al., 2019), posterior parietal cortex (Brodt et al., 2018; Sestieri et al., 2017; Wilber et al., 2017) and anterior cingulate cortex (Frankland et al., 2004; Wartman et al., 2014).

The classical view of hierarchical organization of the neocortex often overlooked the role of primary sensory areas in this function (Weinberger, 2004). Nevertheless, accumulating evidence suggest that primary sensory cortices are also engaged in learning and memory (Ji and Wilson, 2007; Letzkus et al., 2011; Rothschild et al., 2016; Weinberger, 2004). For example, when auditory conditioned stimulus (CS) at a specific frequency is paired with an electric shock on an animal's foot, neurons in the primary auditory cortex (A1) increase responses specifically to the CS frequency (Abs et al., 2018; Bakin and Weinberger, 1990). These results could be extended to the primary somatosensory cortex (S1) and appetitive association learning where sensory cue was coupled with reward instead of a foot shock (Audette et al., 2019). Here the authors coupled whisker stimulation with water reward and found that synaptic strength between higher-order thalamocortical inputs from the posterior medial nucleus (POm) and S1 pyramidal neurons was enhanced after learning. Importantly, learning-induced plasticity is not transient but can last up to 8 weeks (Weinberger et al., 1993), suggesting that primary sensory cortices can support long-term storage of memory. Therefore, memory is not processed by a single brain area but rather represented in multiple brain areas across the neocortical hierarchy (Hübener and Bonhoeffer, 2010; Josselyn et al., 2015).

To understand how memory is processed in the neocortex, it is instructive to understand the cortical circuit organization. Unlike the three-layered archicortex and paleocortex that evolved earlier in evolution, the neocortex displays a stereotypical columnar organization with six distinctive layers, which form a functional unit of the neocortex (Hubel and Wiesel, 1959; Mountcastle, 1997). An interesting aspect of this columnar organization is that different streams of inputs tend to terminate in different layers (Douglas et al., 1995; Felleman and Van Essen, 1991; Harris et al., 2019). While periphery sensory information conveyed by thalamic relay nuclei predominantly target layer 4 (L4) and follow the canonical circuit (L4 -> L2/3 -> L5), long-range top-down inputs from other cortical and subcortical areas tend to terminate in superficial layers, particularly in the outermost layer of the neocortex, L1. In fact, around 90% of synaptic inputs in L1 originate from long-range projections, providing predictive and contextual information that can modulate sensory processing (Cauller, 1995; Cauller et al., 1998; D'Souza & Burkhalter, 2017; Markov et al., 2014; Rockland, 2019).

Recent studies suggest that laminar reorganization of neuronal activity takes place within the neocortical network as memory becomes remote. Using immediate early gene expression, Maviel and colleagues found that neuronal activation level shifts from infragranular layers to supragranular layers during retrieval of remote memory (Maviel et al., 2004). They concluded that the laminar reorganization reflects strengthening of cortico-cortical connections during memory consolidation. Thus, even within a cortical area, memory traces can exist in a diffused manner across cortical layers at different time points. Another recent study showed that top-down inputs from the retrosplenial cortex to L1 of the primary visual cortex (V1) increased activity while L4 responses reflecting bottom-up sensory inputs decreased following learning (Makino and Komiyama, 2015). Therefore, learning might enhance the relative impact of the internal model (top-down) compared to bottom-up sensory information. However, it remains to be determined whether this readjustment is mediated by MTL feedback inputs to the neocortex.

1.3 Dendritic spikes enable integration of top-down and bottom-up information at the cellular level

How do top-down inputs to L1 modulate neocortical neuronal activity? Unlike other cortical layers, L1 lacks cell bodies of excitatory neurons but contain local interneurons and dendrites of pyramidal neurons whose cell bodies are located in L2/3, L5 and L6 (D'Souza and Burkhalter, 2017; Schuman et al., 2019). Therefore, top-down inputs and bottom-up sensory inputs target different subcellular compartments. Specifically, long-range top-down inputs innervate the distal dendritic compartment of pyramidal neurons while bottom-up sensory inputs directly target the perisomatic compartment, in proximity to action potential initiation zone (Larkum, 2013; Larkum and Zhu, 2002). How electrically remote top-down inputs influence somatic action potential firing was a puzzling question until the discovery of dendritic spikes, which later have been shown to efficiently deliver distal inputs to soma and powerfully modulate firing patterns of a pyramidal neuron (Hausser et al., 2000; Stuart and Spruston, 2015).

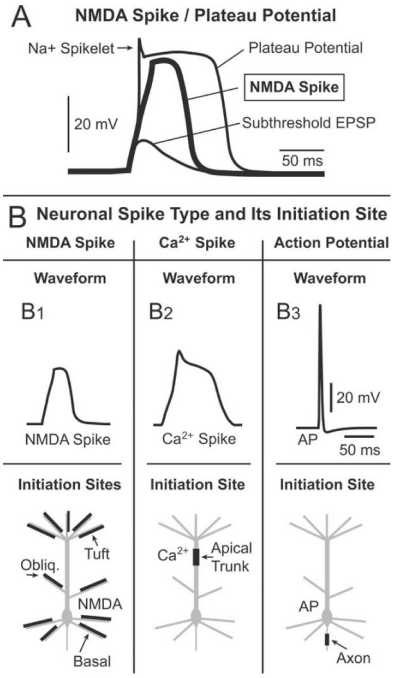

Figure 1.2. Different types of dendritc spikes and their initiation zones. NMDA spikes are initiated in thin dendrites including tuft and basal dendrites. Ca^{2+} spikes initiation zone is on the apical trunk. Action potentials are initiated in the axon initiation segment. Adapted with permission from Antic et al., 2010.

Mainly three types of dendritic spikes have been so far characterized (Figure 1.2). First, dendritic sodium (Na^+) spikes are mediated by voltage-gated Na^+ channels. They typically show narrow widths lower than 5 ms and can be initiated in both distal and basal dendrites. Synaptic inputs to these dendrites can generate dendritic Na^+ spikes (Kampa et al., 2004). Next, dendritic Ca^{2+} spikes, mediated by voltage-gated Ca^{2+} channels, exhibit broader waveform (>10 ms, up to 50 ms) and larger amplitude than Na^+ spikes. Because of the slow dynamics, Ca^{2+} spikes are often observed as plateau potentials. They can deliver bigger charges to the soma and axon, enabling distal inputs to strongly modulate the output of the pyramidal neuron (Larkum et al., 2004) by generating high-frequency bursts of action potentials (Larkum et al., 1999; Schwindt & Crill, 1999; Williams & Stuart, 1999). The Ca^{2+} spike initiation zone is located near

the apical tuft dendrites, making it easier for distal inputs to reach compared to action potential initiation zone (Larkum & Zhu, 2002). The last type of dendritic spike is N-methyl-D-aspartate (NMDA) spikes, mediated by NMDA receptors. NMDA spikes are generated in thin-dendrites such as distal and basal dendrites (Major et al., 2013). Glutamate uncaging study demonstrated that as low as 10 clustered inputs can evoke NMDA spikes as well as distributed inputs but along the same dendrite (Major et al., 2008). Unlike Ca^{2+} spikes, NMDA spikes rarely propagate to the soma, suggesting its role in local computation (Antic et al., 2010). However, multi-branch NMDA spikes can propagate to the Ca^{2+} spike initiation zone and generate Ca^{2+} spikes, which can strongly drive the cells to fire (Grienberger et al., 2014; Palmer et al., 2014).

Somatic action potentials can influence the generation of dendritic spikes as well. Somatically generated action potentials can propagate back to dendrites (Stuart and Sakmann, 1994) and reduce the threshold for Ca^{2+} spike generation, which in turn propagate to the soma to induce high-frequency burst firing in L5 pyramidal neurons (Larkum et al., 1999; Figure 1.3). Therefore, active dendritic mechanisms ensure top-down distal inputs to propagate to the soma, where these inputs can significantly modulate the output of the cell.

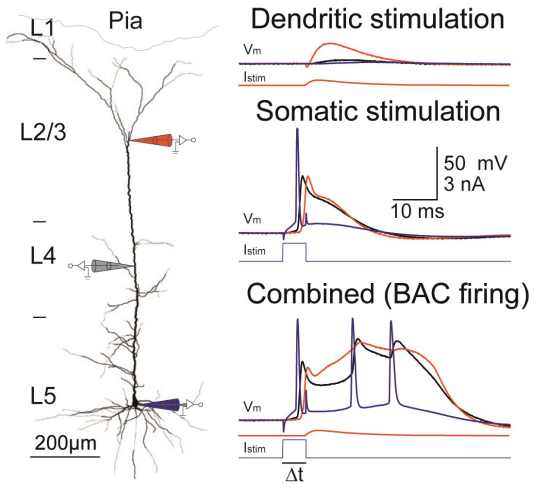

Figure 1.3. Backpropagation-activated Ca^{2+} spike firing. Simultaneous recording of the dendrite and soma from a single layer 5 pyramidal neuron. Subthrehsold dendritic stimulation has almost no effect on somatic membrane potential. Suprthreshold somatic stimulation can generate an action potential that can propagate to the dendrite. The same stimulations in the soma and dendrite generates dendritic Ca^{2+} spikes and triggers burst firing in the soma when given simultaneously. Adapted with permission from Larkum et al., 1999.

Growing evidence from *in vivo* studies suggests that dendritic spikes of L5 pyramidal neurons are implicated with cognitive functions such as sensory perception and sensorimotor processing. First, sensory stimulation has been shown to induce dendritic spikes in both awake and anesthetized rats (Murayama and Larkum, 2009; Murayama et al., 2009). In addition, during active whisker sensing, dendritic spikes in L5 pyramidal neurons integrate sensory and motor information (Xu et al., 2012), and represent sensorimotor signals in a nonlinearly mixed network of L5 pyramidal neurons, which enable adaptive sensing (Ranganathan et al., 2018). Finally, recent studies showed

that disturbing apical dendritic Ca^{2+} activity of L5 pyramidal neurons shifted the perceptual threshold, establishing a causal relationship between dendritic Ca^{2+} activity and sensory perception (Takahashi et al., 2016; Takahashi et al., 2020). In summary, the active dendritic mechanism enables the association of top-down and bottom-up information arriving at different subcellular compartments, enhancing the computational power of cortical pyramidal neurons during cognitive processes. Hoewever, it is still unclear whether this mechanism also contributes to memory formation that involves the integration of sensory information and contextual information.

1.4 Aims of the study

While circuit and cellular mechanisms of memory are extensively studied within the MTL system, the cellular mechanism of memory transfer from the MTL system to the neocortical system is less clear. Most of the studies on cortical-hippocampal interactions focused on prefrontal cortex or medial entorhinal cortex, which are directly connected with the hippocampus (Chrobak and Buzsáki, 1996; Eichenbaum, 2017; Frankland and Bontempi, 2005; Isomura et al., 2006; Peyrache et al., 2009; Rajasethupathy et al., 2015). The present study aims to understand how MTL areas interact with primary sensory cortices that are not directly connected with the hippocampus during declarative memory formation. Based on the cytoarchitecture of the neocortex, we hypothesize that feedback inputs from the MTL mediate memory formation in the neocortex by strengthening top-down cortico-cortical connections in neocortical L1. In order to test our hypothesis,

1) We adapted the microstimulation detection task as a learning paradigm, which allows us to identify a neocortical area to investigate during memory formation.
2) Using anatomical tracings, we sought to identify an MTL structure that provides a direct feedback input to L1 of S1.
3) By interfering this input, we sought to establish a causal relationship between L1-specific MTL input and memory formation.
4) We examined how MTL inputs to L1 regulate learning-induced activity changes in neocortical L5 pyramidal neurons.
5) Finally, we explored the role of dendritic Ca^{2+} activity on memory formation.

Chapter 2. Methods

Animals. All experiments and procedures were approved and conducted in accordance with the guidelines given by Landesamt für Gesundheit und Soziales Berlin. The following animal lines were used in this study: C57BL/6J wild-type mice, Gpr26-cre transgenic mice (Oram et al., 2015; Zolnik et al., 2020), SST::channelrhodopsin2 (ChR2) transgenic mice (SST-IRES-Cre mice (JAX stock #018973) crossed with Ai32 mice (JAX stock #024109) (Madisen et al., 2012), Rbp4-cre transgenic mice (MMRRC #031125-UCD)(Gerfen et al., 2013) and Wistar rats (Charles River). Male animals were used except for two female Rbp4-cre mice for two-photon dendritic imaging. The animals were housed in reversed 12 h light/dark cycle (light on between 21:00 and 09:00) and all the behavioral experiments were performed during dark period of the cycle.

Anasthesia. For surgical procedures, animals were anesthetized under ketamine/xylazine (65 mg kg^{-1}/10 mg kg^{-1} for mice, 100 mg kg^{-1}/ 5 mg kg^{-1} for rats, Intraperitoneal injection). Depth of anesthesia was assessed by firm toe pinch. When toe pinch reflex was no longer induced, animals were head-fixed to a stereotaxic frame with an ear bar. Animals were kept on a thermal blanket during entire surgery and recovery. Rest of the procedures followed the same anesthesia unless otherwise mentioned.

Headpost implant and craniotomy. A light-weight custom made aluminum headpost (mouse) or a metal bolt (rat) was implanted on the skull of the animal under anesthesia. For mice used in chemogenetic experiments, the implantation was performed at least 10 days after viral injection. After the scalp and periosteum were removed, the skull was disinfected with 70% ethanol. A thin layer of light curing dental adhesives (OptiBond, Kerr&Charisma; Heraeus Kulzer) was applied to the dry skull. A head-post was fixed on the skull on the left hemisphere with a dental cement (Paladur, Heraeus Kulzer).

Two or three days before the microstimulation training or/and juxtacellular recording, craniotomy was performed under the anesthesia. 1.5 mm x 1.5 mm cranial window was made above the right S1 centered at Anterioposterior axis (AP) -1.25 mm and mediolateral axis (ML) +3.25 mm from bregma for mice and 2 mm x 2 mm craniotomy centered at AP -2.5 mm and ML +5.5 mm from bregma was made for rats. For juxtacellular

recordings in the rat perirhinal cortex, 2 mm x 2 mm craniotomy was made on AP -4.5 mm and ML 5.0 mm from bregma. Then a recording chamber was implanted above the cranial window for chronic access to this region. The dura was left intact and the craniotomy was covered with silicon (Kwik-Cast; World Precision Instruments).

Habituation. Head-restraint habituation began at least three days after the head-post implantation. Habituation duration at the first day was 5 min and then gradually increased for 5 days until the animal sat calmly for 1 h. Animals were water restricted from the second day (1 ml/day) of the habituation and then trained to receive the saccharin (Sigma-Aldrich) water (0.5% for mice and 0.1% for rats) from the licking port from the fourth day of the habituation. Licking was monitored using a piezo-based sensor attached to the licking port. Weight and health of the animal were monitored daily.

Microstimulation detection task. After head-restraint and licking habituation, training for microstimulation detection task started (Doron et al., 2014; Houweling and Brecht, 2008; Voigt et al., 2008). Animals were water deprived with daily access to 1 ml water at least 48 hours prior to the onset of the training. A 200 ms of current pulses was applied to L5 (700 µm (mouse) or 1500 µm (rat) from pia) of S1 through a tungsten microelectrode (Microprobes). The microstimulation pulse consisted of 40 cathodal pulses at 200Hz with 0.3 ms pulse duration. Inter-trial interval (ITI) was randomly distributed by Poisson delay with time constant 3 s. Licks within the ITI was mildly punished by an additional 1.5 s delay to the next stimulus presentation.

In the first session, initial high intensity pulses (160 µA for all mice; median 155 µA ranging from 70-200 µA for rats) was coupled with a drop of water reward (pairing period). After five pairing trials, testing period began where animals were rewarded only if they licked the licking port within 100 to 1,200 ms (response window) after stimulus onset. Tongue lick responses were detected with piezo-based sensor (mouse) or beam breaker (rat). The time of the first lick after the stimulus onset was taken as reaction time. Trials with reaction time between 0.1 s to 1.2 s from the stimulus onset were counted as hits and trials with no lick or reaction time longer than 1.2 s were counted as misses. When animals licked prematurely within 0.1 s from stimulus onset, that trial was aborted. Once animals reached 80% hit rate, pulse intensity was gradually decreased during and across the sessions until it

reached the target intensity of 10 μA (mouse) or 5 μA (rat). The number of total trials were not fixed per session but a session was terminated either when animals stopped licking to free water presentation or when they reached the intensity threshold, which was defined as the lowest intensity with hit rate ≥80%. Control animals reached to the target intensity within 3-5 days (median 3 days) of training. Expert animals were defined as animals that performed the task with ≥80% hit rate at the target intensity. Untrained animals received microstimulation at the target intensity (10 μA for mice and 5 μA for rats) without any pairing trial.

Behavioral quantification. The performance of the animals during microstimulation detection task was quantified by computing cumulative difference of the number of hit trials and the number of miss trials. We define the cumulative value at the last trials as learning score (i.e. number of total hit trials – number of total miss trials). Since the learning score compares the number of hit trials and the number of miss trials, it is dependent on the total number of trials. Note that the total number of trials per session was not fixed and dependent on subject's behavior during the session. To compensate for the various total number of trials across animals, we normalized the learning score with the total number of trials, resulting in a value ranging from -1 to 1. Negative value indicates higher proportion of miss trials than hit trials while positive value indicates that hit trials number was higher compared to miss trials number.

Pharmacology. To inhibit neuronal activity in the hippocampus and perirhinal cortex, a glass pippete was filled with lidocaine (AlleMan Pharma; 1%, wt/vol) and inserted into the ipsilateral hippocampus or perirhinal cortex based on stereotaxic coordinates (Franklin and Paxinos, 2001; Paxinos and Watson, 1998). The drug (150 nl) was injected by a gentle pressure at least 20 min before the training onset. To generate epileptic mouse model (Häussler et al., 2012; Riban et al., 2002), kainate (50 nL, 20 mM) was injected into the hippocampus (AP: -2 mm, ML: -1.4 mm, dorsoventral axis (DV): -1.8 mm). To inhibit Ca^{2+} spikes in apical dendrites, 100 μM baclofen was injected 3 min prior to the training at a depth of 150 μm in S1. Injections (150 nl each) was made every 20 min throughout the training.

Chemogenetic manipulation of perirhinal axonal activity. Mice (>4 weeks) were anesthetized and lidocaine was injected around the surgical site before the scalp incision. The periosteum was removed and small craniotomy was made on the injection sites. Injection coordinates for the perirhinal cortex were AP -1.8 mm, ML ± 4.2 mm, DV -4.2 mm and for POm were AP -2 mm, ML +1.2 mm, DV -3.0 mm from bregma. AAV1/2-hSyn1-hM4D(Gi)-mCherry-WPRE-hGHp(A) (Viral Vector Facility of the University of Zurich) was injected bilaterally except for n=2 mice injected to the right perhinal cortex (0.15–0.20 µl per side). The training for microstimulation detection task started at least after 3 weeks of expression.

In order to activate hM4Di receptor, Clozapine-N-Oxide (CNO; Tocris Bioscience) dissolved in extracellular solution (final concentration 10 µM) was back-loaded in a glass pipette and applied into L1 (150 µm) of S1 by gentle pressure at least 20 min before the microstimulation training. CNO was applied into two adjacent sites (150 µl each) of the craniotomy to maximize the CNO diffusion area.

Estimation of chemogenetic effect on cortical layers. First to quantify the spread of CNO across cortical layers, 0.5% Chicago Sky Blue 6B (CB; Sigma-Aldrich) diluted in ringer solution was back loaded in a glass pipette and applied with gentle pressure in L1 (150 µm) of S1, where CNO was applied. Then mice were sacrificed and the brain was extracted before post-incubation in 4% paraformaldehyde (PFA) for at least 24 hours. Coronal brain sections were made using a vibratome (Leica VT1000S, Leica Biosystems) and mounted on slide glasses with DAPI-containing mounting medium (ROTI Mount FluorCare DAPI; Carl Roth). Then brain sections were imaged under an epifluorescence microscope (Leica DMI4000 B; Leica Biosystems).

Fluorescence intensity was quantified with ImageJ software by plotting a line profile across the cortical layers with a bin size of 2.594 µm. The average gray value of each images was then normalized by subtracting the minimum intensity of each section and dividing with maximum intensity of each section. Average intensity of CB was convolved with the average intensity of Enhanced Yellow Fluorescent Protein (EYFP) in perirhinal axons in S1 measured from anterograde tracing to calculate the estimated effect of chemogenetic manipulation as a function of cortical depths. Then layer boundaries were marked based on Lefort et al., 2009.

Quantification of DREADD expression. hM4Di-mCherry fluorescence intensity was quantified with ImageJ software by plotting a line profile, across 1000 µm above and below the rhinal fissure with a bin size of 2.594 µm. The average gray value of each image was then normalized by subtracting minimum intensity of each section and dividing by the intensity at the rhinal fissure of each section. The boundaries of the perirhinal cortex was defined as 250 µm above and 750 µm below the rhinal fissure based on stereotaxic coordinates (Franklin and Paxinos, 2001). Expression rate was calculated by measuring area under the curve within the perirhinal cortex or outside the perirhinal cortex divided by the total area under the curve.

Optogenetic manipulations. For optogenetic activation of Somatostatin (SST)-expressing neurons, SST::ChR2 transgenic mice expressing ChR2 in SST+ cells were used. ChR-expressing SST+ neurons were photostimulated by a 465 nm LED light (Doric Lenses Inc.) at the total power of 2 mW delivered via an optic fiber placed above the craniotomy. A 500-ms continuous light pulse started at 300 ms before the microstimulation onset during all trials. To prevent light leakage from photostimulation into the animals' eyes, the recording chamber was covered with a black rubber.

Retrograde tracing and analysis. Wistar ats and C57BL/6J mice (>2 weeks old) were anesthetized under ketamine/xylazine before head-fixed at the stereotaxic frame. After incision of the scalp, skull was cleaned with 70% ethanol and a craniotomy over S1 (Mice: 1 mm x 1 mm, centered at AP -1 mm, ML +3.25 mm; rats: 2 mm x 2 mm, centered at AP -2.5 mm, +ML 5.5 mm) was made on the basis of stereotaxic coordinates. Retrograde tracer, Fast Blue (Polysciences; 1% in dH2O), was soaked in a sterile piece of tissue and then applied onto the surface of S1 for 5 min for mice and 10 min for rats. Seven days later, animals were perfused transcardially with phosphate-buffered saline followed by 4% PFA (Carl Roth) and the brain was extracted. 100 µm-(mouse) or 150 µm-(rat) thick coronal brain sections were made using a vibratome (Leica VT1000S; Leica Biosystems) and mounted on slide glasses with synthetic mounting medium (ROTI Mount; Carl Roth). Fast Blue labelled cells in the perirhinal cortex were detected manually under an epifluorescence microscope (Leica DMI4000 B; Leica Biosystems). These areas were identified based on stereotaxic coordinates

(Franklin and Paxinos, 2001; Paxinos and Watson, 1998). The number of counted cells in each coronal section was normalized by the total number of counted cells per brain.

Anterograde tracing and analysis. For anterograde tracing and optogenetic ex-vivo experiments AAV1.hSyn.hChR2(H134R)-EYFP.WPRE.hGH (Penn Vector Core) was injected in the perirhinal cortex of >2 weeks old C57BL/6J mice and Wistar rats. Anesthesia was induced and maintained with isoflurane at 5% and 2%, respectively for mice. Rats were under anesthesia with ketamine/xylazine. Animals were kept on a thermal blanket during entire surgery and recovery. Animals were placed in a stereotaxic frame and craniotomies were performed based on stereotaxic coordinates: AP -1.8 mm, ML ± 4.1 mm, DV -4.2 mm from bregma for mice / AP -3.8 mm, ML ± 6.0 mm, DV -7.0 mm from bregma for rats. Injections were carried out using graduated pipettes broken back to a tip diameter of 10-15 µm, at a rate of ~25 nl/min for a total volume of 50-70 nl (mouse) or 100 nl (rat). Incubation time was at least 3 weeks before transcradial perfusion or ex-vivo experiment.

AAV1.hSyn.hChR2(H134R)-EYFP.WPRE.hGH containing acute brain sections were imaged using an Olympus BX51 Microscope with a 4x objective. Fluorescence intensity was quantified with ImageJ software by plotting a line profile across the cortical layers that calculates the brightness value. The average gray value of each images was normalized by subtracting the minimum intensity of each section (baseline) and dividing by the maximum intensity of each section.

***Ex-vivo* electrophysiology.** After 3-4 weeks of virus expression, sagittal or coronal slices (300 µm thick) were prepared from 35-50 day old C57BL/6J mice. Whole-cell patch-clamp recordings were performed from visually identified layer5 pyramidal neurons and layer1 interneurons using infrared Dodt-gradient contrast video microscopy. The extracellular solution contained 125 mM NaCl, 25 mM $NaHCO_3$, 25 mM Glucose, 3 mM KCl, 1.25 mM NaH_2PO_4, 2 mM $CaCl_2$, 1 mM $MgCl_2$, pH 7.4 at ~33 °C. The intracellular solution contained 115 mM K^+-gluconate, 20 mM KCl, 2 mM Mg-ATP, 2 mM Na_2-ATP, 10 mM Na_2-phosphocreatine, 0.3 mM GTP, 10 mM HEPES, 0.05 mM Alexa 594 and biocytin (0.2%), pH 7.2. Whole-cell voltage recordings were performed from the soma (4-6 MΩ) using a Multiclamp 700b (Molecular devices) amplifier. Data was acquired with an ITC-18 board (InstruTech) and analyzed using Igor software (WaveMetrics). Optogenetic synaptic

stimulation was performed via a 470 nm LED (2 ms pulses) located in L1 around the tuft dendrite. To activate hM4Di receptor, CNO was applied in the bath solution (final concentration 10 μM).

In vivo **juxtacellular recording and analysis.** Following head-restraint habituation, juxtacellular recordings were performed from deep layer neurons from S1 and the perirhinal cortex in awake head-fixed animals during microstimulation detection task. For experiments during learning, control mice that do not express hM4Di receptors were also treated with CNO in L1 of S1 in order to exclude the indirect effect of CNO on neuronal activity (Gomez et al., 2017). The glass pipette (4–8 MΩ) for juxtacellular recording during microstimulation detection task was filled with extracellular solution containing: 135 mM NaCl, 5.4 mM KCl, 1.0 mM $MgCl_2$, 1.8 mM $CaCl_2$ and 5 mM HEPES (pH 7.2). The juxtacellular signal was amplified and low-pass filtered at 3 kHz by a patch-clamp amplifier (NPI) and sampled at 25 kHz by a Power1401 data acquisition interface (CED) under the control of Spike2 software (CED). The mean depth of juxtacellular recordings in S1 are following: S1 in mice: 1145.0±19.15 μm, S1 in rats: 1462±25.41 μm, which is likely an overestimate of the true depth due to oblique penetrations and dimpling. For perirhinal recording in rats, the pipette was inserted with 17° toward lateral and 50° toward anterior to avoid potential damage to S1. Mean of the diagonal distance from the pia for perirhinal recordings in rats was 6339.64 ±122.07 μm.

Recorded neurons were separated into putative fast-spiking interneurons and regular-spiking pyramidal neurons based on spike half-width and firing rate. Cells with spike half-width lower than 0.5 ms and firing rate higher than 8 Hz were classified to fast-spiking neurons. Only regular-spiking neurons were used for further analysis.

All the cells and trials recorded over days were pooled together for comparing activity (firing rate or burst rate) changes during microstimulation trials. Bursts were identified as at least two spikes with an inter-spike interval of ≤15 ms (66.7 Hz). Burst rates were calculated by dividing the number of total burst events with total recording time (event/s). Time window between 1 and 0 s before the stimulus ([-1 0] s) was used to calculate the baseline activity and 0.2 – 2.5 s ([+0.2 +2.5] s) after the stimulus was used to calculate post-stimulus activity. Spikes could not be detected during the stimulation period ([0 0.2] s) due to electric artifacts. For firing rate and burst rate change analysis in perirhinal

recordings, the difference between pre-stimulus frequency and post-stimulus frequency was divided by average pre-stimulus frequency.

For z-score normalization, peri-stimulus time histograms (PSTHs) were computed for each cell with a bin size of 50 ms and the stationary rate and standard deviation were computed based on the PSTHs in the period [-1,0] s. Z-score of cells with no spikes during [-1, 0] s period could not be computed and not shown. Z-score of burst rate was computed in the same manner but using PSTHs based on burst rate instead of firing rate. PSTHs in period [0.2 – 2.5] s were used to define significantly modulated cells during learning. For multiple comparisons, p-values of 0.05 were corrected by Bonferroni method and converted to z-score (z=3.267 for 46 bins in period of [0.2 – 2.5] s). Bins with z-score higher than bonferroni corrected z-score were considered as significantly modulated bins. Cells with at least one significantly modulated bin were defined as modulated cells. For burst rate, cells having spikes in period [-1 0] s but no bursts were classified as non-modulated cells.

For the classification of L5 neurons in expert animals, PSTHs were calculated for each cell by averaging spikes in time bins of 100 ms for times within 2 seconds before and after microstimulation during hit-trials only. For each cell, the stationary rate and standard deviation were computed based on the PSTHs in the period [-2,0] s. Cells were classified as ON cell or OFF cell if PSTHs in the period [0.3,0.4] s was either more than 3*standard deviations (SDs) above the stationary rate, or less than 3*SD below it, respectively. Other cells were classified as NR cells.

Two-photon Ca^{2+} imaging and analysis. For dendritic Ca^{2+} imaging, AAV2/1-Syn-Flex-GCaMP6s-WPRE.SV40 (Addgene) was injected (100 nl) through a glass pipette (tip diameter, 5–10 μm) into the left S1 of adult Rbp4-Cre mice on the basis of stereotaxic coordinates (AP -1.5 mm and ML 3.2 mm from bregma). Injection depth was at 700 μm deep from the pial surface. After three weeks, a 3-mm craniotomy was made over the injection site and sealed with a 3-mm glass coverslip with cyanoacrylate glue. A light-weight head-post was implanted on the skull of the right hemisphere with light-curing adhesives and a dental cement. Habituation of mice to head fixation and following imaging experiment began 4 weeks after the virus injection.

Two-photon dendritic Ca^{2+} imaging during the microstimulation detection task was performed with a resonant-scanning two-photon microscope (Thorlabs) equipped with

GaAsP photomultiplier tubes (Hamamatsu Photonics). Ti:Sapphire laser (Mai Tai eHP Deep See; Spectra-Physics) was used to excite GCaMP6s at 940 nm (typically 30–40 mW at the sample) and signal was imaged through a 16×, 0.8 NA water immersion objective (Nikon). Full-frame images (256 pixels × 256 pixels, 175 μm × 175 μm) were acquired from apical dendrites of Rbp4+ L5 pyramidal neurons expressing GCaMP6s using ScanImage 4.1 software (Vidrio Technologies). Mean imaging depth was 154±2.1 and sampling frequency was at 58.6 Hz. Tungsten electrodes for microstimulation were inserted through the access port on the chronic glass window.

For axonal calcium imaging, AAV2/1-Syn-GCaMP6s-WPRE (Addgene) was injected into the bilateral perirhinal cortex of adult C57BL/6J mice on the basis of stereotaxic coordinates (AP -1.8 mm, ML ±4.2 mm and DV -4.2 mm from bregma). Three weeks after the injection, a 3-mm chronic glass window was implanted over the left S1. Images (512 pixels × 512 pixels, 133 μm × 133 μm) were acquired from GCaMP6s-expressing axonal fibers in L1 of S1 (at a depth of 30 μm) at sampling frequency 30.3 Hz. For each mouse, imaging was performed in the same field of view with the same laser power throughout the experimental period.

All analysis for Ca^{2+} imaging was performed using custom-written scripts in MATLAB (MathWorks). First, whole-frame cross-correlation was used to correct horizontal and vertical drifts of imaging frames due to animal motion, by registering each frame to a reference image. The reference image was generated by averaging any given consecutive 100 frames in which motion drifts were minimal. Next, based on average intensity and standard deviation projections across movie frames, regions of interest (ROIs) for apical dendrites of L5 neurons were manually selected. Time series of Ca^{2+} fluorescence was obtained by averaging pixel values inside of each ROI. Then neuropil contamination was corrected by subtracting the local, peri-dendritic neuropil signals. For axonal imaging, axonal Ca^{2+} signals were extracted from field ROIs (~100 μm × 100 μm). Fluorescence change (ΔF/F0) was calculated as $(F - F0)/F0$, where F0 was the baseline fluorescence value in the ROI throughout the whole imaging session.

For the classification of dendrites, PSTHs were calculated for each dendrite by averaging Ca^{2+} responses during hit trials. For each dendrite, the baseline fluctuation, i.e., SD, was computed from the PSTH in the period [-1,0] s. Dendrites were classified to ON dendrites or OFF dendrites if the PSTHs in the period [0, 2] s was either more than 3*SD

above the baseline, or less than 3*SD below, respectively. Other dendrites were classified as NR dendrites.

Statistics. All statistics were performed using MATLAB. Unless otherwise stated, all values are indicated as mean±standard error of the mean (s.e.m.). Statistical significance was determined using Wilcoxon signed-rank test within group and Wilcoxon rank-sum test between groups at a significance level of 0.05. For comparing proportions, chi-square test was performed. For non-parametric multiple comparisons, Kruskal-Wallis test was followed by post-hoc Dunn-Sidàk test. No statistical tests were run to predetermine the sample size and blinding and randomization were not performed.

Chapter 3. Results

3.1 Adapting microstimulation detection task as a learning paradigm

3.1.1 Assessing learning in rats and mice during the microstimulation detection task

In order to investigate the influence of the MTL inputs on the neocortex during learning, we first sought to devise a learning paradigm that allows us to precisely identify the cortical area to investigate. An attractive behavioral task that can offer these possibilities is the microstimulation detection task, which involves behavioral report of direct cortical stimulation (Doron et al., 2014; Houweling and Brecht, 2008). Here, whisker stimulus is replaced by a small intracortical current injection to the barrel area of S1 and animals receive water reward upon a successful report of the stimulation (Figure 3.1a). Direct current injection into the sensory cortex enables to define the area of interest and the temporal window precisely, where and when the underlying neuronal mechanisms of memory formation can be examined. We examined if this task is optimal for neurophysiological investigation of memory formation in primary sensory cortices by characterizing the learning behavior of two rodent species.

We trained rats and mice to associate short (200 ms) direct electrical pulses in the S1 with sweetened water reward. Stimulation electrode was placed in L5 (Figure 3.1a), where microstimulation detection threshold is the lowest (Houweling & Brecht, 2008 and personal communication with the authors). The first training session consisted of pairing period and testing period (Figure 3.1b). First, the animals received a pairing block (5 repetitions) of microstimulation followed by a water reward regardless of their licking responses (pairing period; see Methods). Following a block of pairing trials, we tested learning by making the reward available only if the animal actively licked within a response window of 100 – 1200 ms following microstimulation onset (testing period). Premature licking between 0 – 100 ms abolished the trial (aborted) and licking outside of the response window was not rewarded (miss). After a block of testing trials, hit rate was calculated as the total number of hit trials divided by the total number of trials, and another pairing block was given when the hit rate was lower than 80%, defined as target hit rate. Testing period continued at ever decreasing

intensity whenever block hit rates reached the target hit rate. When the subjects failed to reach the target rate, intensity was increased back to that of the previous block.

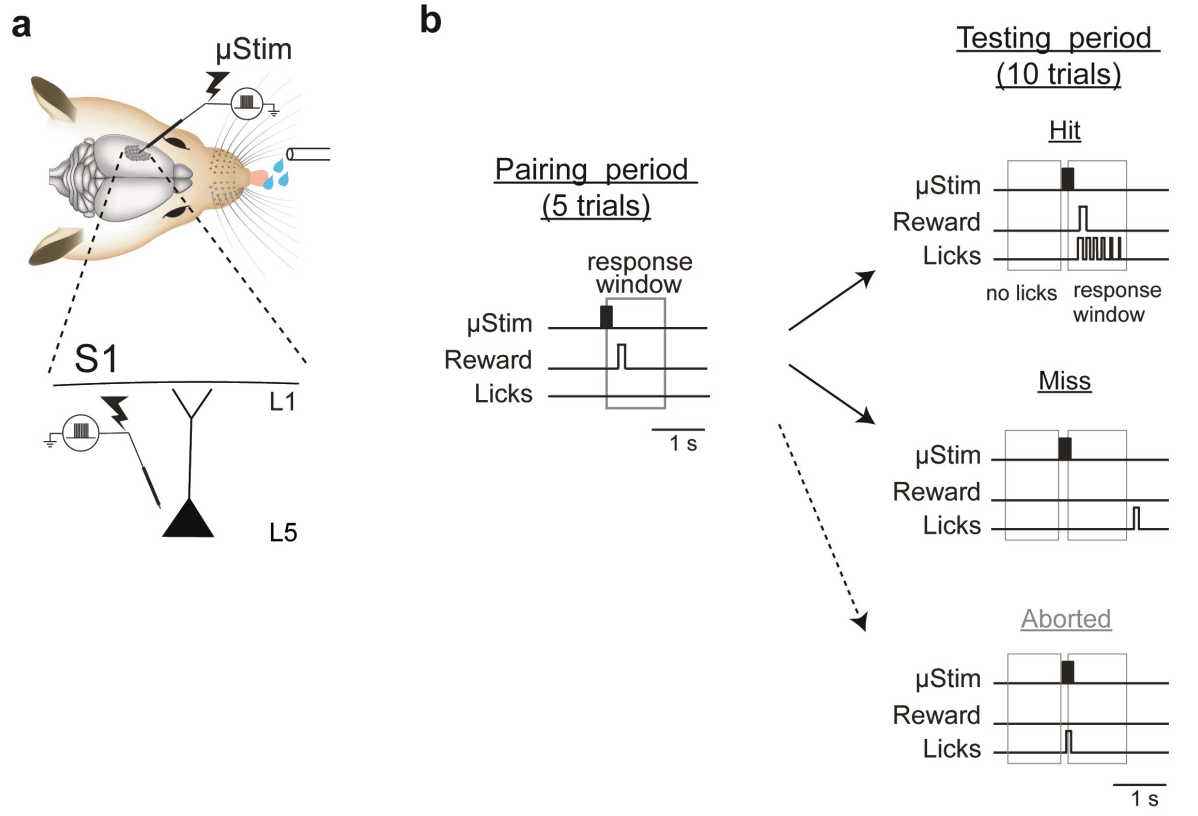

Figure 3.1. Behavioral paradigm. a) Schematic of the microstimulation (µStim) detection task. Rodents were trained to associate µStim and water reward provided from a licking port. Inset, a magnified view in S1 showing a tungsten electrode placed in L5. **b)** Training protocol. The training session consists of a pairing period and testing period. After 5 pairing trials, animals had to lick within the response window upon microstimulation to receive water reward. Premature licking (<0.1 s from µStim onset) aborted the trial.

Previous studies trained rats to behaviorally report microstimulation (Doron et al., 2014; Houweling et al., 2010) but this has rarely performed in mice. While the lareger size of the rat brain is more accessible for surgical procedures necessary for complex eletrophysiological techniques, mice allows genetic manipulations with a wide range of knock-out and transgenic lines, which is less available in rats (Ellenbroek and Youn, 2016). It is, therefore, valuable to establish a behavioral paradigm that can be used in the two most popular model species in neuroscience. Here we trained rats and mice to microstimulation detection task and compared their learning behaviors. Both rodent species learned to associate microstimulation and reward rapidly, as observed by their reliable licking responses within a short time window after microstimulation onset during the first session (Figure 3.2a-d). We quantified their performance in several different ways. First, the number

of pairing blocks was used to estimate the speed of the stimulus-reward association (Figure 3.2e). Since more pairing blocks were presented to animals with low performance (hit rate ≤80%) during testing period, a smaller number of pairing blocks indicates faster association ability. Most rats (n=21/24 rats) required one or two pairing blocks while a few of them needed more than two pairing blocks (n=3/24 rats). Similarly, mice required less than three pairing blocks (except for one outlier mouse that required eight pairing blocks), suggesting that this task is a fast-learning paradigm for both species (median number of pairing blocks: rats 1 block, n=24 vs. mice 1 block, n=20, Wilcoxon rank-sum test, p=0.8). Second, we computed the average hit rates, which were calculated for each block (group of trials at the same intensity), to estimate the overall performance of each animal (Figure 3.2c-d,f). Both rats and mice showed average hit rates around 70% after one training session (rats 73.2±1.9 % vs. mice 75.7±4.1%, Wilcoxon rank-sum test, p=0.1). Animals licked shortly after microstimulation, resulting in an average reaction time during hit trials around 0.3 to 0.4 ms (Figure 3.2g, rats 0.3±0.01 s vs. mice 0.4±0.02 s, Wilcoxon rank-sum test, p=0.2). This is markedly shorter than the maximum limit of the response window (1.2 s after microstimulation onset).

We gradually reduced stimulation intensity if the animals performed well (hit rate ≥80%) at a given intensity. In addition to stimulus-reward association, the ability to report decreasing current intensity was also estimated during the microstimulation detection task. Indeed, both rats and mice were able to reduce microstimulation intensity gradually over blocks and reached an intensity threshold at the end of the session (Figure 3.2c-d). We defined intensity threshold as the lowest intensity with the hit rate ≥80% reached in a session. We compared the intensity improvement by computing the relative difference between the initial intensity and intensity threshold ((initial intensity – intensity threshold)/initial intensity). On average, rats were able to behaviorally report the weak stimulation that is by 80% lower than the initial intensity after one session while mice reached on average around 60% reduction relative to the initial intensity (Figure 3.2h; rats 82.3±2.92% vs. mice 54.7±4.7%, Wilcoxon rank-sum test, p<0.001). This suggests that rats were better in adapting to decreasing intensity than mice.

We also quantified spontaneous licking behaviors of rats and mice. Overall, we found that mice were more impulsive than rats, observed by higher overall licking rate compared to rats (Figure 3.2i; rats 1.2±0.06 Hz vs. mice 8.8±1.3 Hz, Wilcoxon rank-sum test, p<0.001).

In addition, their licking pattern was more irregular than rats, indicated by higher coefficient of variation in inter-lick interval (rats 3.0±0.2 vs. mice 13.0±2.9, Wilcoxon rank-sum test, $p<0.001$). Since we penalized impulsive licking by postponing the next trial, higher spontaneous licking (inter-trial licking) in mice resulted in a significantly higher interval between microstimulation trials (inter-trial interval) (Figure 3.2j; rats 8.1±0.4 s vs. mice 11.9±1.9, Wilcoxon rank-sum test, $p = 0.006$).

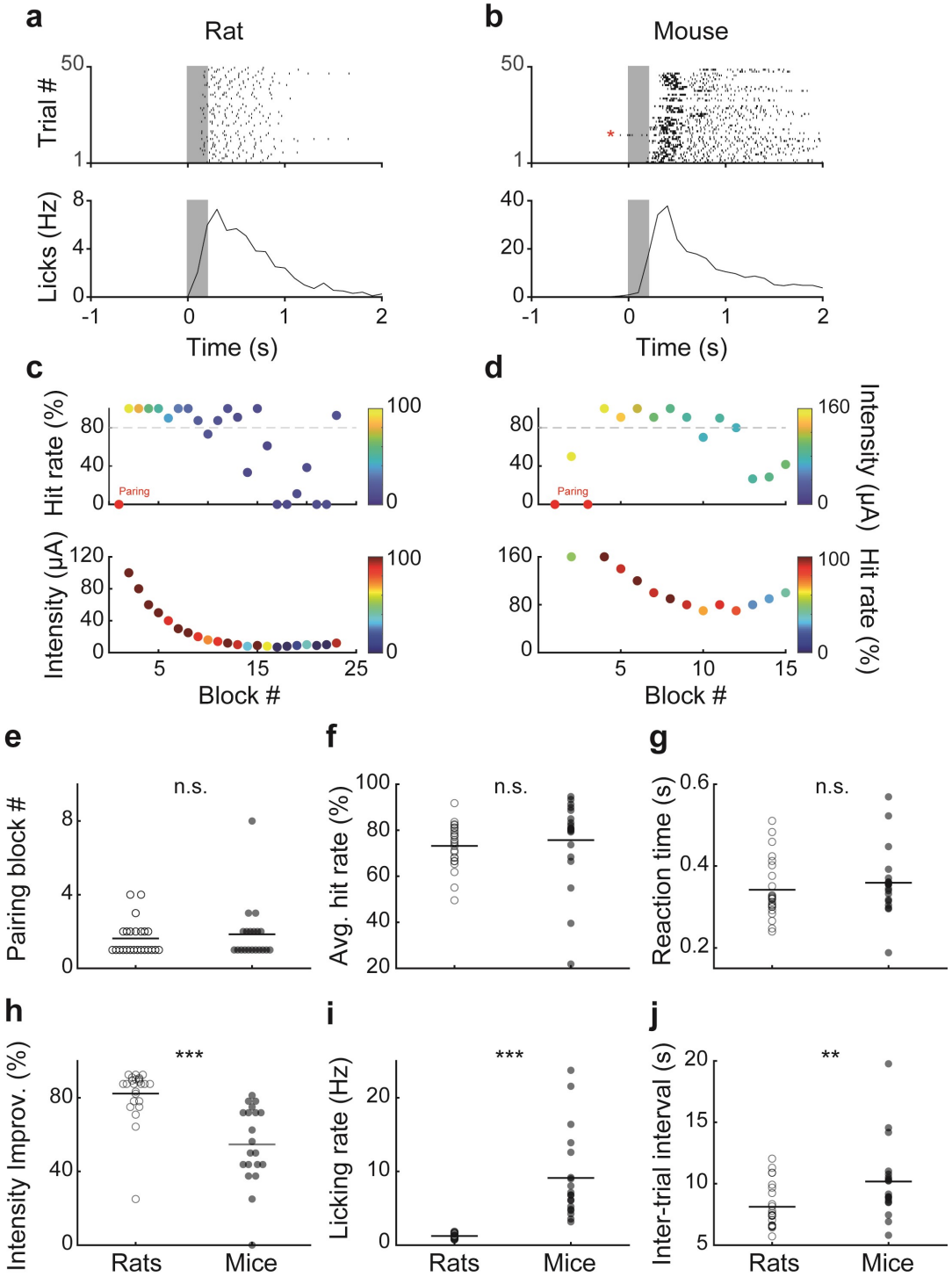

Figure 3.2. Comparison of learning behaviors in rats and mice. a, b) Raster plot of licks (top) and peri-stimulus time licking rate (bottom) during the first training session in an example rat and mouse, respectively. Black ticks in the raster plot indicates licks. Red asterisk indicates an abolished trial due to premature licking. **c, d)** Trajectory of hit rate (top, colormap indicates the intensity) and stimulus intensity (bottom, colormap indicates the hit rate) during the first session in the same example rat and mouse, respectively. Gray dashed line: target hit rate (80%). Red dots: pairing blocks. **e)** Comparison of required number of pairing blocks in rats (n=24) and mice (n=20). **f-j)** Same as **e)** for the average hit rate, reaction time, intensity improvement, licking rate and inter-trial interval. Wilcoxon rank-sum test, n.s., not significant, **p<0.01, ***p<0.001.

Previous studies using the microstimulation detection task trained rats to respond to very low current intensity before they were subjected to respond to single neuron stimulation (Doron et al., 2014; Houweling and Brecht, 2008). We tested if mice can also be trained to perform this task at low intensity by training a subset of mice on subsequent days while gradually lowering microstimulation threshold (see Methods) and compared their performance with that of rats. Once rats and mice performed reliably (hit rate ≥80%) at the lowest target intensity (5 μA for rats and 10 μA for mice), we switched the microstimulation-only testing period to a mixture of microstimulation trials at the target intensity and intermittent catch trials with no current injection (Figure 3.3a). On average both expert rats and mice showed hit rate higher than 85% to microstimulation trials (Figure 3.3b&d; Expert rats 86.5±3.4 %, n = 18 & expert mice 94±3.6 %, n=11). However, they also responded to catch trials (false-positive rates), where no microstimulation was presented but licks were counted during the response window, but significantly lower than to microstimulation trials (Expert rats 35.7±5.5 %, Wilcoxon sign rank test, p<0.001, & expert mice 40.8±7.5 %, Wilcoxon sign rank test, p<0.001). This resulted in an effect size (hit rate – false-positive rate) of approximately 50% in both expert rats and mice (Figure 3.3f; Expert rats 50.8±6.6 % vs. expert mice 53.9±6.3 %, Wilcoxon rank-sum test, p=1). Relatively high false-positive rate might be due to the long response window (0.1 s to 1.2 s after microstimulation onset) that we used for counting hits. We therefore compared the reaction time (RT) to microstimulation trials and catch trials and found that reaction time to catch trials was twice longer than to microstimulation trials in both expert rats and mice (Figure 3.3c&e; Expert rats: microstimulation RT 0.3±0.02 s vs. catch RT 0.6±0.03 s, Wilcoxon signed-rank test, p<0.001; Expert mice: microstimulation RT 0.3±0.02 vs. catch RT 0.6±0.02 s, Wilcoxon signed-rank test, p<0.001). This suggests that high false-positive rate most likely resulted from spontaneous lickings rather than false perception of microstimulation.

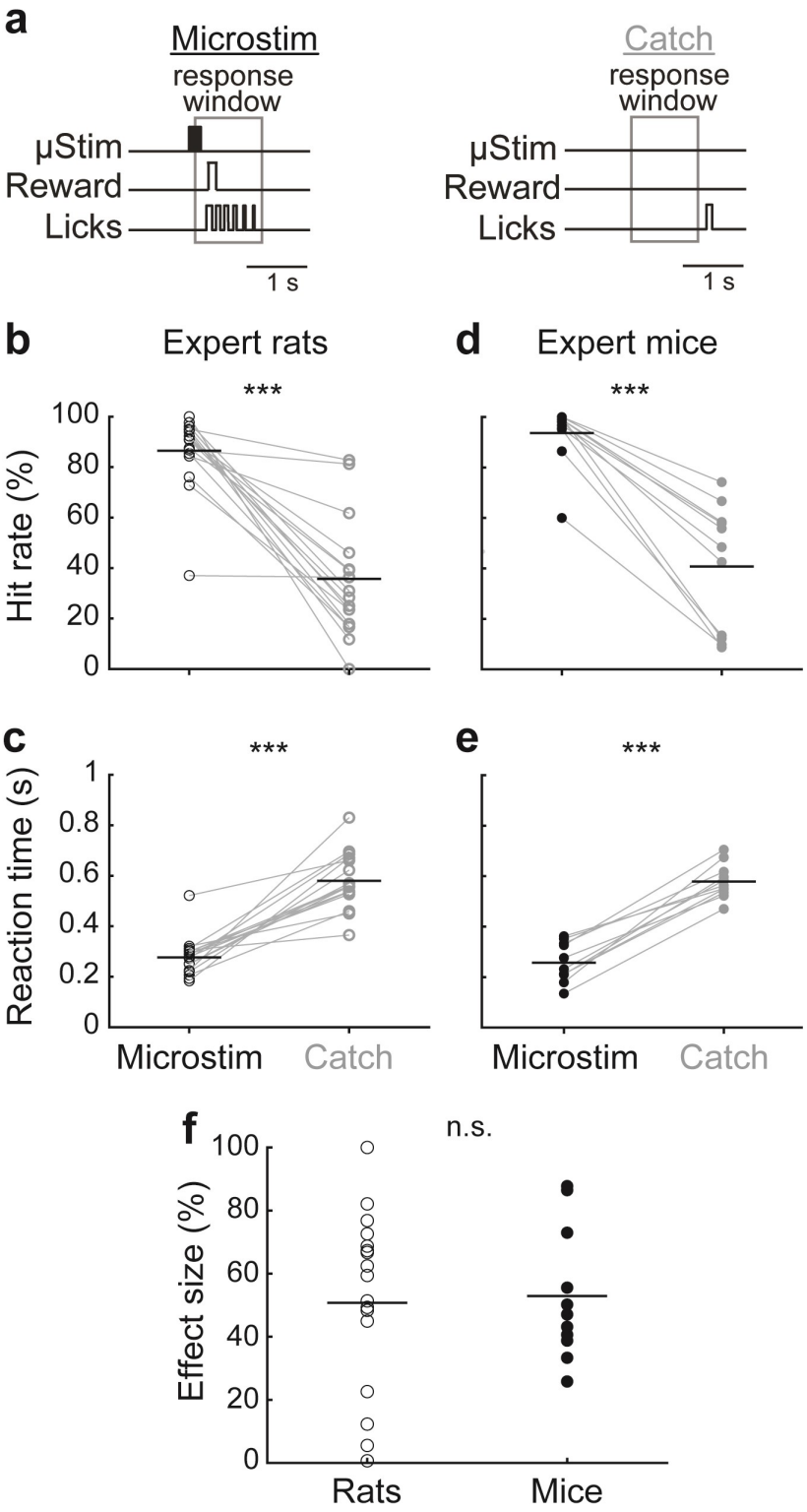

Figure 3.3. Comparison of microstimulation learning behavior in expert rats and mice. a) Expert animals received mix trials where μStim trials and catch trials were randomly presented. During catch trials, no current was injected. **b, c)** Hit rate and reaction time for μStim trials and catch trials in expert rats (n=18), respectively. Wilcoxon signed-rank test, ***p<0.001. **d, e)** Same as **b, c)** for expert mice (n=11). Wilcoxon signed-rank test, ***p<0.001. **f)** Effect size (hit rate – false-positive rate) of expert rats and expert mice. Wilcoxon rank-sum test, n.s., not significant.

So far, we have compared learning behaviors of rats and mice using average-based analysis that provides us an overview of the performance. However, these metrics might not capture all aspects of learning, for instance, how the performance of animals progresses during a session. Therefore, we developed a novel metric to quantify learning by computing the cumulative difference between the number of successful and failed licking responses to microstimulation (Σ[hits-misses]). Here, the learning score was defined as a cumulative value at a given trial and the final learning score, i.e. total number of hits – misses, was used to compare performances among different experimental groups. The learning score across trials can describe how the performance of animals improves during a session, which can be complemented by a single number metric value (final learning score) that can be easily compared among different experimental groups (see Methods). We tested if the learning score can distinguish animals that learned stimulus-reward association from animals that did not learn by comparing trained animals (rats and mice) and untrained animals. Here we tested the behavior of untrained mice only but we expect that untrained rats will display a comparable behavior. In order to prevent stimulus-reward association in untrained mice, we did not present any pairing block to this group but directly proceeded to the testing period (Figure 3.4a). Because untrained animals were not initially conditioned to associate microstimulation and reward, we hypothesized they would perform poorly at the microstimulation detection task. Indeed, untrained mice obtained poor scores at all behavioral metrics, previously used to characterize learning behavior in conditioned animals (Figure 3.2). Specifically untrained mice showed significantly lower hit rate and higher reaction time compared to control animals that received pairing periods (Figure 3.4b&c; hit rate: untrained 22.5±3.3 %, n=5 vs. control 75.6±1.8 %, n=43, Wilcoxon rank-sum test, $p<0.001$; RT: untrained 0.7±0.04 s vs. control 0.4±0.01 s, Wilcoxon rank-sum test, $p<0.001$), indicating that untrained mice did not successfully learn to associate the microstimulation and reward. To test whether this difference is reflected in the learning score, we compared the learning scores of untrained mice with control animals. Both control rats and mice showed a gradual increase of learning score over the session and reached positive value after the first session (learning score normalized by total number of trials: control rats 0.4±0.04, n=24 vs. control mice 0.5±0.05, n=19). Consistent with previous results showing comparable learning behaviors of the two species (Figure 3.2), normalized learning score of rats and mice did not differ significantly (Wilcoxon rank-sum test, $p=0.08$). Therefore, we

pooled two groups together to compare with untrained mice. Contrary to control animals, untrained mice showed a decreasing trend in learning score, which resulted in a negative normalized learning score (Figure 3.4d&e; untrained -0.5±0.05 vs. control 0.4±0.03, n=43, Wilcoxon rank-sum test, p<0.001). In conclusion, learning scores can well describe learning trajectories over the session and distinguish the level of association learning in different groups. In the rest of this study, we used learning score to compare the level of learning among different experimental groups.

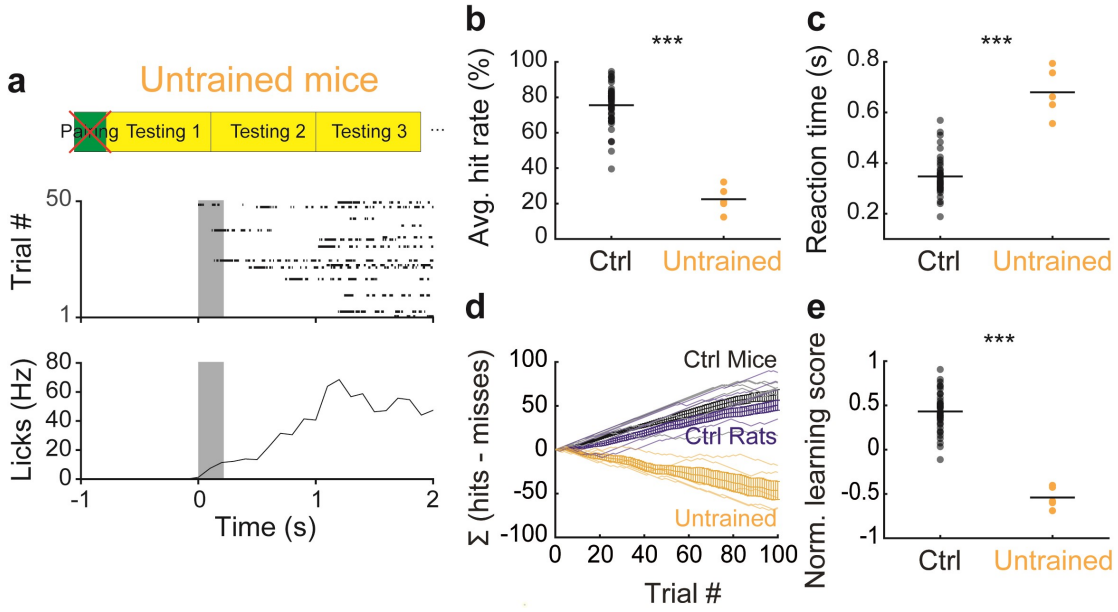

Figure 3.4. Learning score can describe the stimulus-reward association level. a) Training protocol for untrained mice. Untrained mice did not receive pairing trials, where µStim was coupled to reward. Lower, raster plot of licks (top) and peri-stimulus time licking rate (bottom) during the first training session in an example untrained mouse. **b)** Comparison of average hit rates between controls (both mice and rats, n=43) and untrained mice (n=5). **c)** Same as **b)** for reaction time. **d)** Cumulative differences between hit and miss trials (learning score) showing a learning trajectory during the first session. **e)** Normalized learning scores of control and untrained animals. Each dot corresponds to individual animal and black line represents the average. Wilcoxon rank-sum test, ***p<0.001.

3.1.2 Microstimulation-reward association learning is hippocampal-dependent

We next tested if learning to associate intracortical microstimulation and reward is dependent on the hippocampus, an MTL area known to be essential for declarative memory (Squire et al., 2004). To do this, two models of disruption of hippocampal activity were employed (Figure 3.5a). First, we tested a transient inhibition of hippocampal activity by blocking Na^+ channels via lidocaine injection. This manipulation ensured that the hippocampal activity was not permanently changed but only during the memory formation

period. HPC-inhibited animals (n=7 rats and n=3 mice) required slightly, but not significantly, more number of pairing blocks than control animals (control median 1 block, n=43 vs. HPC median 2 blocks, n=10, Wilcoxon rank-sum test, p=0.1). These animals showed low performance during the testing period, measured by lower hit rate (control 76.6±1.8 % vs. HPC 48.2±7.8 %, Wilcoxon rank-sum test, p<0.001; Figure 3.5b, HPC) and longer reaction time (control 0.3±0.01 s vs. HPC 0.4±0.04 s, Wilcoxon rank-sum test, p=0.04; Figure 3.5c, HPC) compared to controls. Moreover, contrary to controls that showed gradual increase of the learning score over a session, the learning score of hippocampus-inhibited animals did not improve but rather stayed at the basal level, indicating that their miss rate was as high as hit rate (Figure 3.5d, red). Interestingly, we found that learning impairment was slightly stronger, albeit not significantly, in hippocampus-inhibited mice than rats (HPC rats 0.03±0.2 vs. HPC mice -0.3±0.2 Wilcoxon rank-sum test, p=0.2). This might be due to the larger size of the rat hippocampus (Kalisch et al., 2006; Stein et al., 2012) that led to an incomplete hippocampal inhibition compared to mice by the same volume of lidocaine injection. The hippocampus-inhibited group showed a significantly lower normalized learning score than the control group (Figure 3.5e, red; HPC -0.07±0.1 vs. control 0.4±0.03, n=43, Wilcoxon rank-sum test, p <0.001), suggesting that hippocampal activity during training is necessary for memory formation during our learning paradigm.

Next, we tested the effect of chronic hippocampal disruption on learning using a mouse model of temporal lobe epilepsy. Here mice were injected with kainate in the hippocampus, resulting in epileptic seizures and permanatly disrupted hippocamapal activity (Häussler et al., 2012; Riban et al., 2002). Epileptic mice did not show any significant difference in number of pairing blocks (median 1 block, n=6, Wilcoxon rank-sum test, p=0.6), average hit rate (80.5±2.0 %, Wilcoxon rank-sum test, p=0.3; Figure 3.5b, Epileptic) and reaction time (0.4±0.04, Wilcoxon rank-sum test, p=0.9; Figure 3.5c, Epileptic) compared to controls. Interestingly, epileptic mice showed a gradual increase in learning score, resulting in slightly higher average normalized learning score than control albeit not significant (Figure 3.5d&e, blue; epileptic 0.6±0.05 vs. control 0.4±0.03, Wilcoxon rank-sum test, p=0.1). Higher or similar learning scores in epileptic mice on the first training session suggests that epileptic activity in the hippocampus might not affect initial learning. However, previous studies showed that temporal lobe epilepsy often accompanies long-term memory deficits (Tramoni-Negre et al., 2017). To test their performance change in long-term, we continued

training epileptic mice for several days. Contrary to the improved performance in control mice over days, the learning score of epileptic mice deteriorated after three days (Figure 3.5f; day 3: control 0.7±0.05, n=12 vs. epileptic 0.3±0.09, n=6, Wilcoxon rank-sum test, $p<0.001$), indicating that normal hippocampal activity is required to form a stable long-term memory. Taken together, learning during the microstimulation detection task is dependent on the hippocampus.

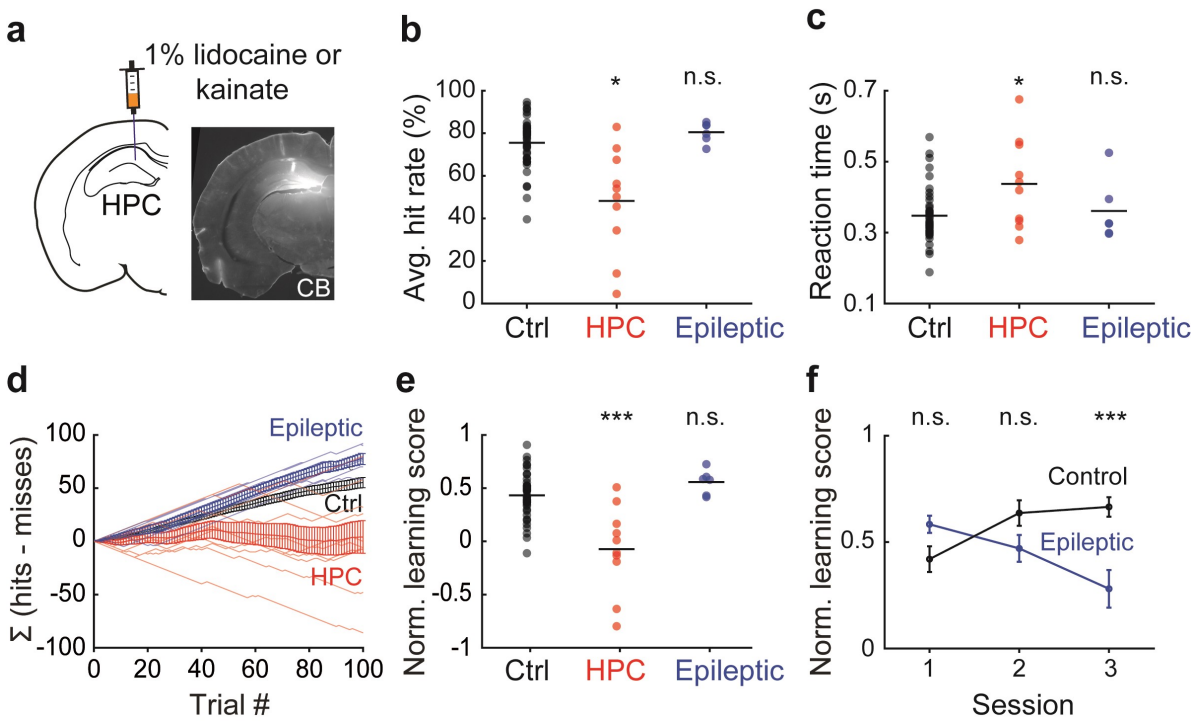

Figure 3.5. Microstimulation detection task is hippocampal-dependent. a) Left, schematics of transient (1% lidocaine) and chronic (kainate) manipulation of hippocampal activity. Right, Chicago Sky Blue (CB) dye injected in the hippocampus (HPC). **b)** Average hit rate of control animals (n=43), animals with lidocaine injection in the hippocampus (HPC, n=10) and epileptic groups (n=6). **c)** Same as **b)** for reaction time. **d)** Cumulative difference between hit and miss trials of controls (black), HPC-inhibited animals (red) and epileptic mice (blue) during the first training session. **e)** Normalized learning score of three groups. Each dot corresponds to individual animal and black line represents the average. **f)** Normalized learning score of control and epileptic mice over three sessions. Wilcoxon rank-sum test against control, n.s. $p>0.05$,*$p<0.05$, ***$p<0.001$.

In summary, we have described rapid and robust learning during the microstimulation detection task in rats and mice. Because it involves a direct current injection into the sensory neocortex (S1 in this case), this task is inherently neocortex-dependent. Our results indicate that this task is dependent on the hippocampus as well (Figure 3.5). Using this learning paradigm, we could now investigate circuit and cellular mechanisms underlying hippocampal-dependent memory formation in the neocortex.

3.2 Perirhinal input to neocortical layer 1 mediates memory formation

3.2.1 The perirhinal cortex sends monosynaptic feedback inputs to layer 1 of the primary somatosensory cortex

The complementary memory systems model suggests that interactions between two memory systems, the MTL and neocortex, are crucial for declarative memory (Alvarez and Squire, 1994; Kumaran et al., 2016; McClelland et al., 1995, 2020). However, there is no known direct anatomical connection between the hippocampus and primary sensory cortices. Instead, the hippocampus is connected via neighboring areas such as the entorhinal cortex and perirhinal cortex (Squire et al., 2004). We performed anatomical tracing experiments to identify a MTL structure that provides monosynaptic inputs to S1 (Figure 3.6a).

We hypothesized that the projection pattern of MTL inputs follows the general cortical connectivity rule in which feedback inputs preferentially target L1 (Cauller et al., 1998; D'Souza and Burkhalter, 2017; Rockland, 2019; Roth et al., 2016; Rubio-Garrido et al., 2009). In order to identify presynaptic regions that directly project to L1 of S1, we applied the retrograde dye, Fast Blue (FB), to L1 of S1 (Figure 3.6b). FB-labeled neurons in S1 were found in supragranular and infragranular layers but not in L4. Because most axons and dendrites of L4 neurons rarely reach L1 but until L2/3 (Staiger et al., 2004), this result indicates that FB did not spread to L2/3 but remained limited in L1 (Figure 3.6c). The retrograde tracing revealed presynaptic neurons in various brain areas, including the primary (M1) and secondary motor (M2) cortices, secondary somatosensory cortex (S2), cingulate cortex, retrosplenial cortex, striatum and POm, consistent with previous reports (Petersen, 2019) (Figure 3.6d). Among MTL structures, we found FB-labeled presynaptic neurons in deep layers of the perirhinal cortex. Interestingly, unlike other areas that project to L1 ipsilaterally we found presynaptic neurons in both ipsilateral and contralateral perirhinal cortex, suggesting that S1 receives bilateral information from the perirhinal cortex (Figure 3.6e-f&h). We performed this experiment in both rats and mice and consistently found FB-labelled neurons in bilateral perirhinal cortices. Most FB-labeled cells were found in the rostral part of the perirhinal cortex (-1.3 mm~ -3 mm from the bregma in mice and -3 mm ~ -5.5 mm from the bregma in rats) (Figure 3.6g). Therefore, the projection pattern of

perirhinal neurons displays gradient along rostral-caudal axes, consistent with previous reports (Agster and Burwell, 2009).

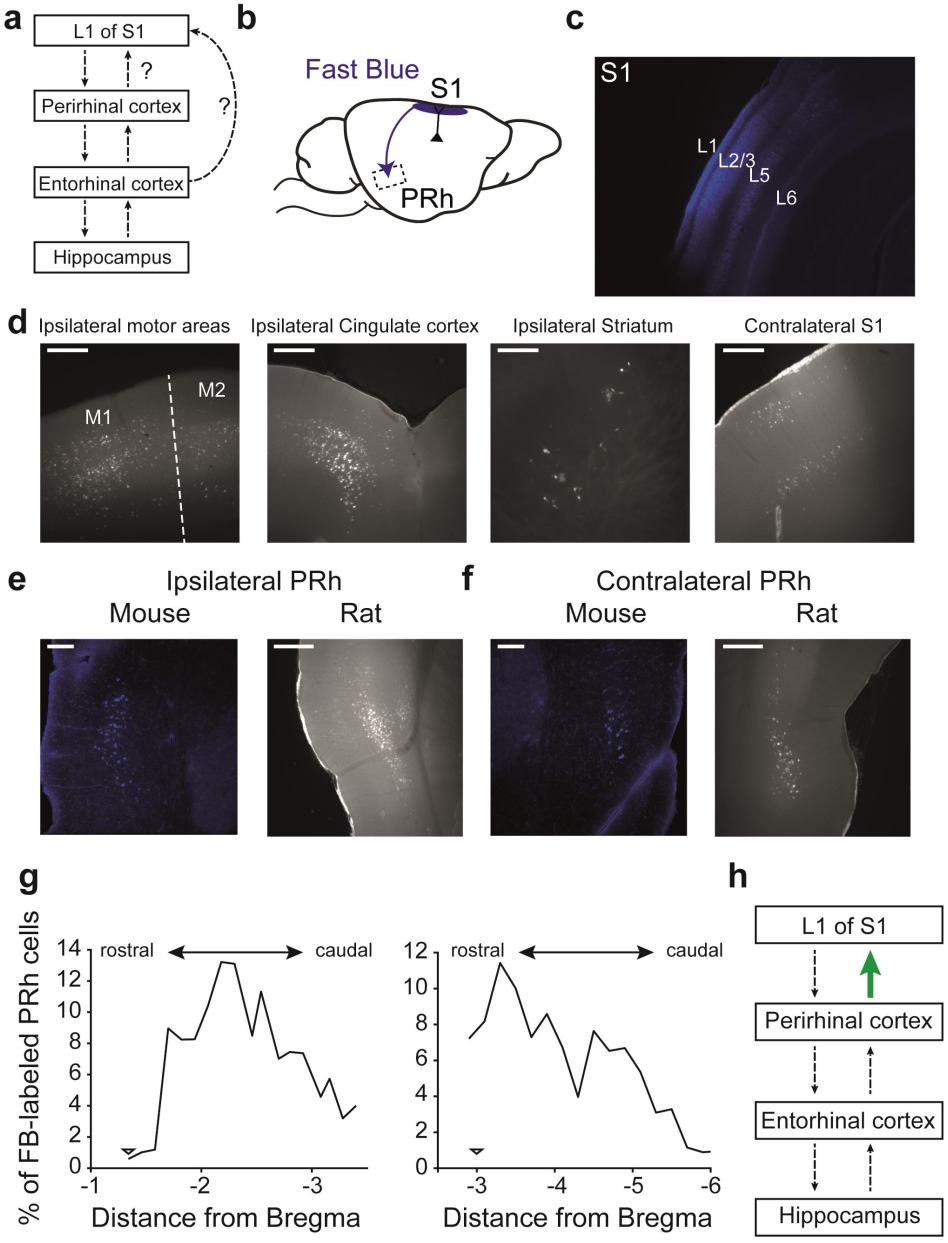

Figure 3.6. Identification of presynaptic area to L1 of S1 using retrograde tracing. a) Examined anatomical connectivity. The HPC is connected to sensory cortices via the entorhinal cortex and perirhinal cortex (PRh). **b)** Schematic of retrograde tracing. Fast Blue (FB) was applied on the surface of S1. **c)** FB-labelled cells in S1 avoided L4, confirming that FB was limited to L1. **d)** FB-labelled presynaptic neurons were found in different cortical areas including the M1, M2, cingulate cortex, striatum and contralateral S1. Scale bar: 250 µm. **e, f)** FB-labelled presynaptic neurons in the ipsilateral and contralateral PRh in the mouse and rat brain, respectively. Scare bar: 100 µm for the mouse brain and 250 µm for the rat brain. **g)** Rostro-caudal distribution of FB-labelled neurons in PRh in the mouse (left, n=6 brains) and rat brain (right, n=2 brains). Arrows indicate the starting point of PRh. **h)** Summary of the retrograde tracing where we found PRh projects to L1 of S1 (highlighted in green).

Next, to examine the laminar projection pattern of perirhinal neurons to S1, we expressed Enhanced Yellow Fluorescent Protein (EYFP) in perirhinal neurons via Adeno-associated viral (AAV) vector (Figure 3.7a-b). Based on retrograde tracing results (Figure 3.6), we targeted the rostral part of the ipsilateral perirhinal cortex (see Methods). We found that axons of perirhinal neurons expressing EYFP were densely labeled in L1 of S1 in both rats and mice (Figure 3.7c-d), confirming that the perirhinal cortex projects axons to L1 of S1. Indeed, we found the highest EYFP intensity in L1, followed by deeper layers and lowest in middle layers, confirming that perirhinal input to S1 is a feedback-type (Felleman and Van Essen, 1991; Harris et al., 2019). Taken together, these results suggest that the perirhinal cortex is the major output structure in MTL system that provides feedback projections to L1 of S1.

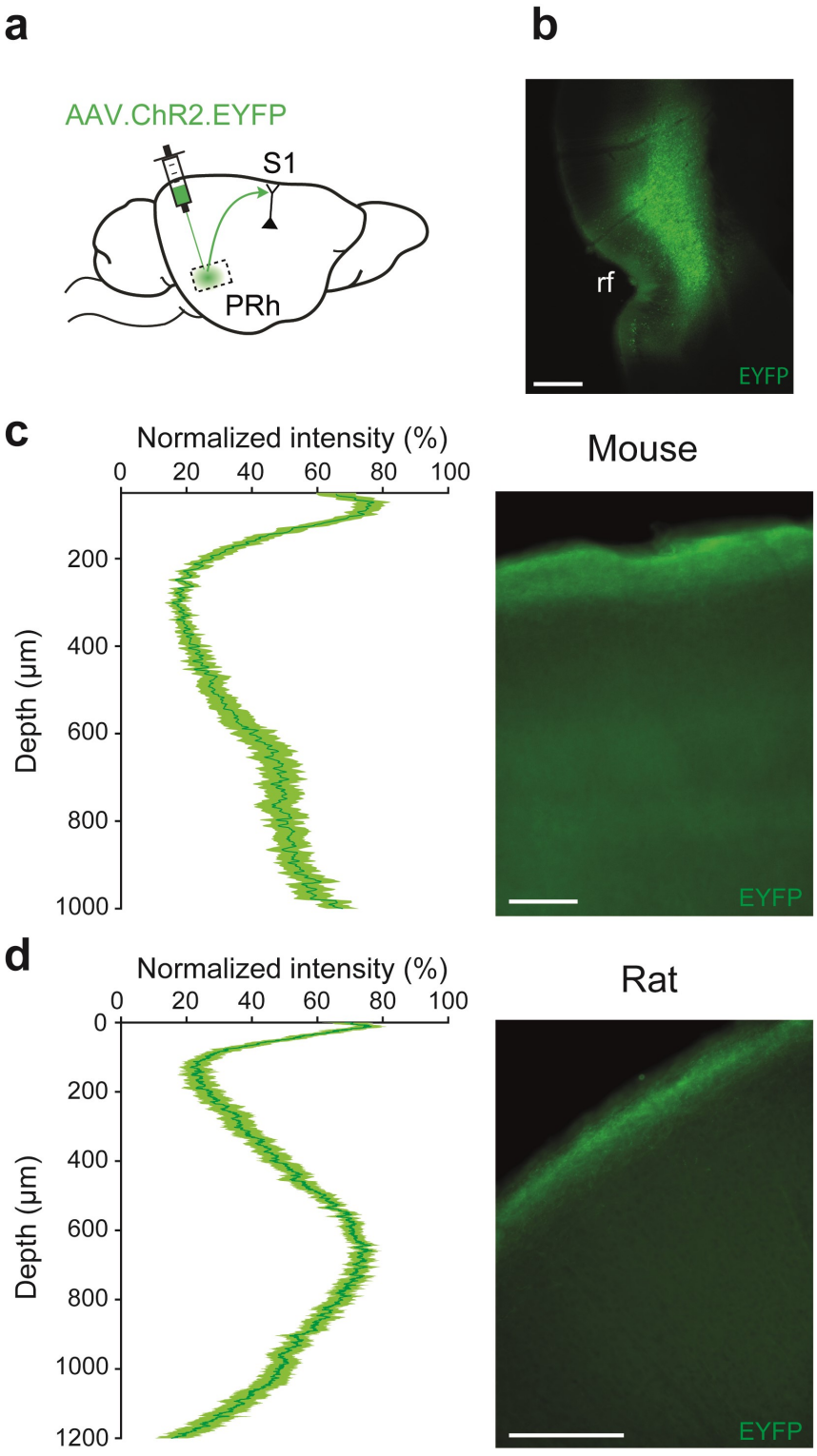

Figure 3.7. Projection pattern of PRh axons to S1. a) Schematic of anterograde tracing. AAV.ChR2.EYFP was injected to PRh and their axons in S1 was imaged. **b)** EYFP expression in PRh. rf: rhinal fissure Scale bar: 500 µm. **c)** EYFP-expressing axons in the S1 of the mouse brain. Left, quantification of EYFP level across cortical depths (n=20 brain sections). Right, representative image showing strong EYFP level in L1. Scale bar: 250 µm. **d)** Same as **c)** for the rat brain (n=16 brain sections).

3.2.2 Functional involvement of the perirhinal cortex in the microstimulation detection task

Next, we examined if learning during the microstimulation detection task is dependent on perirhinal activity. To this end, we injected Na^+ channel blocker, lidocaine, into the ipsilateral perirhinal cortex to transiently inhibit its neuronal activity (Figure 3.8a). Rats were used in this experiment since targeting the perirhinal cortex without damaging S1 was technically more challenging in the smaller mouse brain. Since both the behavior during the microstimulation detection task and anatomical connectivity between the perirhinal cortex and S1 is conserved in rats and mice (Figure 3.2-3.3 and 3.6-3.7), we assumed that the role of the perirhinal cortex in learning in mice would be conserved. The performance during microstimulation learning was quantified using the learning score (Σ[hits-misses]) as described before (Figure 3.4). Perirhinal-inhibited rats could not improve the learning score over the session, resulted in a significantly lower normalized learning score than in control rats (PRh -0.1±0.09, n=4 vs. control 0.4±0.04, n=24, Kruskal-Wallis test, p=0.007, post-hoc Dunn-Sidàk test, p=0.01; Figure 3.8b&c). Next, to examine if perirhinal activity continuously influences the animal's performance after learning, we injected lidocaine in the perirhinal cortex after several days of training. Contrary to its effect on the initial phase of learning, perirhinal inhibition with lidocaine did not affect the performance of the trained rats (Figure 3.8b&c, dark green). The learning score of trained rats was significantly higher than perirhinal inhibited rats during learning (PRh-trained 0.5±0.1, n=6 vs. control rats, Kruskal-Wallis test, p=0.007, post-hoc Dunn-Sidàk test, p=0.9; PRh-trained vs. PRh, post-hoc Dunn-Sidàk test, p=0.01), implying that perirhinal activity is not necessary after memory is stabilized, potentially, in the neocortex. These results suggest that perirhinal activity mediates the initial stage of memory formation but does not have a causal influence on the retrieval of learned behavior.

The fact that the perirhinal activity is necessary for learning does not necessarily indicate that its effect on learning is exerted by influencing activity in S1. We hypothesized that if perirhinal output influences S1 activity, its axons in S1 should be engaged during the task. Since perirhinal activity is necessary in the initial phase of learning (Figure 3.8a-c), we examined how the activity of perirhinal axons in L1 of S1 change after the first training session. To this end, we expressed a genetically encoded calcium indicator, GCaMP6s, in perirhinal neurons and measured their axonal Ca^{2+} activity in L1 of S1 (Figure 3.8d).

Consistent with anterograde tracing result showing that perirhinal neurons project to L1 of S1 (Figure 3.7), we found GCaMP6s expressing axons in L1 (Figure 3.8e). We compared Ca^{2+} activity of perirhinal axons in response to microstimulation before and after one training session to evaluate learning-triggered activity changes in these axons. These axons mildly responded to microstimulation before training but Ca^{2+} responses of perirhinal axons were significantly enhanced after microstimulation was associated with reward (Figure 3.8f; post-stimulus dF/F0: before learning 11.9±0.7%, n=227 trials from n=3 mice vs. after learning 15.0±0.7%, n=185 trials from n=3 mice, Wilcoxon rank-sum test, $p<0.001$). When we analyzed axonal Ca^{2+} activity in individual mice separately, we still observed significantly enhanced axonal Ca^{2+} activity after one training session, suggesting that this effect was not caused by one outlier mouse (Wilcoxon rank-sum test, mouse 1, p=0.03; mouse 2, p=0.009, mouse 3, p=0.01; Figure 3.8f). Interestingly, perirhinal axons did not respond to reward alone (i.e. not paired with microstimulation) (pre-stimulus dF/F0 7.8±1.2% vs. post-stimulus dF/F0 6.9±1.1%, n=66 trials from n=3 mice, Wilcoxon signed-rank test, p=0.1). These results indicate that synaptic transmission between perirhinal axons and cellular components in L1 occurs during learning.

Next we examined the firing activity of perirhinal neurons while animals were performing the microstimulation detection task. To this end, we performed juxtacellular recording from single perirhinal neurons and examined their responses to microstimulation in S1 (Figure 3.8g). We found that firing rate of these neurons significantly increased during hit trials, when animals licked in response to microstimulation within the response window, but significantly reduced when they failed to do so (miss trials) (Figure 3.8h-i; n=28 neurons from 6 rats; Hit trials: pre-stimulus 3.87±0.39 Hz vs. post-stimulus 5.1±0.5 Hz, Wilcoxon signed-rank test, $p<0.001$, n=287 trials; Miss trials: pre-stimulus 2.8±0.4 Hz vs. post-stimulus 2.6±0.4 Hz, Wilcoxon signed-rank test, p=0.01). Therfore, perirhinal activity reflects behavioral outcome of the task. Together with the axonal Ca^{2+} imaging result, this suggests that perirhinal neurons convey 'hit'-related information to L1 of S1. In summary, perirhinal activity plays a significant role in stimuli-reward association learning by conveying behaviorally relevant information (i.e. hits) to S1 via L1.

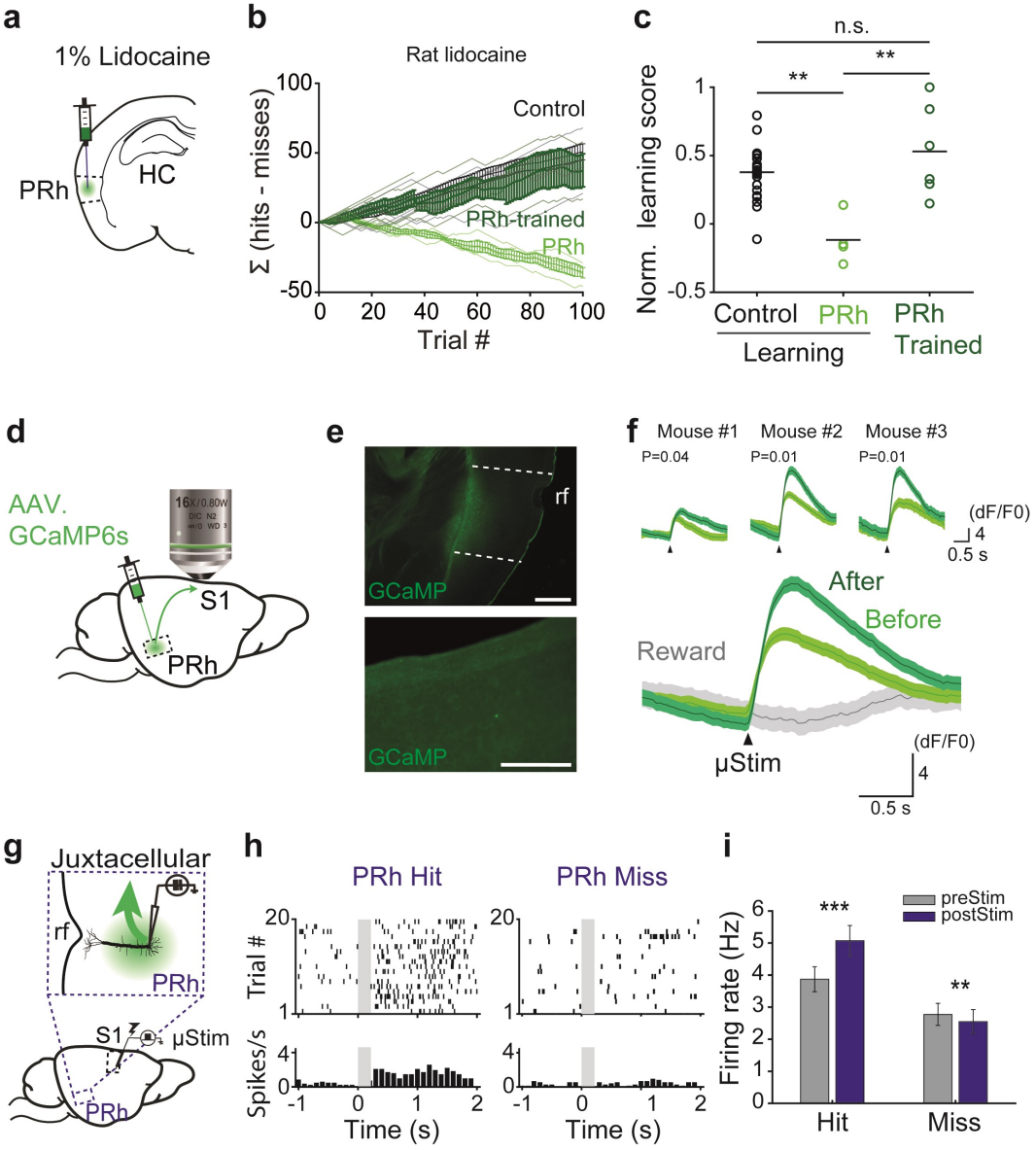

Figure 3.8. Learning to associate microstimulation and reward is dependent on PRh neuronal activity. **a)** Schematic of pharmacological manipulation of PRh activity. 1% lidocaine was injected to PRh before training. **b)** Cumulative differences between hit and miss trials of control (n=24, black), rats with lidocaine-injection in PRh during learning (n=4, light green) and rats with lidocaine-injection in PRh after learning (n=6, dark green). **c)** Normalized learning scores of three groups. Each dot corresponds to individual rats and black line represents the average. Kruskal-Wallis test, p=0.007, post-hoc Dunn-Sidàk test, n.s., not significant, **p=0.01. **d)** Schematic of two-photon Ca^{2+} imaging of PRh axons in L1 of S1. **e)** Representative images showing GCaMP expression in PRh (upper, scale bar: 500 μm) and axons in S1 (lower, scale bar: 250 μm). rf: rhinal fissure. **f)** Average Ca^{2+} responses (and s.e.m.) in PRh axons in L1 upon microstimulation before (light green) and after the first training session (green) and during passive reward reception (gray). Upper inset, average Ca^{2+} responses (and s.e.m.) of PRh axons in three individual mice. P-values were estimated with Wilcoxon rank-sum test. **g)** Schematic of juxtacellular recording in PRh during the microstimulation detection task. **h)** Raster plot and peri-stimulus time histograms (PSTHs) during hit and miss trials from an example PRh neuron. **i)** Firing rates of PRh neurons (n=28) before and after μStim during hit and miss trials. Wilcoxon signed-rank test, **p<0.01, ***p<0.001.

3.2.3 Chemogenetic silencing of perirhinal inputs to layer 1 disrupts learning

We have established the functional significance of perirhinal neurons in microstimulation-reward association (Figure 3.8) and their projection patterns to S1 (Figure 3.7). We now sought to examine the causal role of the perirhinal inputs to L1 on learning. To specifically inhibit these inputs to L1 of S1 during the entire period of the training, we employed a state of art chemogenetic tool (inhibitory designer receptors exclusively activated by a designer drug, DREADD), provent to be efficient in long-term inhibition of neuronal transmission (Roth, 2016; Wiegert et al., 2017). In particular, intracranial application of external ligand of hM4Di receptor, Clozapine-N-oxide (CNO), in a defined brain area guarantees to down-regulate synaptic transmission at the axon terminals located in postsynaptic area without altering somatic activity and its influence over other regions (Stachniak et al., 2014). Therefore, this method allows testing the role of a specific output of the perirhinal cortex without interfering with its influence over other interconnected areas such as the entorhinal cortex and hippocampus.

We first validated the efficacy of hM4Di receptors and the ligand CNO in *ex-vivo* experiments (Figure 3.9a). We co-transfected AAV.mCherry.hM4Di and AAV.EYFP.ChR2 in perirhinal neurons and performed *ex-vivo* whole-cell recordings in brain slices to quantify the effect of hM4Di/CNO on synaptic transmission between perirhinal axons and postsynaptic neurons. Since perirhinal neurons target L1 of S1 (Figure 3.7), we speculated that L1 interneurons and distal dendrites of L5 pyramidal neurons will receive perirhinal inputs. We performed whole-cell recordings using voltage clamp mode in these neurons while activating ChR-expressing perirhinal axons in L1 with 470 nm LED light. Optogenetic activation of ChR2-expressing perirhinal axons evoked excitatory postsynaptic currents (EPSCs) in both L1 interneurons (14.0±7.4 pA) and L5 pyramidal neurons (12.3±4.4 pA), indicating that these neurons receive excitatory inputs from perirhinal axons. Next, to test if activation of hM4Di receptors in perirhinal axons by CNO can block synaptic transmission induced by light stimulation, CNO was applied to the bath solution at a final concentration of 10 µM. After CNO application, light-evoked EPSCs were significantly reduced in both L5 pyramidal neurons and L1 interneurons (L5 pyramidal neurons: baseline 12.3±4.4 pA vs. +CNO 2.2±0.8 pA, n=6, Wilcoxon sign rank test, p=0.03; L1 interneurons: baseline 14.0±7.4 pA vs. +CNO 4.9±2.5 pA, n=7, Wilcoxon sign rank test, p=0.02; Figure 3.9b). In summary, we identified L1 interneurons and dendrites of L5 pyramidal neurons as cellular targets of

perirhinal inputs and validated that hM4Di activation by CNO efficiently down-regulates synaptic transmission in perirhinal axons.

The DREADD system enables specific manipulation of neuronal activity in two-folds. First, brain area-specific expression of hM4Di receptors and second, projection-specific effect by local application of CNO (Roth, 2016). To control the brain area-specific expression of hM4Di receptors, we quantified the expression of hM4Di.mCherry in the perirhinal cortex and neighboring areas. Fluorescence intensity was measured between 1000 µm dorsal and 1000 µm ventral from the rhinal fissure (Figure 3.9c-d; see Methods), which denotes the location of the perirhinal cortex (Kealy and Commins, 2011). Then the intensity was normalized by the intensity at the rhinal fissure to account for the different total expression and different imaging conditions for each brain (see Methods). We divided the areas into areas dorsal to perirhinal cortex (dorsal than 250 µm from the rhinal fissure), the perirhinal cortex (between 250 µm dorsal and 750 µm ventral from the rhinal fissure) and areas ventral to perirhinal cortex (ventral than 750 µm from the rhinal fissure) and compared the integral of the normalized fluorescence intensity in these areas. We found the highest expression level in the perirhinal cortex (54% to 78%) and significantly lower expression in both areas dorsal (14% to 43% vs. PRh, Wilcoxon signed-rank test, $p<0.001$) and ventral (0% to 12% vs. PRh, Wilcoxon signed-rank test, $p<0.001$) to the perirhinal cortex (n=11 brains, Figure 3.9e). In order to quantify how much of each area project to L1 of S1, we counted neurons retrogradely labeled with FB and found 84% of FB-labeled neurons in the perirhinal cortex while only 13% and 4% of FB-labeled neurons were found in areas dorsal and ventral to the perirhinal cortex, respectively (n=30 brain sections from n=3 brains; Figure 3.9f).

Next, to control the projection-specific effect of DREADD by local CNO application, we estimated the spread of CNO by injecting Chicago Sky Blue (CB) dye into S1 at the same depth we injected CNO (150 µm) (Figure 3.9g). Although most perirhinal axons arrive in L1 of S1, a considerable proportion of them was found in infragranular layers as well (Figure 3.7). Therefore, this procedure was necessary to make sure that our intended interference was limited to L1. We quantified the dye spread across cortical depths and we found a peak in L1 followed by gradual decrease in deeper depths (n=29 brain sections from n=7 injections; Figure 3.9h). We then computed the product of perirhinal axonal density and CB spread to evaluate the effect of combined hM4Di and CNO as a function of cortical depth (see Methods). This analysis revealed that the strongest effect was in L1 followed by L2/3, where

apical dendrites of L5 pyramidal neurons are located, while the effect on infragranular layers was the lowest (Figure 3.9i, black). Taken together, these results suggest that the majority of DREADD manipulation targeted hM4Di-expressing axons from the perirhinal cortex projecting to L1 of S1.

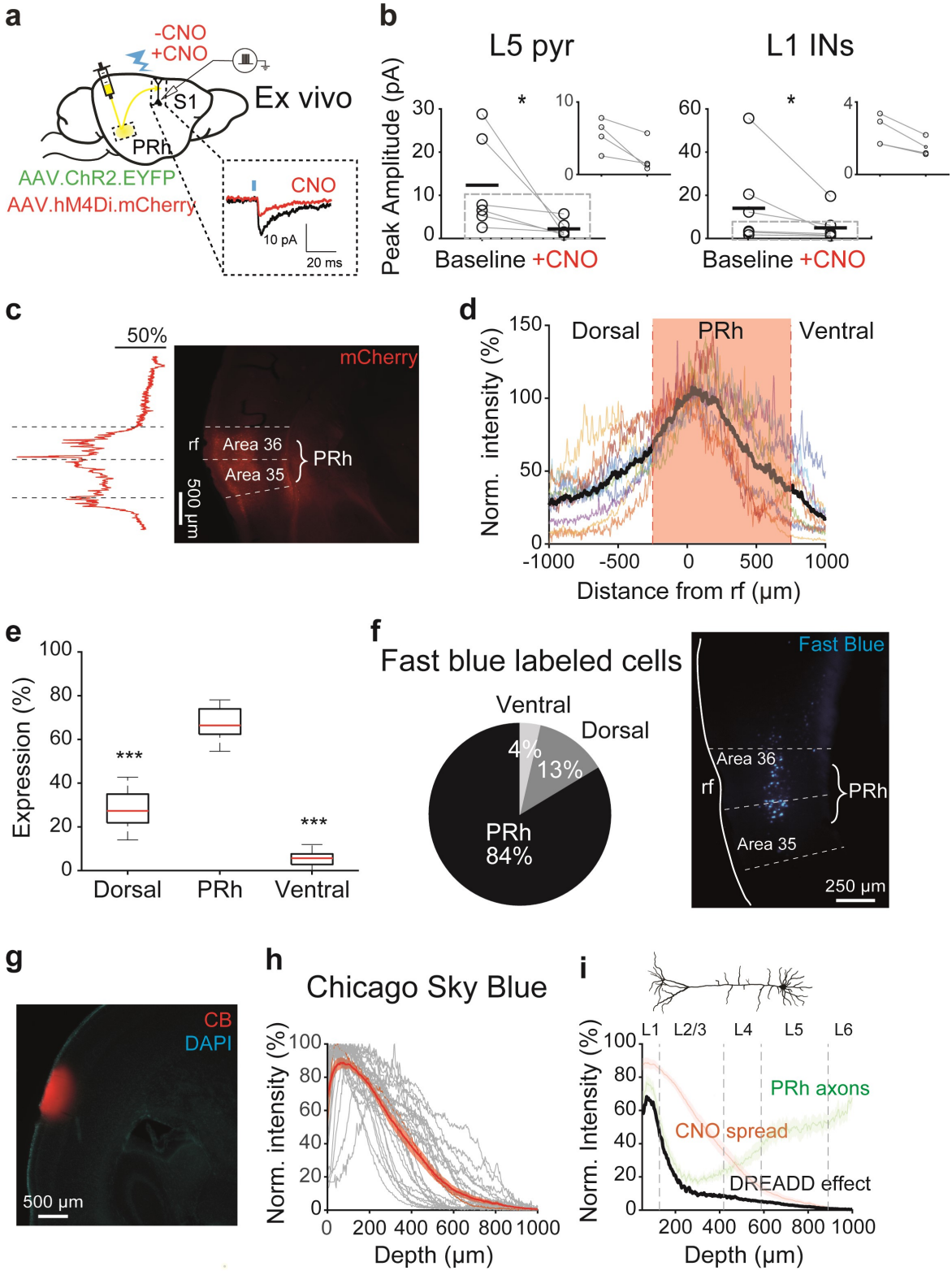

Figure 3.9. Establishing the efficacy and specificity of inhibitory DREADD system. a) Schematic of *ex-vivo* experiments. AAV.ChR2.EYFP and AAV.hM4Di.mCherry were co-injected into PRh. After >3 weeks of incubation, whole-cell recording was performed in *ex-vivo* brain slices during optogenetic activation of ChR2 with and without CNO. Right, example traces from a recorded neuron with (red) and without CNO (black). Blue line shows the light stimulation. **b)** EPSCs of L5 pyramidal neurons (n=6) and L1 interneurons (n=7) before and after CNO application. Light-evoked EPSC amplitudes were significantly reduced after CNO application in both cell classes. Wilcoxon signed-rank test, *p<0.05. Each point represent a cell and black lines indicate the average. Inset, magnified views of dotted boxes with low initial EPSC amplitudes. **c)** Example trace of normalized fluorescent intensity and the corresponding epifluorescent image. hM4Di expression around PRh was quantified by measuring mCherry fluorescent intensity (see Methods). **d)** Normalized mCherry expression between 1000 µm dorsal and 1000 µm ventral from the rhinal fissure (rf), which marks the location of PRh. Colored lines show normalized fluorescence intensity from brains of each mice (n=11) used in this study. Black line shows the average. Red area indicates the PRh. **e)** Quantification of mCherry expression in PRh and neighboring areas (see Methods). Most of the expression was observed in PRh but there was a small leakage into neighboring areas, especially in dorsal areas. Red central lines: median, black bottom and top edges of the box: 25th and 75th percentiles, respectively. Wilcoxon signed-rank test against PRh, ***p<0.001. **f)** Quantification of FB-labelled cells in PRh (n=30 brain sections from n=3 brains) and neighboring areas and an example image. **g)** Spread of CNO was estimated by injecting CB dye at the same depth in S1. Image shows the dye spread. **h)** Quantification of CB intensity across cortical layers. Gray lines show normalized intensity in each brain section (n=29 sections from n=7 injections) and the red line indicates the average normalized intensity and sem. **i)** Estimation of DREADD effect computed by a product of PRh axonal density and CNO spread as a function of cortical depths (see Methods). The morphology of an example L5 pyramidal neuron is shown on top.

After validating the efficacy and specificity of the DREADD system, we examined the role of perirhinal inputs to L1 of S1 on learning by suppressing the hM4Di-expressing perirhinal axons with local application of 10 µM CNO in L1 (150 µm from pia) (see Methods; Figure 3.10a). Remarkably, specific inhibition of this input severely impaired learning (Figure 3.10b-c, red), similar to blocking the hippocampus (Figure 3.5) or perihrhinal cortex (Figure 3.8). Mice in which the perirhinal input to L1 of S1 was suppressed by DREADD could not associate the water reward with the microstimulation. We quantified learning with the learning score (Figure 3.4) and found that the performance of hM4Di/CNO-treated mice measured by this metric did not improve over the session while that of the control mice gradually increased (Figure 3.10b, red). This resulted in a significantly lower normalized learning score compared to control mice (Figure 3.10c, left; control 0.5±0.06, n=20 vs. hM4Di/CNO-treated mice 0.04±0.1, n=12, Wilcoxon rank-sum test, p=0.004). A recent study showed that CNO converts to clozapine that can bind to endogenous receptors at high concentration and effect off-target downstream signal processing (Gomez et al., 2017). To test that CNO alone does not affect learning, we applied CNO in control animals that do not express hM4Di in the same manner we applied in hM4Di-expressing group. CNO application alone without hM4Di expression (hM4Di-/CNO+, n=7 mice) or hM4Di expression without CNO application (hM4Di+/CNO-, n=3 mice) did not affect performance of the animals

compared to mice without any treatment (hM4Di-/CNO-, n=10 mice, Kruskal-Walis test, p=0.1; Figure 3.10d), ruling out the unspecific effect of hM4Di receptor or CNO on learning.

In rats, the perirhinal activity could not affect the performance of the expert animals trained for several days (Figure 3.8). Here we tested whether perirhinal inputs to L1 of S1 affect expert mice. We first trained hM4Di-expressing mice without CNO application until they could perform the task with a hit rate ≥80% at the target intensity (10 μA) (i.e. experts). After three sessions, control mice improved learning scores compared to the first session (0.5±0.06 at session 1, n=20 vs. 0.9±0.04 at session 3, n=3, Wilcoxon rank-sum test, p=0.009). During the last session, we compared the performance of expert mice before and after CNO application and did not find any significant change in their performances (Figure 3.10c, right; 0.8±0.08, n=3 in after CNO, Wilcoxon signed-rank test, p=1). Therefore, the perirhinal cortex and its influence on S1 is involved in early memory formation but does not affect already stabilized memory. Besides, the consistent performance with and without perirhinal suppression suggests that perception of microstimulation was not interfered with by the chemogenetic manipulation.

L1 receives long-range inputs not only from the perirhinal cortex but also from other cortical and subcortical areas (Cauller et al., 1998; Lu and Lin, 1993; Rubio-Garrido et al., 2009). We asked if learning impairment by silencing L1 inputs was unique to perirhinal originated axons or L1 inputs from other areas also can gate learning. We tested the contribution of L1 input from the higher order somatosensory thalamic area, POm, which has been previously shown to be involved in sensory learning related plasticity (Audette et al., 2019; Gambino et al., 2014; Williams & Holtmaat, 2019). In these studies, using whisker stimulation instead of direct S1 stimulation, POm input to L1 has been shown to mediate NMDA receptor-dependent long-term synaptic potentiation in L2/3 pyramidal neurons. To examine the influence of POm inputs in learning during the microstimulation detection task, this time we expressed hM4Di receptors in POm in Gpr26-cre transgenic mice that express Cre-recombinase in POm neurons (Oram et al., 2015; Zolnik et al., 2020) and applied CNO in L1 of S1. Suppression of POm inputs to L1 did not significantly affect the learning of the mice relative to controls (POm 0.3±0.2, n=7 vs. control 0.5±0.06, n=20, Wilcoxon rank-sum test, p=0.1; Figure 3.10e-f). These results suggest that learning impairment during suppression of perirhinal input to L1 is not due to reduced net excitatory inputs in L1 but rather due to a unique and crucial contribution of perirhinal inputs in gating memory formation in S1. We

conclude that the MTL system modulates memory formation in S1 via the perirhinal cortex, of which influence is mainly exerted on L1.

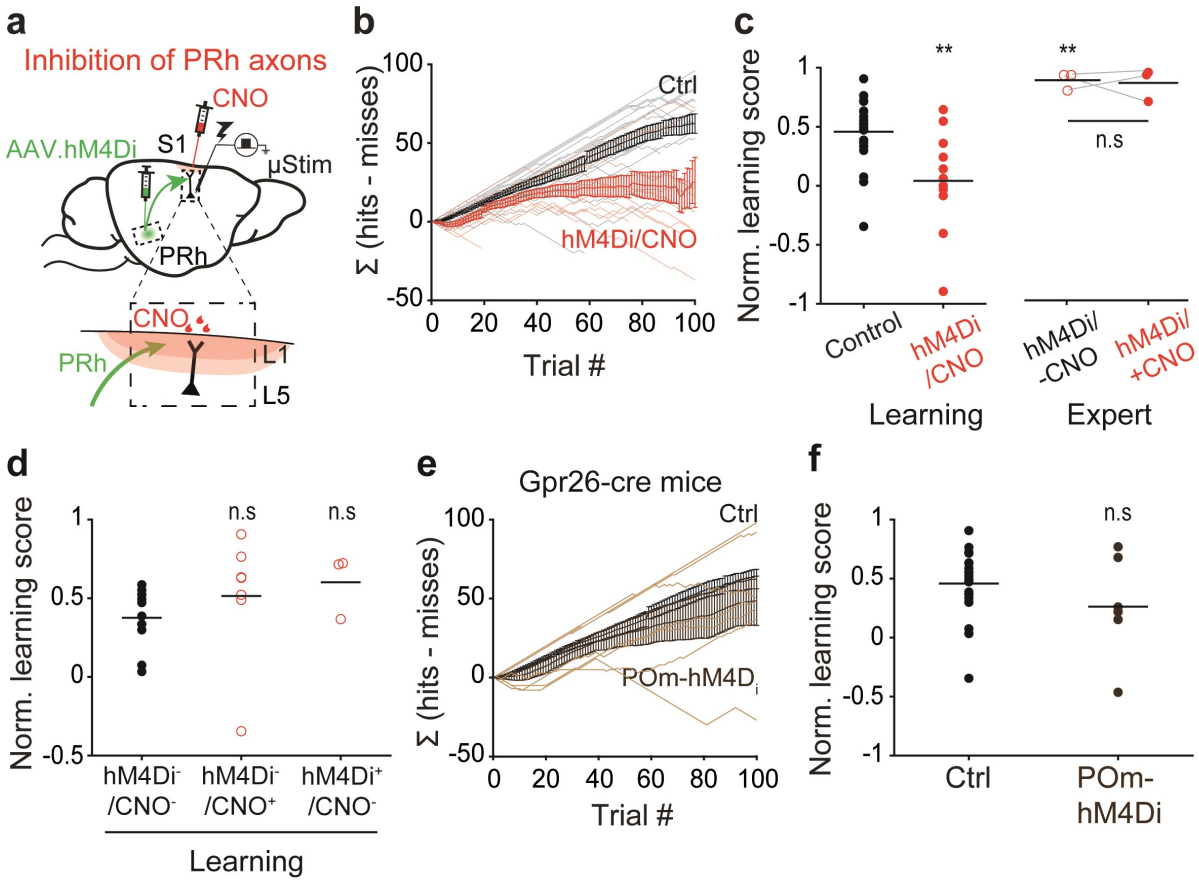

Figure 3.10. L1 inputs from PRh is crucial for the early stage of learning. a) Left, schematic of chemogenetic silencing of PRh projection to L1 of S1. AAV.hM4Di was injected to PRh and CNO was applied in L1 of S1 before the training started. Inset, magnified view of S1 marked in dashed box. **b)** Cumulative differences between hit and miss trials of control mice (n=20, black) and mice with chemogenetic suppression of PRh axons in L1 (n=12, hM4Di/CNO, red). **c)** Effect of PRh axonal suppression on normalized learning score during (left) and after learning (n=3, right, expert). Each dot corresponds to individual mice and black line represents the average. Wilcoxon rank-sum test against control, **p<0.01. Wilcoxon signed-rank test, n.s., not significant. **d)** Normalized learning scores of different controls for DREADD. Both CNO control group (hM4Di-/CNO+, n=7 mice) and hM4Di control group (hM4Di+/CNO-, n=3 mice) showed similar level of learning measured by learning score compared to wild-type group (hM4Di-/CNO-, n=10 mice). Kruskal-walis test, p=0.1. **e)** Cumulative differences between hit and miss trials of control mice (n=20, black) and Gpr26-cre mice with POm axonal suppression (n=7, POm-hM4Di, brown). **f)** Effect of POm axonal suppression on the normalized learning score. Wilcoxon rank-sum test, n.s., not significant.

3.3 Learning enhances the responsiveness of layer 5 pyramidal neurons to top-down inputs

3.3.1 Perirhinal input to layer 1 gates firing modulation in layer 5 pyramidal neurons during learning

The behavioral results suggest that perirhinal inputs influence neuronal activities in S1 to mediate learning. To investigate neurophysiological changes induced by learning and perirhinal input, we performed juxtacellular recordings in S1 while animals were trained to perform microstimulation detection task with and without chemogenetic suppression of perirhinal inputs to L1 of S1 (Figure 3.11a). Same as the behavioral experiments (Figure 3.10), we applied CNO in L1 of S1 in both control and hM4Di-expressing mice prior to the onset of the training session. Juxtacellular recording allowed us to monitor single neuron activity while mice were performing the task (Figure 3.11b-d). We focused on L5 pyramidal neurons in these experiments for several reasons. First, we supposed that the current injection through a microstimulation electrode placed in L5 affected the activity of L5 pyramidal neurons the most. Second, apical dendrites of L5 pyramidal neurons receive inputs from L1 including perirhinal input (Figure 3.9b). Third, L5 pyramidal neurons can integrate somatic and dendritic inputs (Larkum et al., 1999; Shai et al., 2015) and their firing patterns can signal coincidence of two input strems (Larkum, 2013). Lastly, L5 pyramidal neuorns are the major output units of the neocortex, which can broadast output of S1 to other brain areas (Harris and Shepherd, 2015; Shepherd, 2013). Therefore, any changes occurred in the local circuit would likely to be reflected on these neurons. For these reasons, we hypothesized that activity of L5 pyramidal neurons will be subjected to learning and perirhinal inputs.

We examined the spiking activity of L5 pyramidal neurons in S1 during hit trials, when perirhinal neurons enhance firing rate (Figure 3.8). Firing rate changes were quantified by z-score normalization to account for variable spontaneous firing rates. This analysis revealed a heterogeneous responses in this neuronal population (Figure 3.11e). For example, in neuron #34, strong upward modulation was followed by inhibition. On the contrary, neuron #29 showed initial inhibition and then excitation. Also, the timing of the modulation varied across neurons. Overall, we found that successful report of microstimulation modulated (both upward and downward) firing rate of 65% of recorded L5 pyramidal neurons (n=24/37

neurons) in control mice (n=5 mice) while only 33% of them (n=13/36 neurons) in hM4Di/CNO-treated mice (n=5 mice) were significantly modulated (Control vs. hM4Di/CNO, chi-square test, p=0.007; Figure 3.11e,g). At the population level, average firing rate of L5 pyramidal neurons in control mice increased after microstimulation although not statistically significantly (pre-stimulus 2.4±0.4 Hz vs. post-stimulus 3.3±0.7 Hz, n=42 neurons, Wilcoxon signed-rank test, p=0.7; Figure 3.11f). Average firing rate in hM4Di/CNO mice also did not change at the population level (pre-stimulus 1.8±0.4 Hz vs. post-stimulus 1.6±0.4 Hz, n=41 neurons, Wilcoxon signed-rank test, p=0.3; Figure 3.11h).

In vitro studies demonstrated that L1 inputs to apical dendrites could generate high-frequency burst firing in L5 pyramidal neurons, especially when it coincided with somatic inputs (Larkum et al., 1999; Schwindt & Crill, 1999; Williams & Stuart, 1999). To test if perirhinal inputs to L1 that target dendrites of L5 pyramidal neurons (Figure 3.9b) influence burst firing during learning, we examined the burst rate changes in the same population of L5 neurons. We found that significantly more L5 pyramidal neurons in control mice (47%, n=18/37 neurons) were modulated in their burst rate compared to neurons in hM4Di/CNO mice (22%, n=8/36 neurons, Control vs. hM4Di/CNO, chi-square test, p=0.02; Figure 3.11i,k). Interestingly, the average burst rate across control L5 pyramidal neurons was significantly enhanced following the microstimulation (pre-stimulus 0.1±0.03 Hz vs. post-stimulus 0.2±0.07 Hz, Wilcoxon signed-rank test, p=0.03; Figure 3.11j). Conversely, the average burst rate did not change in L5 pyramidal neurons in hM4Di/CNO mice, in which perirhinal input in L1 was downregulated (pre-stimulus 0.1±0.04 Hz vs. post-stimulus 0.1±0.03 Hz, Wilcoxon signed-rank test, p=0.8; Figure 3.11l). Taken together, the output of L5 pyramidal neurons is significantly modulated by learning and this modulation is gated by perirhinal input to L1. Notably, this process involves enhanced burst firing in both single cell and population level.

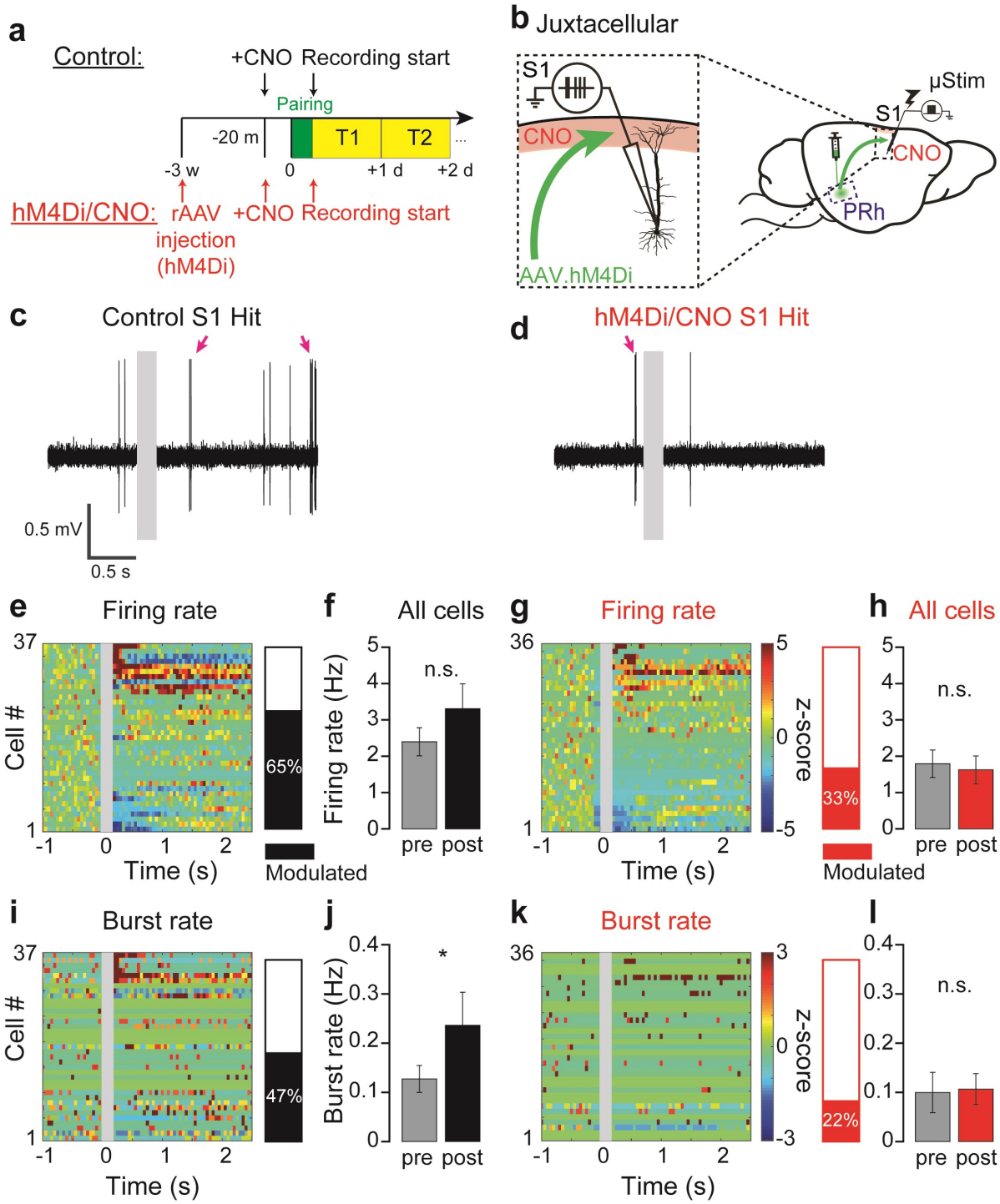

Figure 3.11. Learning-induced activity modulation in L5 pyramidal neurons is dependent on PRh input to L1. a) Timeline for juxtacellular recording during training. CNO was injected to both control and hM4Di groups 20 min before the training onset. T: training session. **b)** Schematics of juxtacellular recording with and without chemogenetic suppression of PRh axons in L1 of S1. **c, d)** Recording traces from an example neuron during a hit trial in control S1 and hM4Di/CNO S1, respectively. Arrows mark bursts. Gray box: μStim. **e)** Left, z-score normalized firing rate PSTHs of L5 pyramidal neurons in control S1. Note that z-scores for cells with no spikes during pre-stimulus period could not be computed and therefore not included in this analysis. Right, fraction of significantly modulated neurons in control S1. **f)** Population averaged firing rate of L5 pyramidal neurons in

control (n=42 cells from 5 mice) S1 during hit trials. **g)** Same as **e)** but for hM4Di/CNO S1. **h)** Same as **f)** but for hM4Di/CNO S1 (n=41 cells from 5 mice). **i)** Left, z-score normalized burst rate PSTHs of L5 pyramidal neurons in control S1. Cell number is identical to **e)** and cells with no burst events during pre-stimulus period are marked with zeros (green). Right, fraction of significantly modulated neurons in control S1. **j)** Population averaged burst rate of L5 pyramidal neurons in control S1 during hit trials. **k)** Same as **i)** but for hM4Di/CNO S1. **l)** Same as **j)** but for hM4Di/CNO S1. Wilcoxon signed-rank test, n.s., not significant, *p<0.05.

3.3.2 Emergence of highly bursting layer 5 pyramidal neurons following learning

We then asked if these modulations in firing responses of L5 pyramidal neurons are transient while learning depends on perirhinal input or remain even after perirhinal input does not affect the learned behavior. To answer this, we examined the firing activity of L5 pyramidal neurons in expert rats that were trained for >3 days. We compared their activities with naive rats that did not learn to associate the microstimulation and water reward in order to disentangle the effect of learning from microstimulation per se (Figure 3.12a). Here again we performed juxtacellular recordings to monitor firing activity of single L5 neurons while rats (n=30 rats) were performing the task (Figure 3.12b). The heterogenous responses observed during learning (Figure 3.11) settled into three distinctive profiles in expert animals (Figure 3.12c&e). Around 10% of L5 pyramidal neurons significantly enhanced firing responses (n=30 out of 273 cells, $L5^{ON}$; Figure 3.12g) while 40% of them significantly decreased (n=108 out of 27 cells, $L5^{OFF}$; Figure 3.12h) shortly after microstimulation (see Methods for classification). Rest of them (n=135 out of 273 cells, $L5^{NR}$;Figure 3.12i) did not show significant responses to microstimulation. Interestingly, increased firing responses in $L5^{ON}$ cells upon microstimulation was dominated by high-frequency burst firing (Figure 3.12e&g, pink). This pattern was not observed in naive rats (n=2 rats) where most of the neurons (95%, n=63 out of 66 cells, $L5^{NR}$) did not show significant change in their firing activity upon microstimulation (Figure 3.12d&f), suggesting that emergence of three subpopulations in expert rats is caused by learning but not by the microstimulation per se. In conclusion, learning correlates with the emergence of an ensemble of L5 pyramidal neurons ($L5^{ON}$) with enhanced burst firing.

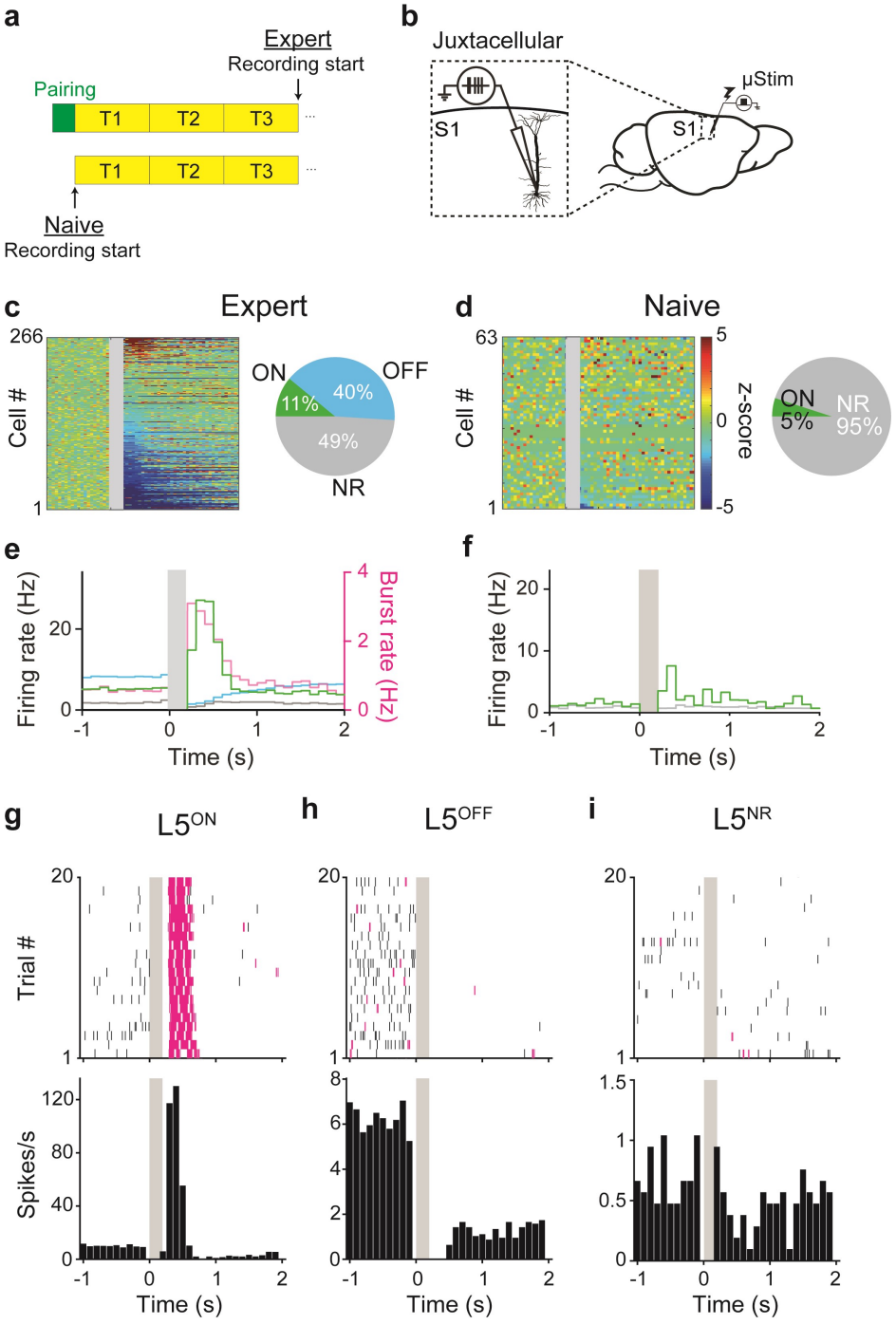

Figure 3.12. Emergence of three distinct subpopulations of L5 pyramidal neurons in S1 following learning. a) Timeline for juxtacellular recording in expert and naive rats. T: training session. **b)** Schematic of juxtacellular recording in S1 during µStim detection task. **c)** Left, z-score normalized PSTHs of L5 pyramidal neurons in expert rats (total n=273 cells) . Right, proportion of $L5^{ON}$, $L5^{OFF}$ and $L5^{NR}$ neurons in expert rats. Note that z-scores for cells with no spikes during pre-stimulus period could not be computed and therefore not included in this analysis. Gray box: µStim. **d)** Same as **c)** but in naive rats (total n=66 cells). **e)** Average PSTHs of each subpopulation in expert rats. Green: $L5^{ON}$, blue: $L5^{OFF}$, gray: $L5^{NR}$, gray box: µStim. **f**) Same as **e)** but in naïve rats. **g-i)** Raster plots and PSTHs from example $L5^{ON}$, $L5^{OFF}$ and $L5^{NR}$ neurons in expert rats. Black ticks: spikes, pink ticks: bursts. gray box: µStim.

3.3.3 Dendritic Ca^{2+} activity in layer 5 pyramidal neurons underlies memory formation

Persistent increase of burst firing in a subpopulation of L5 pyramidal neurons even after learning became independent of perirhinal inputs (Figure 3.12, $L5^{ON}$) led us to speculate that learning might involve enhancement of dendritic activity of L5 pyramidal neurons. To examine this, we expressed GCaMP6s in L5 pyramidal neurons using Rbp4-Cre transgenic mice (Gerfen et al., 2013). This transgenic mouse line expresses Cre-recombinase in L5 pyramidal neurons, enabling expression of Cre-conditional genes (in this case GCaMP6s) specifically in L5 pyramidal neurons. We measured Ca^{2+} transients in 318 apical dendrites (from n=4 mice) at a depth of ~150 μm from pia during the microstimulation detection task in expert mice (Figure 3.13a-e). A small proportion of dendrites exhibited substantial increase in Ca^{2+} activity following microstimulation (10%, 32 out of 318 dendrites, "ON" dendrites; see Methods for classification criteria). Another dendritic subpopulation significantly reduced Ca^{2+} fluorescence (37%, 118 out of 318 dendrites, "OFF" dendrites). The rest were not responsive to microstimulation (53%, 168 out of 318 dendrites "NR" dendrites). Similar proportions of $L5^{ON}$ cells and ON dendrites hinted that ON dendrites might belong to the $L5^{ON}$ cells displaying high burst rates. Tight coupling of dendritic and somatic activity in anesthetized (Helmchen et al., 1999) and awkae behaving animals (Beaulieu-Laroche et al., 2019; Francioni et al., 2019) support this hypothesis. Correlation of both enhanced burst firing and dendritic Ca^{2+} activity with learning suggests that memory formation leads to strengthening of responsiveness of L5 pyramidal neurons to apical dendritic inputs.

To test if learning to associate microstimulation and reward requires activation of dendritic Ca^{2+} activity, we aimed to suppress dendritic Ca^{2+} activity during training sessions. Unfortunately, there is no existing technique, to the best of our knowledge, that can unequivocally and specifically abolish dendritic Ca^{2+} activity in L5 pyramidal neurons without affecting other cellular and network activities. One of the best established methods previously used to suppress dendritic Ca^{2+} activity is to activate G-aminobutyric acid type B ($GABA_B$)–receptor by applying a $GABA_B$–receptor agonist, baclofen, to apical dendrites. A tight coupling between dendritic $GABA_B$ receptors and the dendritic Ca^{2+} channels (Pérez-Garci et al., 2006, 2013) enables efficient blocking of dendritic Ca^{2+} activity (Palmer et al., 2012; Suzuki & Larkum, 2017; Takahashi et al., 2016). We applied 50 μM baclofen every 20

min during the training session to the superficial layer (~150 µm from pia) of S1, where the Ca^{2+} spike initiation zone is located (Larkum & Zhu, 2002) (Figure 3.13f, upper). Blocking dendritic Ca^{2+} activity with baclofen significantly impaired learning (Figure 3.13g-h, blue; Baclofen 0.2±0.05, n=6 vs. control 0.5±0.06, n=20, Wilcoxon rank-sum test, p=0.01), indicating an important role of dendritic Ca^{2+} activity on memory formation. Next, we took a physiological approach recruiting an endogenous cortical circuitry that inhibits dendritic Ca^{2+} activity. Somatostatin (SST)-positive interneurons have been previously shown to suppress dendritic activity via $GABA_A$ receptor-mediated inhibition (Murayama & Larkum, 2009; Palmer et al., 2012; Wang et al., 2004). Moreover, other studies showed that disrupting SST+ interneurons results in preventing learning-induced plasticity and learning (Chen et al., 2015; Cichon & Gan, 2015; Makino & Komiyama, 2015; Williams & Holtmaat, 2019). We optogenetically activated SST+ interneurons expressing ChR2 with 465 nm LED light in SST::ChR2 transgenic mice (Fig. 3.14f, lower; see Methods). Activating SST+ interneuron circuits also prevented learning (SST -0.4±0.07, n=6 vs control 0.5±0.06, n=20, Wilcoxon rank-sum test, $p<0.001$; Figure 3.13g-h, purple). Therefore, dendritic Ca^{2+} activity is crucial for memory formation during microstimulation detection task. Altogether, these results suggest that active properties of dendrites are potential cellular mechanisms for neocortical memory formation. This mechanism can also account for the significance of top-down inputs targeting L1 on learning and the emergence of highly bursting L5 pyramidal neurons in traned animals.

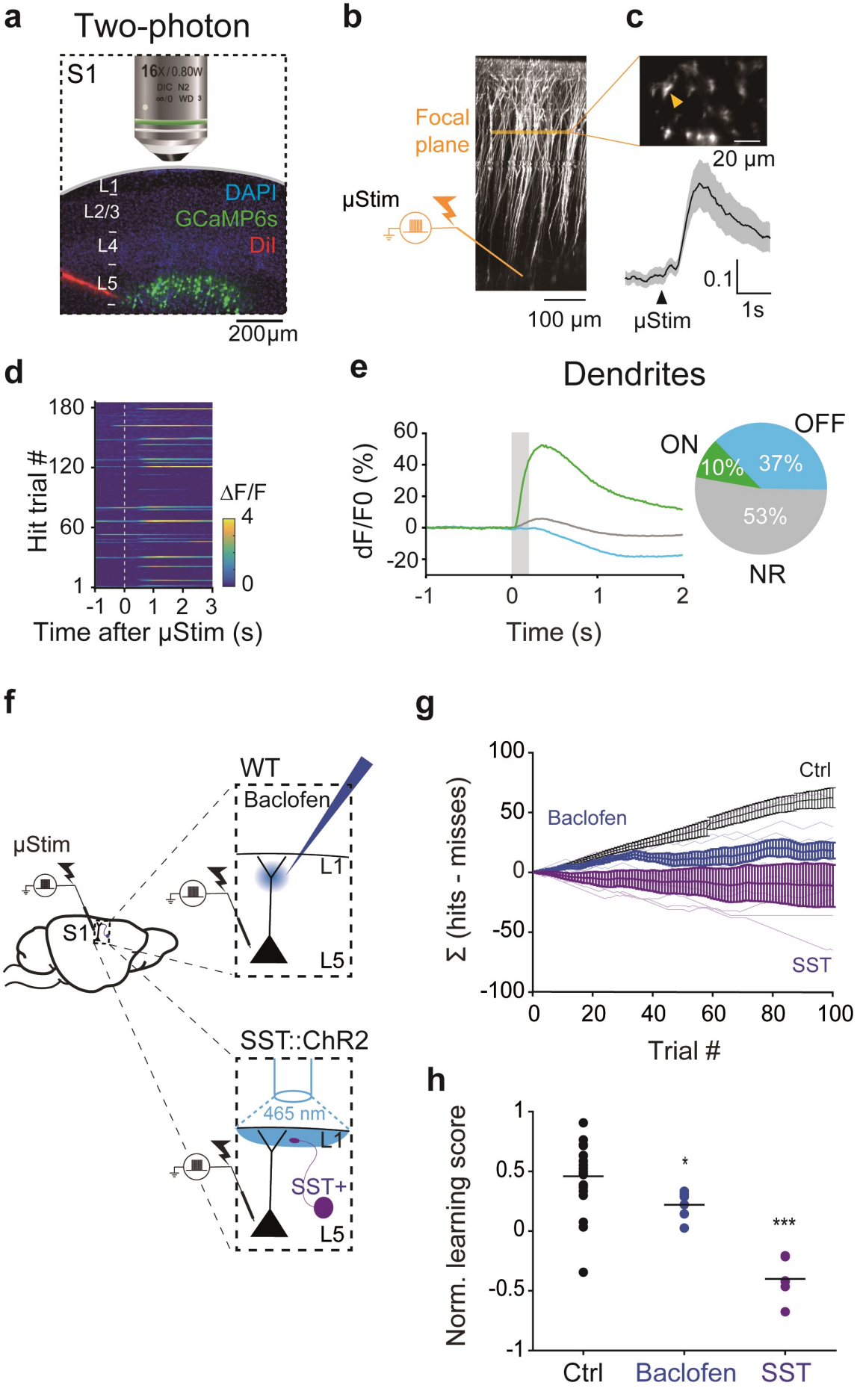
a
Two-photon
S1
16X/0.80W
DIC N2
∞/0 WD 3
L1
L2/3
L4
L5
DAPI
GCaMP6s
DiI
200μm
b
c
Focal plane
μStim
100 μm
20 μm
0.1
1s
μStim
d
Hit trial #
180
120
60
1
-1 0 1 2 3
Time after μStim (s)
ΔF/F
4
0
e
Dendrites
dF/F0 (%)
60
40
20
0
-20
-1 0 1 2
Time (s)
ON
OFF
10%
37%
53%
NR
f
WT
Baclofen
μStim
S1
L1
L5
SST::ChR2
465 nm
L1
SST+
L5
g
Σ (hits - misses)
100
50
0
-50
-100
0 20 40 60 80 100
Trial #
Ctrl
Baclofen
SST
h
Norm. learning score
1
0.5
0
-0.5
-1
*
***
Ctrl
Baclofen
SST

Figure 3.13. Dendritic Ca^{2+} activity of L5 pyramidal neurons is crucial for memory formation. a) Schematic of two-photon dendritic Ca^{2+} imaging during behavior. DiI trace shows the location of the microstimulation electrode. **b)** Z-stack image of recorded dendrites and µStim electrode in L5. **c)** Horizontal imaging plane (upper) (~150 µm from pia) and average (with s.e.m) Ca^{2+} responses (lower) for all trials from a dendrite marked with a yellow arrow. **d)** Ca^{2+} responses in an example apical dendrite marked in **c)** during µStim trials (n=180). **e)** Left, average peri-stimulus time Ca^{2+} responses in ON, OFF and NR dendrites (total n=318 dendrites) during hit trials. Gray box: µStim. Right, the fraction of ON, OFF and NS dendrites. **f)** Schematic of pharmacological and optogenetic manipulations of dendritic activity. Upper inset, application of baclofen in superficial layers of S1 in WT mice. Lower inset, optogenetic activation of SST+ interneurons during µStim detection task in SST::ChR2 transgenic mice. Blue light (465 nm) was shed on the surface of the craniotomy. **g)** Cumulative differences between hit and miss trials of control (n=20, black), baclofen-injected mice (n=6, blue) and SST::ChR2 mice (n=6, purple) during the first session. **h)** Normalized learning scores of control, baclofen-injected mice and SST::ChR2 mice at the first session. Each dot corresponds to individual mice and black line represents the average. Wilcoxon rank-sum test against control, *p<0.05, ***p<0.001.

Chapter 4. Discussion

The present study describes an MTL-neocortical pathway that mediates hippocampal-dependent learning and a potential cellular mechanism underlying neocortical memory formation via L1. Both inhibiting neuronal activity and the axonal output of the perirhinal cortex to L1 of S1 profoundly impaired learning but did not affect the performance of expert animals, suggesting that this pathway is crucial for memory formation but not sensory detection per se. Next, we found that learning to associate microstimulation with reward enhanced high-frequency burst firing in an ensemble of L5 pyramidal neurons in S1, which was dependent on perirhinal inputs to L1 of S1. Learning was also correlated with an enhancement of dendritic Ca^{2+} activity in L5 pyramidal neurons and suppressing dendritic Ca^{2+} activity resulted in learning impairment. We conclude that neocortical L1 is a crucial anatomical substrate for sensory association memory, channeling top-down contextual inputs that trigger dendritic Ca^{2+} spikes and burst firing in a sparse population of L5 pyramidal neurons (~10%).

4.1 Microstimulation detection task is a hippocampal-dependent learning paradigm

Prior to investigation on cellular mechanisms of neocortical memory formation, we first adapted and characterized the learning behavior of rats and mice during the microstimulation detection task. Intracortical microstimulation has been previously used in human, primate and rodent research to establish a causal link between neuronal activity and sensory perception (Houweling and Brecht, 2008; Newsome et al., 1990; Penfield and Rasmussen, 1950; Romo et al., 1998, 2000). While it is not possible to exactly describe the sensation evoked by sensory cortical stimulation in animals, human studies suggest that microstimulation in S1 induces tactile sensation that is comparable to sensation induced by natural stimuli (Penfield and Rasmussen, 1950). In rodents, microstimulation has been used at the initial step in an attempt to train rats to report single neuron stimulation (Doron et al., 2014; Houweling and Brecht, 2008). However, these studies did not investigate how animals initially learn to associate the cortical microstimulation and reward and mechanisms underlying this process.

In this study, we characterized learning behavior during the microstimulation detection task by assessing the behaviors of the two most popular rodent models: rats and mice. Both species displayed indistinguishable performance measured by several behavioral metrics (Figure 3.2-3.3), suggesting that this paradigm can be used in cross-species studies to investigate evolutionarily conserved neuronal mechanisms underlying their behaviors. In addition, the knowledge gained from one species could be generalized to the other. Even at low intensity (≤10 μA) trials, mice showed a comparable performance to rats (i.e. experts), suggesting that mice can also be trained to behaviorally report a weak cortical stimulation. Nevertheless, whether mice can detect single neuron stimulation, which uses several orders of magnitude lower than 10μA (Houweling et al., 2010), should be tested in the future. Even though two rodent species exhibited equivalent learning behaviors, there were also differences between them, namely, impulsiveness. Mice were generally more impulsive than rats, reflected in their licking behavior (Figure 3.2i). The high spontaneous licking resulted in longer inter-trial intervals since impulsive licking was mildly punished with a delay for the next trial to initiate (Figure 3.2j; see Methods). These results suggest that although both rats and mice can learn to behaviorally report microstimulation in the sensory cortex rapidly and robustly, their innate behavior such as impulsiveness can affect the session duration and performance depending on the task design. One possible prediction from this result is that increasing the delay between microstimulation and reward might be more difficult for mice to learn than for rats. Future experiments involving modified versions of this task should consider such factors in task design.

Characterizing behavior during this behavioral paradigm also allowed us to consider several modifications to optimize the task. For instance, both rats and mice exhibited much shorter reaction time than the maximum response window not only at the expert level (Figure 3.3c&e, microstimulation) but also already after the first training session (Figure 3.2g), indicating that response window can be shortened for more precise estimation of the performance. Consistent with this, long response window potentially overestimated the response rate to catch trials, where lick rate was measured while no stimulus was presented (Figure 3.3c&e, catch). Next, precise manipulation of stimulation patterns during the microstimulation detection task proposes a possibility to investigate perceptual learning, where discrimination of sensory stimuli improves through training (Seitz, 2017). By presenting stimuli with different intensities while coupling only one stimulus to reward, one

can investigate how training improves the animal's ability to distinguish a target stimulus from others and the underlying neuronal mechanisms in this process. In fact, this possibility is not limited to stimulus intensity but also other stimulus properties such as frequency and duration.

Using two models of disrupted hippocampal activity – transient inactivation of neuronal activity by application of sodium channel blocker and chronic disruption of hippocampal activity by inducing mouse-model of epilepsy – we showed that normal hippocampal activity is crucial for memory formation as well as for a stable long-term memory (Figure 3.5). Given that the hippocampus is well known to be involved in episodic memory formation and spatial navigation, it seemed surprising at the first sight that this simple sensory association learning is hippocampal dependent. Although hippocampal activity was not directly measured in this study, several studies reported tactile information processing in the hippocampus (Bellistri et al., 2013; Itskov et al., 2011; Pereira et al., 2007; Zhao et al., 2020). Pereira et al., recorded simultaneously in the Cornu Ammonis 1 (CA1) region of the hippocampus and S1 during passive whisker stimulation and active tactile discrimination task and found that CA1 neurons significantly responded to whisker stimulation. Another recent study showed that the hippocampus does not encode physical properties of stimuli per se but in conjunction with the animal's location and maintain the tactile information even after reward was given (Itskov et al., 2011). These results suggest that somatosensory information can be readily integrated into memory representation in the hippocampus. Future studies, directly monitoring hippocampal activity during the microstimulation detection task, will be able to elucidate how hippocampal neurons associate direct cortical stimulation and reward and how different subfields of the hippocampus contribute to this type of learning. Alternatively, the involvement of the hippocampus in the microstimulation detection task might be due to the temporal relationship between stimuli and reward in our paradigm, where reward was given only when animals responded at a certain time window. Neither premature licking (less than 0.1 s from the stimulus onset) nor delayed licking (more than 1.2 s from the stimulus onset) was rewarded (see Methods). This means that animals had to take an action in a defined time window by withholding the licking for at least 0.1 s and rapidly respond within 1.2 s. The hippocampus contains time cells supporting the tracking of the lapsed time from the stimulus onset, enabling animals to respond at the correct timing (MacDonald et al., 2011;

Pastalkova et al., 2008). Lastly, salient or novel events are shown to engage hippocampal activity (Dolan and Fletcher, 1997; Jafarpour et al., 2019; Kumaran and Maguire, 2006; Ranganath and D'Esposito, 2001). Although we speculate that microstimulation evokes a similar sensation induced by natural stimuli, the initial high intensity of microstimulation might induce a novel sensation that animals had never experienced before.

The microstimulation detection task possesses several advantages for memory research over other learning paradigms using natural stimuli. First, direct cortical stimulation bypasses multisynaptic pathways from whiskers to S1 (Feldmeyer et al., 2013; Petersen, 2007), minimizing brain circuits involved in learning and makes it easier to isolate neocortical contribution in learning and memory. Second, because the experimenter controls the stimulation pattern as well as the location and timing of current injection, this task allows defining the area of interest and the temporal window precisely, where and when the underlying neuronal mechanisms of memory formation can be examined. Specifically, this characteristic enables to scrutinize activity changes in the stimulated area during learning as well as to investigate the contribution of a specific input arriving in that area. Next, this task requires relatively short time (one session) to train animals, avoiding overtraining, during which different subjects could develop different strategies to learn the task. In conclusion, the microstimulation detection task is an effective learning paradigm for investigating interactions between MTL and neocortical memory systems as well as neuronal mechanisms of memory storage in the neocortex.

4.2 Neocortical layer 1 is a major anatomical target of memory

Our retrograde and anterograde tracing results indicate that the perirhinal cortex is the last output station of MTL system that directly projects feedback inputs to S1 (Figure 3.6-3.7). Notably, perirhinal axons strongly target L1 of S1 and specific inhibition of these axons in L1 resulted in a similar level of learning impairment as ipsilateral perirhinal inhibition with Na^+ channel blocker (Figure 3.8, 3.10). Therefore, a major output pathway of the MTL system to S1 is routed via the perirhinal cortex, which exerts its influence on neocortical L1 to mediate memory formation. The importance of perirhinal input to L1 on learning implies that this input might form memory by interacting with other long-range cortico-cortical inputs to L1 containing contextual information (Cauller, 1995). One implication of this

unique connectivity of L1 is that internal model (ex. memory) might be reflected in altered activity in this layer.

L1 contains local interneurons and dendrites of pyramidal neurons located in deeper cortical layers. ChR2-assisted functional mapping of the connectivity between the perirhinal cortex and L1 of S1 found that perirhinal axons target both L1 interneurons and dendrites of L5 pyramidal neurons (Figure 3.9a-b). Although we did not classify interneuron types receiving perirhinal inputs, previous studies reported that other L1-targeting long-range inputs (from M1 and POm) recruit vasoactive intestinal polypeptide (VIP)-expressing interneurons (Lee et al., 2013; Williams & Holtmaat, 2019). Another recent study that characterized neuron-derived neurotrophic factor (NDNF)-expressing interneurons found that the perirhinal cortex innervates this class of interneurons in L1 of A1, which display experience-dependent activity changes after learning (Abs et al., 2018). While VIP+ interneurons can disinhibit dendrites of pyramidal neurons by inhibiting dendrite-targeting SST+ interneurons (Pfeffer et al., 2013), NDNF+ interneuron can directly suppress dendritic activity via $GABA_B$ receptors (Abs et al., 2018). Although it is unclear how seemingly opposing effects (i.e. excitation and inhibition) contribute to dendritic activity during learning, this might be able to explain our two-photon imaging results that identified distinctive subpopulations of L5 pyramidal dendrites following learning. One group of dendrites strongly enhanced Ca^{2+} activity (ON dendrites) while another group showed strong negative responses (OFF dendrites) upon microstimulation (Figure 3.13e). Perirhinal inputs as well as other long-range inputs could potentially mediate this process by disinhibiting one group of dendrites by activating VIP+ neurons while inhibiting others by activating NDNF+ interneurons.

Although perirhinal input to L1 was necessary in learning, this input was not required once memory was formed (i.e. in experts) (Figure 3.10c, expert). Together with the fact that dendritic Ca^{2+} activity is enhanced in highly trained animals during sensory detection tasks (in our study and Takahashi et al., 2016&2020), this implies that other cortico-cortical inputs to L1 may as well have contributed to excitation of dendrites. Here we tested the contribution of another L1-targeting input originating in POm in learning (Figure 3.10e-f). Contrary to perirhinal input to L1, suppressing POm axonal activity in L1 using the same chemogenetic approach did not disrupt learning. One possible explanation is that since our paradigm bypasses the thalamus that normally delivers peripheral sensory input to S1,

thalamocortical circuits might not be strongly involved in the microstimulation detection task. In fact, rhythmic whisker stimulation that begins from the periphery has been shown to induce POm-dependent long-term potentiation in L2/3 pyramidal neurons (Gambino et al., 2014). Therefore, it is possible that POm inputs contribute to peripheral sensory perception and sensory learning that involves thalamo-cortical circuits (Audette et al., 2017). Alternatively, POm input to L1 might contribute to dendritic excitation in later stages of learning when learning becomes independent of perirhinal inputs. In addition to perirhinal and POm inputs, L1 receives long-range inputs from the motor cortex (both M1 and M2), S2, cingulate cortex, retrosplenial cortex and striatum (Figure 3.6; Aronoff et al., 2010; Petersen, 2019). These pathways can well be engaged during the microstimulation detection task and provide top-down inputs necessary to generate dendritic spikes in the later period. Based on these observations, we hypothesize that perirhinal inputs to L1 serves as a gating signal for the enhancement of cortico-cortical feedback inputs (Figure 4.1). The perirhinal cortex initially provides an instructive signal that allows synaptic plasticity between weak cortico-cortical inputs and dendrites to occur and this role becomes less required as cortico-cortical connections strengthen during memory consolidation. The instructive role of perirhinal inputs during learning might be replaced by prefrontal inputs for remote memory (Frankland and Bontempi, 2005). This hypothesis is in line with the systems memory consolidation model, which posits the role of the MTL system in strengthening connections between neocortical areas (Diekelmann and Born, 2010; Klinzing et al., 2019). Our study proposes that, at least in primary sensory areas, strengthening of cortico-cortical connections during memory consolidation occur primarily in L1.

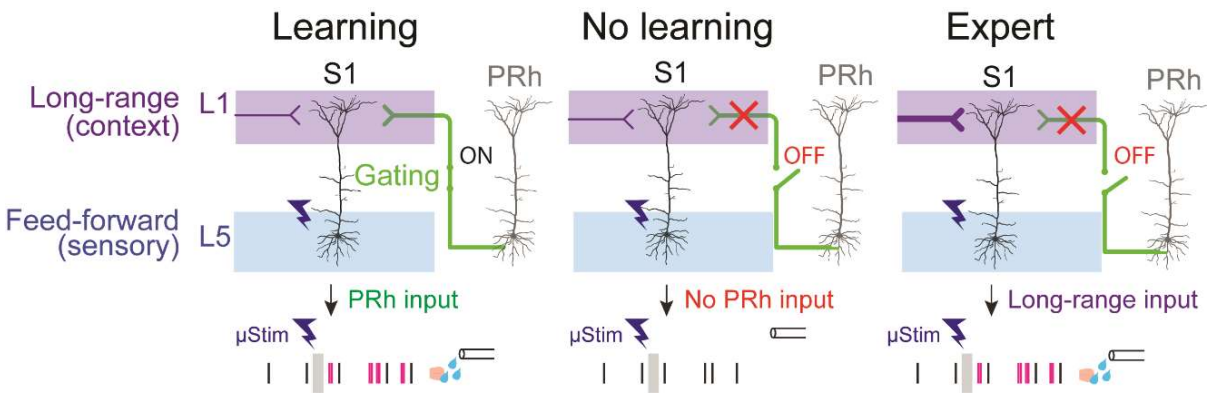

Figure 4.1. Gating model of neocortical memory formation. a) During learning, PRh input to L1 gates other cortico-cortical inputs to the same layer, which activate dendrites and induce burst firing upon a stimulus, leading to a successful behavior (licking). At this stage, cortico-cortical inputs are not strong enough to activate dendritic Ca^{2+} activity alone. **b)** When PRh input is blocked, cortico-cortical inputs are not able to activate dendrites and burst firing, resulting in unsuccessful behavior. **c)** After several days of training, cortico-cortico inputs are strengthened (i.e. memory consolidation) and do not require PRh input to activate dendrites and burst firing.

Nevertheless, we should consider other possibilities why perirhinal axonal inhibition did not affect trained animals. First, as seen from anterograde tracing, the perirhinal cortex does not only send axons to L1 but also to deeper layers. Thus, it is possible that inputs in deeper layers can compensate for the L1 pathway when it is not functional. Second, we cannot rule out the possibility that chemogenetic inhibition by CNO was not complete. Although we attempted to inhibit the entire cranial window, a few axons could have survived our manipulation and a small population of these axons might have been sufficient to mediate learning but at a slower rate. Lastly, information from the MTL system might recruit other pathways bypassing the perirhinal cortex to arrive S1. For example, the retrosplenial cortex is directly connected to the hippocampus (via subiculum) and to S1, positioned similarly to the perirhinal cortex (Figure 3.6; Cenquizca & Swanson, 2007; Nitzan et al., 2020). In addition, the entorhinal cortex sends weak projections to S1 as well (Kerr et al., 2007). Further experiments are required to examine how diverse L1 inputs differentially contribute to memory formation in the neocortex.

4.3 The potential role of dendrites in learning and memory

What is the cellular mechanism of memory formation mediated by L1 inputs? One of the major cellular targets of L1 inputs is apical dendrites of L5 pyramidal neurons (Ramaswamy and Markram, 2015). In this study, we have provided several lines of evidence that dendritic Ca^{2+} activity plays a key role in learning. First, chemogenetic suppression of perirhinal input to L1 impaired learning and reduced burst responses in L5 pyramidal neurons (Figure 3.11). Tight coupling between somatic burst firing and dendritic Ca^{2+} activity in awake behaving animals (Beaulieu-Laroche et al., 2019; Francioni et al., 2019) implies that down-regulation of perirhinal input to L1 reduced dendritic Ca^{2+} activity in these neurons as well. Indeed, the estimation of chemogenetic effect revealed that this manipulation mostly

affected the apical dendritic compartment of L5 pyramidal neurons (Figure 3.9i), where it receives perirhinal input (Figure 3.9b). In addition, *in vitro* studies demonstrated that burst firing can be caused by apical dendritic inputs and dendritic spikes (Helmchen et al., 1999; Larkum et al., 1999; Larkum & Zhu, 2002; Pérez-Garci et al., 2006). Therefore, perirhinal inputs must have controlled somatic burst firing by activating dendritic activity in L5 pyramidal neurons. Second, baclofen application, which has been shown to effectively abolish dendritic Ca^{2+} spikes (Palmer et al., 2014; Suzuki & Larkum, 2017; Takahashi et al., 2016), caused learning impairments (Figure 3.13g-h, blue). Finally, optogenetic activation of dendrite-targeting SST+ interneuron also resulted in disruption of learning (Figure 3.13g-h, purple). Taken together, these results suggest that a key process of learning entails active dendritic mechanisms modulated by L1 inputs.

How do active dendrites contribute to memory formation and consolidation? First, dendritic spikes are highly implicated in synaptic plasticity. A single burst-event induced by dendritic spikes in CA1 neurons has been shown to potentiate synaptic strength for few hours (Remy and Spruston, 2007). Another recent study in the hippocampus characterized a new synaptic plasticity rule, termed behavioral timescale synaptic plasticity (BTSP) (Bittner et al., 2015, 2017; Zhao et al., 2020). This rule is governed by dendritic plateau potentials, which support a few second-long plasticity window that is several magnitudes longer than Hebbian plasticity (Bittner et al., 2017). Intriguingly, BSTP mediates place field formation in CA1 pyramidal neurons, which display similar long-lasting high frequency bursts to those we observed in L5 pyramidal neurons during and after learning (Figure 3.11&3.12). Consistent with the observation by Bittner et al., two-photon imaging of CA1 dendrites in mice performing spatial task in virtual reality revealed that local dendritic spikes underlie place cell formation (Sheffield and Dombeck, 2019, 2015). It is tempting to speculate that a similar plasticity mechanism might underlie this remarkable resemblance displayed in the hippocampus and S1 pyramidal neurons' firing behavior during learning. Second, theoretical studies illustrated that active dendritic mechanisms increase the memory capacity. Poirazi and Mel showed that compartmentalized dendrites with non-linear integration could learn 46 times more number of patterns than dendrites with linear integration in yes/no recognition task (Poirazi and Mel, 2001). This model opened a possibility that memory information can be stored not only in synaptic connections between neurons but also at a subcellular level. In line with this, brain areas in the frontal lobe that are considered to be

highly associated with long-term memory contain pyramidal neurons with more complex dendritic arborizations than posterior sensory areas (Elston, 2000). These results suggest that non-linear integration by active dendrites can support synaptic plasticity required for memory formation as well as long-term storage of memory information.

Synaptic plasticity for long-term memory require new protein synthesis (Kandel, 2001; Shrestha et al., 2020) that mediates structural changes (Bailey & Kandel, 1993; Hofer et al., 2009; Xu et al., 2009). As dendrites receive the majority of synaptic inputs (Larkman, 1991) and undergo experience-dependent structural changes such as new spine formation (Li et al., 2017; Yang et al., 2014), it is likely that protein synthesis in dendrites plays a significant role in memory storage. Indeed, messenger RNA and ribosomes were found in distal dendrites, indicating a local protein translation (Holt et al., 2019; Martin et al., 1997). Local protein synthesis ensures rapid induction of long-term plasticity in subcellular compartments, which would otherwise take a few hours to days to traffic proteins from the soma (~1 μm/s) (Griffin et al., 1976). This process also undergoes experience-dependent regulations (Sambandan et al., 2017). Recent advances in single-molecule imaging and metabolic labeling methods can detect newly synthetized proteins in a particular neuronal compartment, for instance in dendrites (Holt et al., 2019), opening a possibility to identify proteins translated by learning and investigating their specific role in long-term memory. Furthermore, blocking local protein synthesis specifically in distal and apical dendrites will be instrumental for probing the crucial role of this cellular compartment for memory storage.

4.4 Cellular correlates of memory in the neocortex

Neuronal responses could differ in response to the same bottom-up sensory inputs depending on the context provided by top-down inputs, leading to different behavioral responses. Our results indicate that top-down MTL inputs (via the perirhinal cortex) to L1 gates learning-induced modulation of L5 pyramidal neuronal responses (Figure 3.11). Heterogeneous responses of L5 pyramidal neurons developed into three distinctive classes following learning, in particular in a subset of L5 pyramidal neurons exhibiting enhanced dendritic Ca^{2+} activity and burst firing to the same cortical stimulation aimed at the soma (Figure 3.12&3.13). These results suggest that memory formation in the neocortex (i.e. not dependent on perirhinal input) enhances responsiveness of L5 pyramidal neurons to distal dendritic inputs. What synaptic processes might occur during learning to mediate these

changes? First, the amplitude of distal dendritic inputs can be potentiated by synaptic plasticity in upstream areas that project to L1. Indeed, we found that perirhinal axons increase activity following the first training session (Figure 3.8f). Consistent with this, axonal activity of the retrosplenial cortex in L1 of V1 (Makino and Komiyama, 2015) was shown to increase after learning. Second, synapses between L1 inputs and distal dendrites can be strengthened. *In vitro* studies showed that distal synapses potentiate when distal dendritic inputs are paired with burst firing (Froemke et al., 2010; Letzkus et al., 2006; Sjöström & Häusser, 2006). Since L5 pyramidal neurons showed increased burst firing during learning, it is likely that distal synapses with perirhinal or other L1 inputs were potentiated. Moreover, L1 inputs have been shown to induce heterosynaptic plasticity, in which strengthening synaptic connections is indirectly induced by neighboring synapses (Chistiakova and Volgushev, 2009). For example, POm inputs to L2/3 apical dendrites in L1 can gate synaptic plasticity between L2/3 and L4 pyramidal neurons, while POm synapses with L2/3 remain unchanged (Williams & Holtmaat, 2019). Similarly, a recent neuronal model reflecting active dendritic properties suggests that L1 inputs targeting distal dendrites can provide a teaching signal that determines the sign of long-term plasticity in perisomatic synapses by inducing burst firing (Payeur et al., 2020).

As discussed above, one of the major consequences of dendritic Ca^{2+} spikes is burst firing. Especially, long-lasting bursts can be induced when distal dendritic inputs and somatic inputs coincide in a same L5 pyramidal neuron *in vitro* (Larkum et al., 1999). Based on this observation, a recent hypothesis implicated L5 pyramidal neuron as an association unit in the neocortex (Larkum, 2013). Termed backpropagation-activated Ca^{2+} spike (BAC) firing hypothesis, this hypothesis suggests that association of feedback inputs and feedforward inputs can occur at the cellular level, in which coincidence of two information streams will be expressed as high-frequency burst firing in the soma. Consistent with this hypothesis, we observed that burst firing was reduced when distal dendritic input (perirhinal input to L1) was inhibited while somatic input (microstimulation) remained constant, suggesting that bursts might be a product of coincidence detection during learning. Downregulating perirhinal input to L1 not only reduced burst firing but also impaired learning (Figure 3.10b-c, hM4Di/CNO), implying that a key aspect of learning is providing top-down inputs to L5 pyramidal neurons.

Moreover, BAC firing hypothesis predicts that burst firing can serve as an indicator for neurons participating in conscious behavior. Interestingly, we found a subset of L5 pyramidal neurons ($L5^{ON}$) exhibiting enhanced burst firing (Figure 3.12). Although we did not directly test if $L5^{ON}$ cells store memory (i.e. whether artificial activation of theses neurons retrieve memory), our study signifies a potential role of bursts as a way of neural communication employed by the neocortical neurons to represent memory. Indeed, burst coding has been suggested to provide extra information than single isolated spikes (Lisman, 1997). A recent study showed that bursts in subicular bursting neurons contain more spatial information than isolated spikes (Simonnet and Brecht, 2018), corroborating this hypothesis. Several studies suggested how bursts facilitates an efficient neural communication. For example, increased burst firing can drive postsynaptic neurons more reliably by synaptic facilitation (Malinow et al., 1994; Stevens and Wang, 1995) and non-linear integration of EPSPs in postsynaptic neurons (Thomson, 2000). Therefore, bursts could induce stronger sensation or behavioral response by activating downstream areas robustly. In line with this, irregular action potentials containing bursts have been shown to be more detectable by rats (Doron et al., 2014). Furthermore, burst coding has been suggested to provide an additional computational power such as multiplexing (Naud and Sprekeler, 2018). According to this model, bottom-up and top-down information can be simultaneously broadcasted by ensemble event rate and burst probability, respectively. In fact, correlation of burst firing and cognitive functions is not limited to S1 pyramidal neurons. For instance, a recent study found that a small population of L2/3 pyramidal neurons in A1 display high-frequency burst firing following sensory association learning (Wang et al., 2020). In addition, CA1 pyramidal neurons fire in bursts during place field formation (Bittner et al., 2015).

Overall, our results suggest that memory is formed by upregulating responsiveness of L5 pyramidal neurons to top-down inputs arriving distal dendrites, which can powerfully modulate neuronal responses to sensory stimuli by triggering dendritic spikes. Our results corroborate the BAC firing hypothesis that predicted cellular correlates of memory can be identified by examining their firing patterns (i.e. bursts). Based on our results and others, we hypothesize that high-frequency burst firing in an ensemble of L5 pyramidal neurons can efficiently reinstate memory traces and retrieve learned behavior.

4.5 Memory traces in different neocortical hierarchies

Conventionally, memory research has focused on higher-order association areas (Eichenbaum, 2000; Frankland and Bontempi, 2005) and somewhat overlooked primary sensory areas. This view is based on previous studies using immediate early genes (IEGs; ex. c-fos, zif268, arc/arg3.1 and homer), often used as a marker for synaptic plasticity owing to their activity-dependent expression (Guzowski et al., 2005). These studies found that remote fear memory recall (≥30 days after the first experience) engages medial prefrontal cortex, parietal cortex and retrosplenial cortex (Maviel et al., 2004; Wheeler et al., 2013). Inhibiting these areas impaired remote memory recall (Frankland et al., 2004; Todd and Bucci, 2015; Todd et al., 2016) and activating neurons in these regions could elicit memory recall (Cowansage et al., 2014), confirming their role in long-term memory. In contrast, the present study demonstrated that MTL inputs to the primary sensory cortex is crucial for memory formation.

Interestingly, while monitoring brain-wide memory traces underlying fear memory, Wheeler et al., observed an increased number of Fos-expressing neurons in S1 after remote memory retrieval compared to recent memory recall, although it did not fulfill the author's criteria for the reliable contribution (Wheeler et al., 2013). Therefore, primary sensory areas can be engaged in long-term memory as well. In the present study, we found highly responsive neurons in S1, which emerged after animals were trained for several days, at the stage when learning became independent of perirhinal inputs (Figure 3.12). These neurons in primary sensory areas were found only after a few days of training but they might maintain their activity for longer-term (≥30 days) to support remote memory. However, it is worth noting that neuronal populations identified by electrophysiological properties might not completely overlap with those defined by IEG expression. For instance, expression of IEGs often occur slowly (Josselyn et al., 2015) and Fos-labeling might not able to detect all $L5^{ON}$ neurons.

While our study provides several lines of evidence for memory trace in S1, how diffused memory traces in the neocortex are represented and processed at different hierarchical levels remains to be answered. First, how do multiple memory traces in different brain areas distinctively contribute to memory? As suggested previously for prefrontal cortex (Frankland and Bontempi, 2005; Wiltgen et al., 2004), higher-order association areas with their widespread connections with other neocortical areas might

integrate and coordinate activities in distributed neocortical memory traces rather than directly encode the contents of the memory. Instead, specific sensory features of memory might reside in primary sensory areas. Similarly, index theory suggested that hippocampal information might serve as an an index to neocortical activity pattern that is associated with an episode (Teyler and DiScenna, 1986; Teyler and Rudy, 2007). Second, how do sparse and distributed memory traces communicate each other to form a cohesive memory? Our results suggest that cortico-cortical projections to L1, strengthened during memory consolidation, might trigger burst firing in a specific set of neurons. These cortico-cortical inputs from multiple memory traces might be coordinated by higher-order areas and provide a contextual information to sensory areas and activate an ensemble of neurons associated with sensory features coupled to that context. Finally, primary sensory areas and higher-order areas might require different duration to develop memory traces. Primary sensory areas might form memory traces faster than higher-order areas or vice versa. Future studies monitoring multiple cortical areas simultaneously for long-term will be able to characterize the time course of neural representations of memory as well as their interactions.

4.6 Limitation of the present study

The findings of this study have to be seen in light of several limitations. First, a learning paradigm using artificial stimuli requires further examinations to find out whether the same circuit and cellular mechanisms are responsible for natural learning behavior. For example, our behavioral paradigm using direct cortical stimulation bypasses thalamocortical sensory pathways. It is probable that subcortical and thalamocortical pathways also contribute to learning using peripheral sensory stimuli (Audette et al., 2019; Gambino et al., 2014; Williams and Holtmaat, 2019). However, multiple pathways reaching the neocortex from the periphery can obscure the contribution of the neocortex on learning by redundant processing and the microstimulation detection task provides an advantage over other learning paradigms using peripheral stimulus in this sense. Next, in real-life situations learning and memory often involves different sensory modalities rather than a single modality used in this paradigm. Further studies are required to examine if the same circuit and cellular mechanisms described in this study are also employed in more ethological

learning paradigms requiring multimodal sensory processing and how different circuits interact to mediate multimodal memory formation.

Another limitation pertains to the recording method we used to measure neuronal activity during learning. We used juxtacellular recording that allowed us to measure single-neuron activity at high resolution. While this method allowed us to isolate spikes from a single neuron at high fidelity and especially enabled a reliable burst analysis, it could not offer us to investigate neuronal interactions during learning because we could record only one cell at a time. Given recent views regarding neuronal ensemble coding (Buzsáki, 2010; Harris, 2005; Luczak et al., 2015; Yuste, 2015), it would be interesting to investigate how a subpopulation of $L5^{ON}$ neurons we observed here represent high-dimensional memory information and how they interact with each other.

Furthermore, we confined our recordings primarily in L5 for several reasons discussed earlier (see Results section 3.3) (Larkum, 2013). This does not mean that we excluded a possibility that neurons in other layers or interneurons do not contribute to memory. In fact, it would be of a great interest to record different layers simultaneously and investigate how different layers contribute to memory formation and represent memory in different ways, for example, using a silicon probe (also see Outlook). This method will also allow us to record the same population for long-term, making it possible to track activity changes in the same neurons at different learning stages.

Finally, our behavioral paradigm consisted of continuous behavioral epochs. Thus, we were not able to disentangle the neuronal activity caused by different behavioral states such as stimulus receiving, decision making and reporting (licking). Developing a behavioral paradigm with separate epochs will make training more difficult and longer but will enable us to disentangle the contribution of each behavioral state.

4.7 Outlook

It is commonly regarded that transfer of memory from the MTL system to the neocortex primarily happens during offline periods (i.e. immobile or sleep) and often referred to as memory consolidation in order to distinguish it from memory encoding in the hippocampus during online periods (Buzsáki, 1989). The interaction between the medial temporal system and neocortex plays a pivotal role in memory consolidation (Born, 2010; Diekelmann and Born, 2010; Klinzing et al., 2019). Our study suggests that this interaction is

also essential during online memory formation stage, as blocking output of the medial temporal system (i.e. the perirhinal cortex) to S1 during training impaired learning. We also showed that this interaction occur through a particular layer of the neocortex, L1. It is tempting to speculate that L1 is also a target of offline memory consolidation. In agreement with this hypothesis, a recent study showed that top-down input from M2 to L1 of S1 during NREM sleep supports memory consolidation (Miyamoto et al., 2016). In addition, dendritic Ca^{2+} activity has been shown to increase during sleep spindles, cortical oscillations coupled to hippocampal SWRs (Seibt et al., 2017). Another study showed that dendrite-targeting SST+ interneurons decrease activity during spindles, releasing dendrites from inhibition (Niethard et al., 2018). More direct evidence for the role of L1 and dendritic Ca^{2+} activity in offline memory consolidation could be provided by simultaneous recording of dendritic activity in S1 and spiking activity and local field potential in the perirhinal cortex or/and hippocampus during sleep. Under those settings, one could investigate the coupling of L1 activity to sleep oscillations tightly associated with memory consolidation such as spindles and SWRs and provide insights into how these oscillations create favorable conditions for memory consolidation.

Another outstanding question is how different cortical layers contribute to memory processing and at different stages. Although our study focused on the role of L5 pyramidal neurons in learning and memory, L2/3 pyramids might contribute to long-term memory as well (Li et al., 2019; Xie et al., 2014). In accordance with this hypothesis, immediate early gene expression levels redistribute from deep layers to superficial layers in the parietal cortex as the memory becomes remote (Maviel et al., 2004). Examination of laminar reorganization during memory consolidation in primary sensory areas will shed light on our understanding in the contribution of each cortical layer in long-term memory.

Finally, our study focused on changes occur at the single neuron level while recent advancement in multi-unit recording techniques and spike sorting algorithms emphasizes the significance of neural ensemble coding, in which a group of neurons encode abstract representations (Buzsáki, 2010; Harris, 2005; Yuste, 2015). In this perspective, memory is represented by a group of neurons (ex. engrams) rather than by a single neuron. In fact, our study also found that a small subpopulation of neurons (~10% $L5^{ON}$ cells) actively respond to reward-associated stimuli (Figure 3.12). Based on our results presented here, it is tempting to speculate that formation of neural ensembles encoding a particular memory

communicate via burst firing during memory retrieval. Recording somatic activities of the entire population of $L5^{ON}$ neurons using two-photon microscopy or multi-unit recording will be able to reconcile knowledge from single neuron level and population level. More specifically, these methods can establish more direct relationship between memory and burst firing in $L5^{ON}$ cells. For example, one could examine if bursts correlate with different level of learning and then if bursts rate returns to baseline after the animal is detrained.

Abbreviations

µStim	Microstimulation
A1	Primary auditory cortex
AAV	Adeno-associated virus
AP	Anterioposterior axis
BAC	Back-propagation-activated Ca^{2+} spike
bAP	Back-propagating action potential
BTSP	Behavioral timescale synaptic plasticity
CA1	Cornu Ammonis 1
CB	Chicago Sky Blue
ChR2	Channelrhodopsin 2
CNO	Clozapine-N-Oxide
CS	Conditioned stimulus
DREADD	Designer Receptors Exclusively Activated by Designer Drugs
DV	Dorsoventral axis
EPSC	Excitatory postsynaptic current
EYFP	Enhanced Yellow Fluorescent Protein
FB	Fast blue
$GABA_B$	G-aminobutyric acid type B
GFP	Green Fluorescent Protein
HPC	Hippocampus
IEG	Immediate Early Gene
ITI	Inter-trial interval

L	Layer
M1	Primary motor cortex
M2	Secondary motor cortex
ML	Mediolateral axis
MTL	Medial temporal lobe
NDNF	Neuron-derived neurotrophic factor
NMDA	N-Methyl-D-aspartic acid
PFA	Paraformaldehyde
POm	Posterior medial nucleus
PRh	Perirhinal cortex
PSTH	Peri-stimulus time histogram
rf	Rhinal fissure
ROI	Region of interest
RT	Reaction time
s.e.m.	Standard error mean
S1	Primary somatosensory cortex
S2	Secondary somatosensory cortex
SD	Standard deviation
SST	Somatostatin
SWR	Sharp-wave ripple
V1	Primary visual cortex
VIP	Vasoactive intestinal polypeptide

References

Abs, E., Poorthuis, R.B., Apelblat, D., Conzelmann, K.-K., Spiegel, I., and Letzkus, J.J. (2018). Learning-Related Plasticity in Dendrite-Targeting Layer 1 Interneurons. Neuron *100*, 684–699.

Agster, K.L., and Burwell, R.D. (2009). Cortical efferents of the perirhinal, postrhinal, and entorhinal cortices of the rat. Hippocampus *19*, 1159–1186.

Alvarez, P., and Squire, L.R. (1994). Memory consolidation and the medial temporal lobe: a simple network model. Proc. Natl. Acad. Sci. *91*, 7041–7045.

Antic, S.D., Zhou, W.L., Moore, A.R., Short, S.M., and Ikonomu, K.D. (2010). The decade of the dendritic NMDA spike. J. Neurosci. Res. *88*, 2991–3001.

Aronoff, R., Matyas, F., Mateo, C., Ciron, C., Schneider, B., and Petersen, C.C.H. (2010). Long-range connectivity of mouse primary somatosensory barrel cortex. Eur. J. Neurosci. *31*, 2221–2233.

Audette, N.J., Urban-Ciecko, J., Matsushita, M., and Barth, A.L. (2017). POm Thalamocortical Input Drives Layer-Specific Microcircuits in Somatosensory Cortex. Cereb. Cortex 1–17.

Audette, N.J., Bernhard, S.M., Ray, A., Stewart, L.T., and Barth, A.L. (2019). Rapid Plasticity of Higher-Order Thalamocortical Inputs during Sensory Learning. Neuron *103*, 277–291.

Bailey, C.H., and Kandel, E.R. (1993). Structural Changes Accompanying Memory Storage. Annu. Rev. Physiol. *55*, 397–426.

Bakin, J.S., and Weinberger, N.M. (1990). Classical conditioning induces CS-specific receptive field plasticity in the auditory cortex of the guinea pig. Brain Res. *536*, 271–286.

Beaulieu-Laroche, L., Toloza, E.H.S., Brown, N.J., and Harnett, M.T. (2019). Widespread and Highly Correlated Somato-dendritic Activity in Cortical Layer 5 Neurons. Neuron *103*, 235–241.

Bellistri, E., Aguilar, J., Brotons-Mas, J.R., Foffani, G., and de la Prida, L.M. (2013). Basic

properties of somatosensory-evoked responses in the dorsal hippocampus of the rat. J. Physiol. *591*, 2667–2686.

Bittner, K.C., Grienberger, C., Vaidya, S.P., Milstein, A.D., Macklin, J.J., Suh, J., Tonegawa, S., and Magee, J.C. (2015). Conjunctive input processing drives feature selectivity in hippocampal CA1 neurons. Nat. Neurosci. *18*, 1133–1142.

Bittner, K.C., Milstein, A.D., Grienberger, C., Romani, S., Magee, J.C., and Magee, J.C. (2017). Behavioral timescale synaptic plasticity underlies CA1 place fields. Science *1036*, 1033–1036.

Bontempi, B., Laurent-Demir, C., Destrade, C., and Jaffard, R. (1999). Time-dependent reorganization of brain circuitry underlying long-term memory storage. Nature *400*, 671–675.

Born, J. (2010). Slow-wave sleep and the consolidation of long-term memory. World J. Biol. Psychiatry *11*, 16–21.

Brodt, S., Gais, S., Beck, J., Erb, M., Scheffler, K., and Schönauer, M. (2018). Fast track to the neocortex: A memory engram in the posterior parietal cortex. Science *362*, 1045–1048.

Burwell, R.D. (2006). The Parahippocampal Region: Corticocortical Connectivity. Ann. N. Y. Acad. Sci. *911*, 25–42.

Burwell, R.D., Witter, M.P., and Amaral, D.G. (1995). Perirhinal and postrhinal cortices of the rat: A review of the neuroanatomical literature and comparison with findings from the monkey brain. Hippocampus *5*, 390–408.

Buzsáki, G. (1989). Two-stage model of memory trace formation: A role for "noisy" brain states. Neuroscience *31*, 551–570.

Buzsáki, G. (2010). Neural Syntax: Cell Assemblies, Synapsembles, and Readers. Neuron *68*, 362–385.

Buzsáki, G., and Tingley, D. (2018). Space and Time: The Hippocampus as a Sequence Generator. Trends Cogn. Sci. *22*, 853–869.

Cauller, L. (1995). Layer I of primary sensory neocortex: where top-down converges upon

bottom-up. Behav. Brain Res. *71*, 163–170.

Cauller, L.J., Clancy, B., and Connors, B.W. (1998). Backward cortical projections to primary somatosensory cortex in rats extend long horizontal axons in layer I. J. Comp. Neurol. *390*, 297–310.

Cenquizca, L.A., and Swanson, L.W. (2007). Spatial organization of direct hippocampal field CA1 axonal projections to the rest of the cerebral cortex. Brain Res. Rev. *56*, 1–26.

Chen, J.L., Margolis, D.J., Stankov, A., Sumanovski, L.T., Schneider, B.L., and Helmchen, F. (2015). Pathway-specific reorganization of projection neurons in somatosensory cortex during learning. Nat. Neurosci. *18*, 1101–1108.

Chistiakova, M., and Volgushev, M. (2009). Heterosynaptic plasticity in the neocortex. Exp. Brain Res. *199*, 377–390.

Chrobak, J.J., and Buzsáki, G. (1996). High-frequency oscillations in the output networks of the hippocampal-entorhinal axis of the freely behaving rat. J. Neurosci. *16*, 3056–3066.

Cichon, J., and Gan, W.-B. (2015). Branch-specific dendritic Ca^{2+} spikes cause persistent synaptic plasticity. Nature *520*, 180–185.

Clark, R.E., Broadbent, N.J., and Squire, L.R. (2005). Hippocampus and remote spatial memory in rats. Hippocampus *15*, 260–272.

Cowansage, K.K., Shuman, T., Dillingham, B.C., Chang, A., Golshani, P., and Mayford, M. (2014). Direct Reactivation of a Coherent Neocortical Memory of Context. Neuron *84*, 432–441.

D'Souza, R.D., and Burkhalter, A. (2017). A laminar organization for selective cortico-cortical communication. Front. Neuroanat. *11*, 71.

Diekelmann, S., and Born, J. (2010). The memory function of sleep. Nat. Rev. Neurosci. *11*. 114–126.

Dolan, R.J., and Fletcher, P.C. (1997). Dissociating prefrontal and hippocampal function in episodic memory encoding. Nature *388*, 582–585.

Doron, G., von Heimendahl, M., Schlattmann, P., Houweling, A.R., and Brecht, M. (2014). Spiking Irregularity and Frequency Modulate the Behavioral Report of Single-Neuron Stimulation. Neuron *81*, 653–663.

Douglas, R.J., and Martin, K.A.C. (2004). Neuronal circuits of the neocortex. Annu. Rev. Neurosci. *27*, 419–451.

Douglas, R.J., Koch, C., Mahowald, M., Martin, K.A.C., and Suarez, H.H. (1995). Recurrent excitation in neocortical circuits. Science *269*, 981–985.

Dudai, Y., Karni, A., and Born, J. (2015). The Consolidation and Transformation of Memory. Neuron *88*, 20–32.

Eichenbaum, H. (2000). A cortical–hippocampal system for declarative memory. Nat. Rev. Neurosci. *1*, 41–50.

Eichenbaum, H. (2017). Prefrontal-hippocampal interactions in episodic memory. Nat. Rev. Neurosci. *18*, 547–558.

Ellenbroek, B., and Youn, J. (2016). Rodent models in neuroscience research: Is it a rat race? DMM Dis. Model. Mech. *9*, 1079–1087.

Elston, G.N. (2000). Pyramidal cells of the frontal lobe: all the more spinous to think with. J. Neurosci. *20*

Feldmeyer, D., Brecht, M., Helmchen, F., Petersen, C.C.H., Poulet, J.F.A., Staiger, J.F., Luhmann, H.J., and Schwarz, C. (2013). Barrel cortex function. Prog. Neurobiol. *103*, 3–27.

Felleman, D.J., and Van Essen, D.C. (1991). Distributed Hierarchical Processing in the Primate Cerebral Cortex. Cereb. Cortex *1*, 1–47.

Francioni, V., Padamsey, Z., and Rochefort, N.L. (2019). High and asymmetric somato-dendritic coupling of v1 layer 5 neurons independent of visual stimulation and locomotion. Elife *8*.

Frankland, P.W., and Bontempi, B. (2005). The organization of recent and remote memories. Nat. Rev. Neurosci. *6*, 119–130.

Frankland, P.W., Bontempi, B., Talton, L.E., Kaczmarek, L., and Silva, A.J. (2004). The Involvement of the Anterior Cingulate Cortex in Remote Contextual Fear Memory. Science *304*, 881–883.

Franklin, K., and Paxinos, G. (2001). The Mouse Brain in Stereotaxic Coordinates (San Diego: Academic Press).

Froemke, R.C., Letzkus, J.J., Kampa, B.M., Hang, G.B., and Stuart, G.J. (2010). Dendritic synapse location and neocortical spike-timing dependent plasticity. Front. Synaptic Neurosci. *2*, 1–14.

Gambino, F., Pagès, S., Kehayas, V., Baptista, D., Tatti, R., Carleton, A., and Holtmaat, A. (2014). Sensory-evoked LTP driven by dendritic plateau potentials *in vivo*. Nature *515*, 116–119.

Gerfen, C.R., Paletzki, R., and Heintz, N. (2013). GENSAT BAC Cre-Recombinase Driver Lines to Study the Functional Organization of Cerebral Cortical and Basal Ganglia Circuits. Neuron *80*, 1368–1383.

Gomez, J.L., Bonaventura, J., Lesniak, W., Mathews, W.B., Sysa-Shah, P., Rodriguez, L.A., Ellis, R.J., Richie, C.T., Harvey, B.K., Dannals, R.F., et al. (2017). Chemogenetics revealed: DREADD occupancy and activation via converted clozapine. Science *357, 503–507*.

Graham, K.S., and Hodges, J.R. (1997). Differentiating the roles of the hippocampal complex and the neocortex in long-term memory storage: Evidence from the study of semantic dementia and Alzheimer's disease. Neuropsychology *11*, 77–89.

Grienberger, C., Chen, X., and Konnerth, A. (2014). NMDA receptor-dependent multidendrite Ca^{2+} spikes required for hippocampal burst firing invivo. Neuron *81*, 1274–1281.

Griffin, J.W., Price, D.L., Drachman, D.B., and Engel, W.K. (1976). AXONAL TRANSPORT TO AND FROM THE MOTOR NERVE ENDING*. Ann. N. Y. Acad. Sci. *274*, 31–45.

Guzowski, J.F., Timlin, J.A., Roysam, B., McNaughton, B.L., Worley, P.F., and Barnes, C.A. (2005). Mapping behaviorally relevant neural circuits with immediate-early gene expression. Curr. Opin. Neurobiol. *15*, 599–606.

Harris, K.D. (2005). Neural signatures of cell assembly organization. Nat. Rev. Neurosci. *6*, 399–407.

Harris, K.D., and Shepherd, G.M.G. (2015). The neocortical circuit: Themes and variations. Nat. Neurosci. *18*, 170–181.

Harris, J.A., Mihalas, S., Hirokawa, K.E., Whitesell, J.D., Choi, H., Bernard, A., Bohn, P., Caldejon, S., Casal, L., Cho, A., et al. (2019). Hierarchical organization of cortical and thalamic connectivity. Nature *575*, 195–202.

Hausser, M., Spruston, N., and Stuart, G.J. (2000). Diversity and dynamics of dendritic signaling. Science *290*, 739–744.

Häussler, U., Bielefeld, L., Froriep, U.P., Wolfart, J., and Haas, C.A. (2012). Septotemporal position in the hippocampal formation determines epileptic and neurogenic activity in temporal lobe epilepsy. Cereb. Cortex *22*, 26–36.

Helmchen, F., Svoboda, K., Denk, W., and Tank, D.W. (1999). *In vivo* dendritic calcium dynamics in deep-layer cortical pyramidal neurons. Nat. Neurosci. *2*, 989–996.

Hofer, S.B., Mrsic-Flogel, T.D., Bonhoeffer, T., and Hübener, M. (2009). Experience leaves a lasting structural trace in cortical circuits. Nature *457*, 313–317.

Holt, C.E., Martin, K.C., and Schuman, E.M. (2019). Local translation in neurons: visualization and function. Nat. Struct. Mol. Biol. *26*, 557–566.

Houweling, A.R., and Brecht, M. (2008). Behavioural report of single neuron stimulation in somatosensory cortex. Nature *451*, 65–68.

Houweling, A.R., Doron, G., Voigt, B.C., Herfst, L.J., and Brecht, M. (2010). Nanostimulation: manipulation of single neuron activity by juxtacellular current injection. J. Neurophysiol. *103*, 1696–1704.

Hubel, D.H., and Wiesel, T.N. (1959). Receptive fields of single neurones in the cat's striate cortex. J. Physiol. *148*, 574–591.

Hübener, M., and Bonhoeffer, T. (2010). Searching for Engrams. Neuron *67*, 363–371.

Isomura, Y., Sirota, A., Özen, S., Montgomery, S., Mizuseki, K., Henze, D.A., and Buzsáki, G. (2006). Integration and Segregation of Activity in Entorhinal-Hippocampal Subregions by Neocortical Slow Oscillations. Neuron *52*, 871–882.

Itskov, P.M., Vinnik, E., and Diamond, M.E. (2011). Hippocampal Representation of Touch-Guided Behavior in Rats: Persistent and Independent Traces of Stimulus and Reward Location. PLoS One *6*, e16462.

Jafarpour, A., Griffin, S., Lin, J.J., and Knight, R.T. (2019). Medial orbitofrontal cortex, dorsolateral prefrontal cortex, and hippocampus differentially represent the event saliency. J. Cogn. Neurosci. *31*, 874–884.

Ji, D., and Wilson, M.A. (2007). Coordinated memory replay in the visual cortex and hippocampus during sleep. Nat. Neurosci. *10*, 100–107.

Josselyn, S.A., Köhler, S., and Frankland, P.W. (2015). Finding the engram. Nat. Rev. Neurosci. *16*, 521–534.

Kalisch, R., Schubert, M., Jacob, W., Keßler, M.S., Hemauer, R., Wigger, A., Landgraf, R., and Auer, D.P. (2006). Anxiety and hippocampus volume in the rat. Neuropsychopharmacology *31*, 925–932.

Kampa, B.M., Clements, J., Jonas, P., and Stuart, G.J. (2004). Kinetics of Mg^{2+} unblock of NMDA receptors: Implications for spike-timing dependent synaptic plasticity. J. Physiol. *556*, 337–345.

Kandel, E.R. (2001). The molecular biology of memory storage: A dialogue between genes and synapses. Science *294*, 1030–1038.

Kealy, J., and Commins, S. (2011). The rat perirhinal cortex: A review of anatomy, physiology, plasticity, and function. Prog. Neurobiol. *93*, 522–548.

Keller, G.B., and Mrsic-Flogel, T.D. (2018). Predictive Processing: A Canonical Cortical Computation. Neuron *100*, 424–435.

Kerr, K.M., Agster, K.L., Furtak, S.C., and Burwell, R.D. (2007). Functional Neuroanatomy of the Parahippocampal Region: The Lateral and Medial Entorhinal Areas. Hippocampus 697–

708.

Kitamura, T., Ogawa, S.K., Roy, D.S., Okuyama, T., Morrissey, M.D., Smith, L.M., Redondo, R.L., and Tonegawa, S. (2017). Engrams and circuits crucial for systems consolidation of a memory. Science *356*, 73–78.

Klinzing, J.G., Niethard, N., and Born, J. (2019). Mechanisms of systems memory consolidation during sleep. Nat. Neurosci. *22*, 1598–1610.

Krubitzer, L., and Kahn, D.M. (2003). Nature versus nurture revisited: An old idea with a new twist. Prog. Neurobiol. *70*, 33–52.

Kumaran, D., and Maguire, E.A. (2006). An unexpected sequence of events: Mismatch detection in the human hippocampus. PLoS Biol. *4*, 2372–2382.

Kumaran, D., Hassabis, D., and McClelland, J.L. (2016). What Learning Systems do Intelligent Agents Need? Complementary Learning Systems Theory Updated. Trends Cogn. Sci. *20*, 512–534.

Larkman, A.U. (1991). Dendritic morphology of pyramidal neurones of the visual cortex of the rat: III. Spine distributions. J. Comp. Neurol. *306*, 332–343.

Larkum, M. (2013). A cellular mechanism for cortical associations: An organizing principle for the cerebral cortex. Trends Neurosci. *36*, 141–151.

Larkum, M.E., and Zhu, J.J. (2002). Signaling of layer 1 and whisker-evoked Ca^{2+} and Na^{+} action potentials in distal and terminal dendrites of rat neocortical pyramidal neurons *in vitro* and *in vivo*. J. Neurosci. *22*, 6991–7005.

Larkum, M.E., Zhu, J.J., and Sakmann, B. (1999). A new cellular mechanism for coupling inputs arriving at different cortical layers. Nature *398*, 338–341.

Larkum, M.E., Senn, W., and Lüscher, H.R. (2004). Top-down dendritic input increases the gain of layer 5 pyramidal neurons. Cereb. Cortex *14*, 1059–1070.

Latchoumane, C.-F. V., Ngo, H.-V. V., Born, J., and Shin, H.-S. (2017). Thalamic Spindles Promote Memory Formation during Sleep through Triple Phase-Locking of Cortical,

Thalamic, and Hippocampal Rhythms. Neuron *95*, 1–12.

Lavenex, P., and Amaral, D.G. (2000). Hippocampal-neocortical interaction: A hierarchy of associativity. Hippocampus *10*, 420–430.

Lee, J.Q., Zelinski, E.L., McDonald, R.J., and Sutherland, R.J. (2016). Heterarchic reinstatement of long-term memory: A concept on hippocampal amnesia in rodent memory research. Neurosci. Biobehav. Rev. *71*, 154–166.

Lee, S., Kruglikov, I., Huang, Z.J., Fishell, G., and Rudy, B. (2013). A disinhibitory circuit mediates motor integration in the somatosensory cortex. Nat. Neurosci. *16*, 1662–1670.

Lefort, S., Tomm, C., Floyd Sarria, J.C., and Petersen, C.C.H. (2009). The Excitatory Neuronal Network of the C2 Barrel Column in Mouse Primary Somatosensory Cortex. Neuron *61*, 301–316.

Letzkus, J.J., Kampa, B.M., and Stuart, G.J. (2006). Learning Rules for Spike Timing-Dependent Plasticity Depend on Dendritic Synapse Location. J. Neurosci. *26*, 10420–10429.

Letzkus, J.J., Wolff, S.B.E., Meyer, E.M.M., Tovote, P., Courtin, J., Herry, C., and Lüthi, A. (2011). A disinhibitory microcircuit for associative fear learning in the auditory cortex. Nature *480*, 331–335.

Li, D., Wang, G., Xie, H., Hu, Y., Guan, J.-S., and Hilgetag, C.C. (2019). Multimodal memory components and their long-term dynamics identified in cortical layers II/III but not layer Vb. Front. Integr. Neurosci. *13*.

Li, W., Ma, L., Yang, G., and Gan, W.-B. (2017). REM sleep selectively prunes and maintains new synapses in development and learning. Nat. Neurosci. *20*. 427–437.

Lisman, J.E. (1997). Bursts as a unit of neural information: Making unreliable synapses reliable. Trends Neurosci. *20*, 38–43.

Lodato, S., and Arlotta, P. (2015). Generating Neuronal Diversity in the Mammalian Cerebral Cortex. Annu. Rev. Cell Dev. Biol. *31*, 699–720.

Lu, S.M., and Lin, R.C. (1993). Thalamic afferents of the rat barrel cortex: a light- and

electron-microscopic study using Phaseolus vulgaris leucoagglutinin as an anterograde tracer. Somatosens. Mot. Res. *10*, 1–16.

Luczak, A., McNaughton, B.L., and Harris, K.D. (2015). Packet-based communication in the cortex. Nat. Rev. Neurosci. *16*, 745–755.

MacDonald, C.J., Lepage, K.Q., Eden, U.T., and Eichenbaum, H. (2011). Hippocampal "Time Cells" Bridge the Gap in Memory for Discontiguous Events. Neuron *71*, 737–749.

Madisen, L., Mao, T., Koch, H., Zhuo, J., Berenyi, A., Fujisawa, S., Hsu, Y.-W.A., Garcia, A.J., Gu, X., Zanella, S., et al. (2012). A toolbox of Cre-dependent optogenetic transgenic mice for light-induced activation and silencing. Nat. Neurosci. *15*, 793–802.

Maingret, N., Girardeau, G., Todorova, R., Goutierre, M., and Zugaro, M. (2016). Hippocampo-cortical coupling mediates memory consolidation during sleep. Nat. Neurosci. *19*, 959–964.

Major, G., Polsky, A., Denk, W., Schiller, J., and Tank, D.W. (2008). Spatiotemporally graded NMDA spike/plateau potentials in basal dendrites of neocortical pyramidal neurons. J. Neurophysiol. *99*, 2584–2601.

Major, G., Larkum, M.E., and Schiller, J. (2013). Active Properties of Neocortical Pyramidal Neuron Dendrites. Annu. Rev. Neurosci. *36*, 1–24.

Makino, H., and Komiyama, T. (2015). Learning enhances the relative impact of top-down processing in the visual cortex. Nat. Neurosci. *18*, 1116–1122.

Malinow, R., Otmakhov, N., Blum, K.I., and Lisman, J. (1994). Visualizing hippocampal synaptic function by optical detection of Ca^{2+} entry through the N-methyl-D-aspartate channel. Proc. Natl. Acad. Sci. U. S. A. *91*, 8170–8174.

Markov, N.T., Vezoli, J., Chameau, P., Falchier, A., Quilodran, R., Huissoud, C., Lamy, C., Misery, P., Giroud, P., Ullman, S., et al. (2014). Anatomy of hierarchy: Feedforward and feedback pathways in macaque visual cortex. J. Comp. Neurol. *522*, 225–259.

Marler, P. (2004). Innateness and the instinct to learn. In Anais Da Academia Brasileira de Ciencias, (Academia Brasileira de Ciencias), pp. 189–200.

Marr, D. (1971). Simple memory: a theory for archicortex. Philos. Trans. R. Soc. London. B, Biol. Sci. *262*, 23–81.

Martin, K.C., Casadio, A., Zhu, H., Yaping, E., Rose, J.C., Chen, M., Bailey, C.H., and Kandel, E.R. (1997). Synapse-specific, long-term facilitation of aplysia sensory to motor synapses: A function for local protein synthesis in memory storage. Cell *91*, 927–938.

Maviel, T., Durkin, T.P., Menzaghi, F., and Bontempi, B. (2004). Sites of neocortical reorganization critical for remote spatial memory. Science *305*, 96–99.

McClelland, J.L., McNaughton, B.L., and O'Reilly, R. (1995). Why There Are Complementary Learning Systems in the Hippocampus and Neocortex: Insights From the Successes and Failures of Connectionist Models of Learning and Memory. Psych. Rev. *102*, 419–457.

McClelland, J.L., McNaughton, B.L., and Lampinen, A.K. (2020). Integration of new information in memory: new insights from a complementary learning systems perspective. Philos. Trans. R. Soc. B Biol. Sci. *375*.

Metzler, P., Rudolph, M., Voshage, J., and Nickel, B. (1991). Zum Begriff der Amnesie und zur quantitativen Beurteilung mnestischer Störungen. Fortschritte Der Neurol. Psychiatr. *59*, 207–215.

Milner, B. (2005). The medial temporal-lobe amnesic syndrome. Psychiatr. Clin. North Am. *28*, 599–611.

Miyamoto, D., Hirai, D., Fung, C.C.A., Inutsuka, A., Odagawa, M., Suzuki, T., Boehringer, R., Adaikkan, C., Matsubara, C., Matsuki, N., et al. (2016). Top-down cortical input during NREM sleep consolidates perceptual memory. Science *352*, 1315–1318.

Moscovitch, M., and Nadel, L. (1997). Memory consolidation , retrograde amnesia and the hippocampal complex. Curr. Opin. Neurobiol. *7*, 217–227.

Mountcastle, V.B. (1997). The columnar organization of the neocortex. Brain *120*, 701–722.

Murayama, M., and Larkum, M.E. (2009). Enhanced dendritic activity in awake rats. Proc. Natl. Acad. Sci. U. S. A. *106*, 20482–20486.

Murayama, M., Pérez-Garci, E., Nevian, T., Bock, T., Senn, W., and Larkum, M.E. (2009). Dendritic encoding of sensory stimuli controlled by deep cortical interneurons. Nature *457*, 1137–1141.

Nadel, L., Samsonovich, A., Ryan, L., and Moscovitch, M. (2000). Multiple Trace Theory of Human Memory: Computational, Neuroimaging, and Neuropsychological Results. Hippocampus *368*, 352–368.

Naud, R., and Sprekeler, H. (2018). Sparse bursts optimize information transmission in a multiplexed neural code. Proc. Natl. Acad. Sci. *115*, E6329–E6338.

Newsome, W.T., Salzman, C.D., and Britten, K.H. (1990). Cortical Microstimulation Influences Perceptual Judgements of Motion Direction. Nature *346*, 174–177.

Niethard, N., Ngo, H.-V. V, Ehrlich, I., and Born, J. (2018). Cortical circuit activity underlying sleep slow oscillations and spindles. Proc. Natl. Acad. Sci. U. S. A. E9220–E9229.

Nitzan, N., McKenzie, S., Beed, P., English, D.F., Oldani, S., Tukker, J.J., Buzsáki, G., and Schmitz, D. (2020). Propagation of hippocampal ripples to the neocortex by way of a subiculum-retrosplenial pathway. Nat. Commun. *11*, 1947.

Oram, T.B., AhissarE., and Yizhar, O. (2015). Head-motion modulation of the activity of optogenetically tagged neurons in the vibrissal thalamus. Soc Neuro Abstr 736.15.

Palmer, L., Murayama, M., and Larkum, M. (2012a). Inhibitory Regulation of Dendritic Activity *in vivo*. Front. Neural Circuits *6*, 26.

Palmer, L.M., Schulz, J.M., Murphy, S.C., Ledergerber, D., Murayama, M., and Larkum, M.E. (2012b). The Cellular Basis of GABAB-Mediated Interhemispheric Inhibition. Science *335*, 989–993.

Palmer, L.M., Shai, A.S., Reeve, J.E., Anderson, H.L., Paulsen, O., and Larkum, M.E. (2014). NMDA spikes enhance action potential generation during sensory input. Nat Neurosci *17*, 383–390.

Pastalkova, E., Itskov, V., Amarasingham, A., and Buzsáki, G. (2008). Internally generated cell assembly sequences in the rat hippocampus. Science *321*, 1322–1327.

Paxinos, G., and Watson, C. (1998). The Rat Brain in Stereotaxic Coordinates (San Diego: Academic Press).

Payeur, A., Guerguiev, J., Zenke, F., Richards, B., and Naud, R. (2020). Burst-dependent synaptic plasticity can coordinate learning in hierarchical circuits. BioRxiv Neurosci. 2020.03.30.015511.

Penfield, W., and Rasmussen, T. (1950). The cerebral cortex of man; a clinical study of localization of function. (Oxford, England: Macmillan).

Pereira, A., Ribeiro, S., Wiest, M., Moore, L.C., Pantoja, J., Lin, S.-C., and Nicolelis, M.A.L. (2007). Processing of tactile information by the hippocampus. Proc. Natl. Acad. Sci. U. S. A. *104*, 18286–18291.

Pérez-Garci, E., Gassmann, M., Bettler, B., and Larkum, M.E. (2006). The GABAB1b Isoform Mediates Long-Lasting Inhibition of Dendritic Ca^{2+} Spikes in Layer 5 Somatosensory Pyramidal Neurons. Neuron *50*, 603–616.

Pérez-Garci, E., Larkum, M.E., and Nevian, T. (2013). Inhibition of dendritic Ca^{2+} spikes by $GABA_B$ receptors in cortical pyramidal neurons is mediated by a direct $G_{i/o}$-βγ-subunit interaction with Ca_V1 channels. J. Physiol. *591*, 1599–1612.

Petersen, C.C.H. (2019). Sensorimotor processing in the rodent barrel cortex. Nat. Rev. Neurosci. *20*, 533–546.

Petersen, C.C.H.H. (2007). The functional organization of the barrel cortex. Neuron *56*, 339–355.

Peyrache, A., Khamassi, M., Benchenane, K., Wiener, S.I., and Battaglia, F.P. (2009). Replay of rule-learning related neural patterns in the prefrontal cortex during sleep. Nat. Neurosci. *12*, 919–926.

Pfeffer, C.K., Xue, M., He, M., Huang, Z.J., and Scanziani, M. (2013). Inhibition of inhibition in visual cortex: The logic of connections between molecularly distinct interneurons. Nat. Neurosci. *16*, 1068–1076.

Poirazi, P., and Mel, B.W. (2001). Impact of active dendrites and structural plasticity on the

memory capacity of neural tissue. Neuron *29*, 779–796.

Rajasethupathy, P., Sankaran, S., Marshel, J.H., Kim, C.K., Ferenczi, E., Lee, S.Y., Berndt, A., Ramakrishnan, C., Jaffe, A., Lo, M., et al. (2015). Projections from neocortex mediate top-down control of memory retrieval. Nature *526*, 653–659.

Rakic, P. (2009). Evolution of the neocortex: A perspective from developmental biology. Nat. Rev. Neurosci. *10*, 724–735.

Ramaswamy, S., and Markram, H. (2015). Anatomy and physiology of the thick-tufted layer 5 pyramidal neuron. Front. Cell. Neurosci. *9*, 233.

Ramos, J.M.J. (2013). Profound retrograde but absence of anterograde amnesia for cued place learning in rats with hippocampal lesions. Behav. Brain Res. *236*, 102–109.

Ranganath, C., and D'Esposito, M. (2001). Medial temporal lobe activity associated with active maintenance of novel information. Neuron *31*, 865–873.

Ranganathan, G.N., Apostolides, P.F., Harnett, M.T., Xu, N.-L., Druckmann, S., and Magee, J.C. (2018). Active dendritic integration and mixed neocortical network representations during an adaptive sensing behavior. Nat. Neurosci.

Remy, S., and Spruston, N. (2007). Dendritic spikes induce single-burst long-term potentiation. Proc. Natl. Acad. Sci. *104*, 17192–17197.

Riban, V., Bouilleret, V., Pham-Lê, B.T., Fritschy, J.M., Marescaux, C., and Depaulis, A. (2002). Evolution of hippocampal epileptic activity during the development of hippocampal sclerosis in a mouse model of temporal lobe epilepsy. Neuroscience *112*, 101–111.

Rockland, K.S. (2019). What do we know about laminar connectivity? Neuroimage *197*, 772–784.

Romo, R., Hernández, A., Zainos, A., and Salinas, E. (1998). Somatosensory discrimination based on cortical microstimulation. Nature *392*, 387–390.

Romo, R., Hernández, A., Zainos, A., Brody, C.D., and Lemus, L. (2000). Sensing without touching: Psychophysical performance based on cortical microstimulation. Neuron *26*, 273–

278.

Roth, B.L. (2016). DREADDs for Neuroscientists. Neuron *89*, 683–694.

Roth, M.M., Dahmen, J.C., Muir, D.R., Imhof, F., Martini, F.J., and Hofer, S.B. (2016). Thalamic nuclei convey diverse contextual information to layer 1 of visual cortex. Nat. Neurosci. *19*, 299–307.

Rothschild, G., Eban, E., and Frank, L.M. (2016). A cortical – hippocampal – cortical loop of information processing during memory consolidation. Nat. Neurosci. 1–12.

Rubio-Garrido, P., Pérez-De-Manzo, F., Porrero, C., Galazo, M.J., and Clascá, F. (2009). Thalamic input to distal apical dendrites in neocortical layer 1 is massive and highly convergent. Cereb. Cortex *19*, 2380–2395.

Sambandan, S., Akbalik, G., Kochen, L., Rinne, J., Kahlstatt, J., Glock, C., Tushev, G., Alvarez-Castelao, B., Heckel, A., and Schuman, E.M. (2017). Activity-dependent spatially localized miRNA maturation in neuronal dendrites. Science *355*, 634–637.

Schuman, B., Machold, R.P., Hashikawa, Y., Fuzik, J., Fishell, G.J., and Rudy, B. (2019). Four unique interneuron populations reside in neocortical layer 1. J. Neurosci. *39*, 125–139.

Schwindt, P., and Crill, W. (1999). Mechanisms Underlying Burst and Regular Spiking Evoked by Dendritic Depolarization in Layer 5 Cortical Pyramidal Neurons. J. Neurophysiol. *81*, 1341–1354.

Scoville, W.B., and Milner, B. (1957). Loss of recent memory after bilateral hippocampal lesions. J. Neurol. Neurosurg. Psychiatry *20*, 11–21.

Seibt, J., Richard, C.J., Sigl-Glöckner, J., Takahashi, N., Kaplan, D.I., Doron, G., De Limoges, D., Bocklisch, C., and Larkum, M.E. (2017). Cortical dendritic activity correlates with spindle-rich oscillations during sleep in rodents. Nat. Commun. *8*, 684.

Seitz, A.R. (2017). Perceptual learning. Curr. Biol. *27*, R631–R636.

Sestieri, C., Shulman, G.L., and Corbetta, M. (2017). The contribution of the human posterior parietal cortex to episodic memory. Nat. Rev. Neurosci. *18*, 183–192.

Shai, A.S., Anastassiou, C.A., Larkum, M.E., and Koch, C. (2015). Physiology of Layer 5 Pyramidal Neurons in Mouse Primary Visual Cortex: Coincidence Detection through Bursting. PLOS Comput. Biol. *11*.

Sheffield, M.E., and Dombeck, D.A. (2019). Dendritic mechanisms of hippocampal place field formation. Curr. Opin. Neurobiol. *54*, 1–11.

Sheffield, M.E.J., and Dombeck, D.A. (2015). Calcium transient prevalence across the dendritic arbour predicts place field properties. Nature *517*, 200–204.

Shepherd, G.M.G. (2013). Corticostriatal connectivity and its role in disease. Nat. Rev. Neurosci. *14*, 278–291.

Shrestha, P., Ayata, P., Herrero-Vidal, P., Longo, F., Gastone, A., LeDoux, J.E., Heintz, N., and Klann, E. (2020). Cell-type-specific drug-inducible protein synthesis inhibition demonstrates that memory consolidation requires rapid neuronal translation. Nat. Neurosci.

Simonnet, J., and Brecht, M. (2018). Burst firing and spatial coding in subicular principal cells. J. Neurosci 19, 3651–3662.

Sjöström, P.J., and Häusser, M. (2006). A Cooperative Switch Determines the Sign of Synaptic Plasticity in Distal Dendrites of Neocortical Pyramidal Neurons. Neuron *51*, 227–238.

Sousa, A.F. de, Cowansage, K.K., Zutshi, I., Cardozo, L.M., Yoo, E.J., Leutgeb, S., and Mayford, M. (2019). Optogenetic reactivation of memory ensembles in the retrosplenial cortex induces systems consolidation. Proc. Natl. Acad. Sci. *17*, 8576–8581.

Squire, L.R., and Alvarez, P. (1995). Retrograde amnesia and memory consolidation: a neurobiological perspective. Curr. Opin. Neurobiol. *5*, 169–177.

Squire, L.R., Stark, C.E.L., and Clark, R.E. (2004). THE MEDIAL TEMPORAL LOBE. Annu. Rev. Neurosci. *27*, 279–306.

Stachniak, T.J., Ghosh, A., and Sternson, S.M. (2014). Chemogenetic Synaptic Silencing of Neural Circuits Localizes a Hypothalamus→Midbrain Pathway for Feeding Behavior. Neuron *82*, 797–808.

Staiger, J.F., Flagmeyer, I., Schubert, D., Zilles, K., Kötter, R., and Luhmann, H.J. (2004). Functional Diversity of Layer IV Spiny Neurons in Rat Somatosensory Cortex: Quantitative Morphology of Electrophysiologically Characterized and Biocytin Labeled Cells. Cereb. Cortex *14*, 690–701.

Stein, J.L., Medland, S.E., Vasquez, A.A., Hibar, D.P., Senstad, R.E., Winkler, A.M., Toro, R., Appel, K., Bartecek, R., Bergmann, Ø., et al. (2012). Identification of common variants associated with human hippocampal and intracranial volumes. Nat. Genet. *44*, 552–561.

Stevens, C.F., and Wang, Y. (1995). Facilitation and depression at single central synapses. Neuron *14*, 795–802.

van Strien, N.M., Cappaert, N.L.M., and Witter, M.P. (2009). The anatomy of memory: an interactive overview of the parahippocampal-hippocampal network. Nat. Rev. Neurosci. *10*, 272–282.

Stuart, G.J., and Sakmann, B. (1994). Active propagation of somatic action potentials into neocortical pyramidal cell dendrites. Nature *367*, 69–72.

Stuart, G.J., and Spruston, N. (2015). Dendritic integration: 60 years of progress. Nat. Neurosci. *18*, 1713–1721.

Suzuki, M., and Larkum, M.E. (2017). Dendritic calcium spikes are clearly detectable at the cortical surface. Nat. Commun. *8*, 276.

Takahashi, N., Oertner, T.G., Hegemann, P., and Larkum, M.E. (2016). Active cortical dendrites modulate perception. Science *354*, 1587–1590.

Takashima, A., Nieuwenhuis, I.L.C., Jensen, O., Talamini, L.M., Rijpkema, M., and Fernández, G. (2009). Shift from hippocampal to neocortical centered retrieval network with consolidation. J. Neurosci. *29*, 10087–10093.

Teyler, T.J., and DiScenna, P. (1986). The Hippocampal Memory Indexing Theory. Behav. Neurosci. *100*, 147–154.

Teyler, T.J., and Rudy, J.W. (2007). The hippocampal indexing theory and episodic memory: Updating the index. Hippocampus *17*, 1158–1169.

Thomson, A.M. (2000). Molecular frequency filters at central synapses. Prog. Neurobiol. *62*, 159–196.

Tierney, A.J. (1986). The evolution of learned and innate behavior: Contributions from genetics and neurobiology to a theory of behavioral evolution. Anim. Learn. Behav. *14*, 339–348.

Todd, T.P., and Bucci, D.J. (2015). Retrosplenial Cortex and Long-Term Memory: Molecules to Behavior. Neural Plast. *2015*.

Todd, T.P., Mehlman, M.L., Keene, C.S., De Angeli, N.E., and Bucci, D.J. (2016). Retrosplenial cortex is required for the retrieval of remote memory for auditory cues. Learn. Mem. *23*, 278–288.

Tramoni-Negre, E., Lambert, I., Bartolomei, F., and Felician, O. (2017). Long-term memory deficits in temporal lobe epilepsy. Rev. Neurol. *173*, 490–497.

Voigt, B.C., Brecht, M., and Houweling, A.R. (2008). Behavioral detectability of single-cell stimulation in the ventral posterior medial nucleus of the thalamus. J. Neurosci. *28*, 12362–12367.

Wang, Y., Toledo-Rodriguez, M., Gupta, A., Wu, C., Silberberg, G., Luo, J., and Markram, H. (2004). Anatomical, physiological and molecular properties of Martinotti cells in the somatosensory cortex of the juvenile rat. J. Physiol. *561*, 65–90.

Wartman, B.C., Gabel, J., and Holahan, M.R. (2014). Inactivation of the Anterior Cingulate Reveals Enhanced Reliance on Cortical Networks for Remote Spatial Memory Retrieval after Sequential Memory Processing. PLoS One *9*.

Weinberger, N.M. (2004). Specific long-term memory traces in primary auditory cortex. Nat. Rev. Neurosci. *5*, 279–290.

Weinberger, N.M., Javid, R., and Lepan, B. (1993). Long-term retention of learning-induced receptive-field plasticity in the auditory cortex. Proc. Natl. Acad. Sci. U. S. A. *90*, 2394–2398.

Wheeler, A.L., Teixeira, C.M., Wang, A.H., Xiong, X., Kovacevic, N., Lerch, J.P., McIntosh, A.R., Parkinson, J., and Frankland, P.W. (2013). Identification of a Functional Connectome for

Long-Term Fear Memory in Mice. PLoS Comput. Biol. *9*.

Wiegert, J.S., Mahn, M., Prigge, M., Printz, Y., and Yizhar, O. (2017). Silencing Neurons: Tools, Applications, and Experimental Constraints. Neuron *95*, 504–529.

Wilber, A.A., Skelin, I., Wu, W., and McNaughton, B.L. (2017). Laminar Organization of Encoding and Memory Reactivation in the Parietal Cortex. Neuron *95*, 1406-1419.

Williams, L.E., and Holtmaat, A. (2019). Higher-Order Thalamocortical Inputs Gate Synaptic Long-Term Potentiation via Disinhibition. Neuron *101*, 91-102.

Williams, S.R., and Stuart, G.J. (1999). Mechanisms and consequences of action potential burst firing in rat neocortical pyramidal neurons. J. Physiol. *521*, 467–482.

Wiltgen, B.J., Brown, R.A.M., Talton, L.E., and Silva, A.J. (2004). New Circuits for Old Memories: The Role of the Neocortex in Consolidation. Neuron *44*, 101–108.

Winocur, G., and Moscovitch, M. (2011). Memory transformation and systems consolidation. J. Int. Neuropsychol. Soc. *17*, 766–780.

Winocur, G., McDonald, R.M., and Moscovitch, M. (2001). Anterograde and retrograde amnesia in rats with large hippocampal lesions. Hippocampus *11*, 18–26.

Witter, M.P., Groenewegen, H.J., Lopes da Silva, F.H., and Lohman, A.H.M. (1989). Functional organization of the extrinsic and intrinsic circuitry of the parahippocampal region. Prog. Neurobiol. *33*, 161–253.

Xie, H., Liu, Y., Zhu, Y., Ding, X., Yang, Y., and Guan, J.S. (2014). *In vivo* imaging of immediate early gene expression reveals layer-specific memory traces in the mammalian brain. Proc. Natl. Acad. Sci. U. S. A. *111*, 2788–2793.

Xu, N.L., Harnett, M.T., Williams, S.R., Huber, D., O'Connor, D.H., Svoboda, K., and Magee, J.C. (2012). Nonlinear dendritic integration of sensory and motor input during an active sensing task. Nature *492*, 247–251.

Xu, T., Yu, X., Perlik, A.J., Tobin, W.F., Zweig, J.A., Tennant, K., Jones, T., and Zuo, Y. (2009). Rapid formation and selective stabilization of synapses for enduring motor memories.

Nature *462*, 915–919.

Yang, G., Lai, C.S.W., Cichon, J., Ma, L., Li, W., and Gan, W.-B. (2014). Sleep promotes branch-specific formation of dendritic spines after learning. Science *344*, 1173–1178.

Yuste, R. (2015). From the neuron doctrine to neural networks. Nat. Rev. Neurosci. *16*, 487–497.

Zhao, X., Wang, Y., Spruston, N., and Magee, J.C. (2020). Membrane potential dynamics underlying context-dependent sensory responses in the hippocampus. Nat. Neurosci. 1–11.

Zolnik, T.A., Ledderose, J., Toumazou, M., Trimbuch, T., Oram, T., Rosenmund, C., Eickholt, B.J., Sachdev, R.N.S., and Larkum, M.E. (2020). Layer 6b Is Driven by Intracortical Long-Range Projection Neurons. Cell Rep. *30*, 3492-3505.

Acknowledgements

I am grateful to all the people who generously offered their help during my PhD. Without them, I would not have been able to reach where I am now and finish this dissertation. My colleagues who directly contributed to this dissertation are acknowledged in the next section of 'statement of contributions'. First, I would like to express my sincere gratitude to my supervisor, Prof. Matthew Larkum, for his outstanding mentorship by being an excellent role model to an aspiring young scientist. He never treated me as his student but rather as his colleague and carefully listened to my opinions. Our discussions were often interesting and insightful, which helped me a lot to shape my ideas. Also, his endless passion for science has been always inspiring and stimulating.

Secondly, I would like to thank Dr. Guy Doron, who supervised me on daily basis until he left the lab. He introduced and taught me *in vivo* electrophysiology and animal behavior as well as programming. In fact, he paved the way to this project by conceiving the initial ideas. I am especially grateful to his advice and help even after moving outside of the academia.

I would like to acknowledge my collaborators, Dr. Naoya Takahashi and Dr. Richard Naud, with whom I was fortunate to work with. I would like to express my gratitude to all the members in Larkum lab for collaborative and friendly atmosphere. I want to send special thanks to Dr. Robert Sachdev, whom I could always ask for advice, and Oded Kruchik for successfully managing rather a chaotic lab. I am grateful to Dr. Jaan Aru and Dr. Aarti Swaminathan for reviewing my dissertation and providing constructive feedbacks.

Lastly and most importantly, I would like to express my deepest gratitude to my family, to whom I am in debt forever, for their endless truth and love towards me. This dissertation is dedicated to them who would be more proud of me than anyone else including myself. Especially my mother, who unfortunately could not see this moment herself, would be very happy to know her first child becoming a PhD. During my PhD, I also had a fortune to form a new family. I am very grateful to my partner Noam, who recently defended his PhD, for his unconditional love and being next to me during the most difficult time of my life. His love is my driving force to continue.

Statement of contributions

All experiments and analysis in this thesis were conceived and designed by my supervisors, Prof. Matthew Larkum and Dr.Guy Doron, and myself. All data not mentioned below are acquired and analyzed by me and the manuscript is solely written by me. Results of Chapter 2 and 3 have been published in a peer-reviewes journal Science (https://doi.org/10.1126/science.aaz3136) and preliminary results were posted on bioRxiv (https://doi.org/10.1101/713883).

Detailed contributions of my colleagues to the data are following:

Dr. Guy Doron (AG Larkum, Humboldt University until August 2018, currently at Bayer, Berlin) provided behavioral and electrophysiological data from rats used throughout this dissertation (but analysis was done by myself).

Dr. Peter Bäuerle (AG Glovelli, Charite University Medicine) provided epileptic mice model used in Figure 3.5 as a collaboration.

Dr. Naoya Takahashi (AG Larkum, Humboldt University until July 2020, currently at Bordeaux Neurocampus) performed two-photon axonal (Figure 3.8) and dendritic Ca^{2+} imaging (Figure 3.13) in behaving animals jointly with me. He also pre-processed and analyzed the data.

Dr. Christina Bocklisch (AG Larkum, Humboldt University) performed *ex-vivo* experiments for validating DREADD efficacy and provided parts of anterograde tracing data used in Figure 3.7. My contribution in these experiments was the stereotaxic viral injection for three mice and data analysis.

Maria Toumazou (AG Larkum, Humboldt University, Berlin) counted cells in PRh labelled with Fast Blue used in Figure 3.6 from mouse brain sections provided by **Dr. Julia Ledderose** (AG Larkum, Humboldt University, Berlin) and rat brain sections prepared by myself.

Dr. Richard Naud (University of Ottawa, Ottawa, Canada) classified L5 pyramidal neurons by their responses, used in figure 3.12.

Moritz Drüke (AG Larkum, Humboldt University, Berlin) collected behavioral data from six wild-type mice and untrained mice (together with **Lisa de Mont**) used in chapter 3.1. He also collected behavioral data from Gpr26-cre transgenic mice used in Figure 3.10 and baclofen-treated mice used in Figure 3.13. My contribution in these experiments was supervising him and performing surgeries for implants and craniotomy as well as stereotaxic viral injections.

Salina Skenderi (AG Larkum, Humboldt University, Berlin) collected behavioral data from SST::ChR2 transgenic mice used in Figure 3.13, under my supervision as a MSc student.

Selbständigkeitserklärung

Hiermit erkläre ich, die Dissertation selbstständig und nur unter Verwendung der angegebenen Hilfen und Hilfsmittel angefertigt zu haben. Ich habe mich anderwärts nicht um einen Doktorgrad beworben und besitze keinen entsprechenden Doktorgrad. Ich erkläre, dass ich die Dissertation oder Teile davon nicht bereits bei einer anderen wissenschaftlichen Einrichtung eingereicht habe und dass sie dort weder angenommen noch abgelehnt wurde.
Ich erkläre die Kenntnisnahme der dem Verfahren zugrunde liegenden Promotionsordnung der Lebenswis-senschaftlichen Fakultät der Humboldt-Universität zu Berlin vom 5. März 2015. Weiterhin erkläre ich, dass keine Zusammenarbeit mit gewerblichen Promotionsbearbeiterinnen/Promoti-onsberatern stattgefunden hat und dass die Grundsätze der Humboldt-Universität zu Berlin zur Sicherung guter wissenschaftlicher Praxis eingehalten wurden.

Berlin, 17. Sep. 2020

Jiyun Shin